Schweizerische Eidgenossenschaft
Confédération suisse
Confederazione Svizzera
Confederaziun svizra

Federal Department of the Environment, Transport, Energy and Communication DETEC

Swiss Federal Office of Energy SFOE
Energy Research and Cleantech

Final Report December 12, 2025

SolHOOD

Solar energy neighbor**hood**s – Optimal design and operation of heat, cold and electricity supply on the neighbourhood scale

Publisher:
Swiss Federal Office of Energy SFOE
Energy Research and Cleantech
CH-3003 Bern
www.energy-research.ch

Co-financing:
Stadt Zürich
Amt für Hochbauten
CH-8021 Zürich
www.stadt-zuerich.ch/hochbau

Subsidy recipients:
Ostschweizer Fachhochschule - OST
SPF Institut für Solartechnik
CH-8640 Rapperswil
www.spf.ch
www.ost.ch

HEIG-VD
Institut de génie thermique
CH-1401 Yverdon-les-Bains
www.heig-vd.ch

Authors:
Neha Dimri, SPF-OST, neha.dimri@ost.ch
Daniel Carbonell, SPF-OST/DCarbo, daniel.carbonell@dcarbo.es
Mikel Arenas, SPF-OST, mikel.arenas@ost.ch
Stefano Pauletta, IGT-HEIG-VD, stefano.pauletta@heig-vd.ch

Collaborators:
Daniel Zenhäusern, Xavier Jobard

SFOE project coordinators:
Andreas Eckmanns, andreas.eckmanns@bfe.admin.ch
Stephan A. Mathez, stephan.a.mathez@solarcampus.ch

SFOE Contract number: SI/502297-1

Abstract

The project SolHOOD targets the decarbonization of Swiss neighborhoods by developing smart planning methods that mitigate the winter energy gap. This was achieved firstly through an overall design optimization, and secondly by using Model Predictive Control (MPC) to optimally control solar-integrated energy systems. Central to this approach is the development of "optihood", an open-source Python-based framework for holistic energy system optimization integrating dynamic 3R3C building models. Applying the optimization framework to an office district identified a centralized high-temperature district heating network, hybridized with solar thermal flat plate collectors, as the techno-economic optimum. This topology yielded an 18 % reduction in total annualized costs compared to a low-temperature district heating solution with decentralized ground-source heat pumps. The optimal design relies on heat pump downsizing for baseload operation (>6000 full load hours) and significant thermal storage (0.3–0.4 m^3 per MWh of heat demand), with solar thermal collectors providing a specific yield of 500 kWh/m^2a and a solar fraction of 11.9 %. In a residential district case study, the analysis quantified the trade-offs of deep decarbonization: achieving a threefold reduction in annual GHG emissions required a 20 % increase in total system costs, primarily to accommodate necessary electrical storage (>1.5 hours of PV peak storage capacity) and expanded solar thermal capacity (200 m^2). While these specific numeric values depend on the underlying cost assumptions, the trends regarding hybridization and storage sizing are applicable to similar district typologies. Regarding operational control, the implementation of a novel MPC strategy demonstrated a fundamental shift in grid interaction. The MPC strategy achieved a 4.2 % reduction in operational costs compared to Rule-Based Control. This, however, represents a conservative estimate; savings are expected to be higher if the optimizer and digital twin models are well aligned. More significantly, the MPC strategy improved the Grid Flexibility Factor by 33.8 %, successfully transforming the district heating system from a grid-stressing to a grid-supporting asset by decoupling thermal generation from peak electricity pricing periods.

Zusammenfassung

Das Projekt SolHOOD zielt auf die Dekarbonisierung von Schweizer Quartieren ab. Es wurden intelligente Planungsmethoden entwickelt werden, die die Winterenergielücke mindern. Dies wird erstens durch eine umfassende Optimierung des Systemdesigns und zweitens durch den Einsatz von modellprädiktiver Regelung (Model Predictive Control - MPC) zur optimalen Steuerung solarintegrierter Energiesysteme erreicht. Zentral für diesen Ansatz ist die Entwicklung von „optihood“, einem open-source, Python-basierten Framework für die ganzheitliche Energiesystemoptimierung, das dynamische 3R3C-Gebäudemodelle. Die Anwendung des Optimierungs-Frameworks auf ein Büroquartier identifizierte ein zentrales Hochtemperatur-Fernwärmenetz, hybridisiert mit solarthermischen Flachkollektoren, als das technisch-wirtschaftliche Optimum. Diese Topologie führte zu einer Reduktion der gesamten annualisierten Kosten um 18 % im Vergleich zu einer Niedertemperatur-Fernwärmelösung mit dezentralen Erdwärmepumpen. Das optimale Design basiert auf einer kleineren Dimensionierung der Wärmepumpen für den Grundlastbetrieb (>6000 Volllaststunden) und einem signifikanten thermischen Speicher (0,3–0,4 m^3 pro MWh Wärmebedarf), wobei die solarthermischen Kollektoren einen spezifischen Ertrag von 500 kWh/m^{2}a und einen solaren Deckungsgrad von 11,9 % lieferten. In einer Fallstudie eines Wohnquartiers quantifizierte die Analyse die Zielkonflikte einer tiefgreifenden Dekarbonisierung: Eine dreifache Reduktion der jährlichen THG-Emissionen erforderte eine Erhöhung der gesamten Systemkosten um 20 %, hauptsächlich um den notwendigen elektrischen Speicher (>1,5 Stunden der PV-Spitzenspeicherkapazität) und eine grösseres Solarthermie-Feld (200 m^2) bereitzustellen. Während diese spezifischen numerischen Werte von den zugrunde liegenden Kostenannahmen abhängen, sind die Trends hinsichtlich Hybridisierung und Speicherdimensionierung auf ähnliche Quartierstypologien übertragbar. In Bezug auf die Betriebsführung zeigte die Implementierung einer neuen MPC-Strategie einen fundamentalen Wandel in der Netzinteraktion. Die MPC-Strategie erzielte eine Reduktion der Betriebskosten um 4,2 % im Vergleich zu einer regelbasierten Steuerung. Noch bedeutender ist, dass die MPC-Strategie den Netzflexibilitätsfaktor um 33,8 % verbesserte und das Fernwärmesystem erfolgreich von einem netzbelastenden zu einem netzdienlichen Akteur transformierte, indem die thermische Erzeugung von den Spitzenzeiten der Strompreise entkoppelt wurde.

Résumé

Le projet SolHOOD vise la décarbonisation des quartiers suisses en développant des méthodes de planification intelligentes qui atténuent le déficit énergétique hivernal. Il y parvient d'une part grâce à une optimisation globale de la conception, et d'autre part en utilisant la commande prédictive par modèle (MPC) pour contrôler de manière optimale les systèmes énergétiques intégrés au solaire. Au cœur de cette approche se trouve le développement d'≪ optihood ≫ : un cadre open-source basé sur Python pour l'optimisation holistique des systèmes énergétiques, intégrant des modèles de bâtiments dynamiques 3R3C. L'application du cadre d'optimisation à un quartier de bureaux a identifié comme l'optimum technico-économique un réseau de chauffage urbain centralisé à haute température, hybridé avec des capteurs solaires thermiques plans. Cette topologie a permis une réduction de 18 % des coûts totaux annualisés par rapport à une solution de chauffage urbain à basse température avec des pompes à chaleur géothermiques décentralisées. La conception optimale repose sur un dimensionnement réduit des pompes à chaleur pour un fonctionnement en charge de base (>6000 heures à pleine charge) et un stockage thermique important (0,3–0,4 m^3 par MWh de demande thermique), avec des capteurs solaires thermiques fournissant un rendement spécifique de 500 kWh/m^2a et une fraction solaire de 11,9 %. Dans une étude de cas de quartier résidentiel, l'analyse a quantifié les compromis de la décarbonation profonde : atteindre une réduction par facteur de trois des émissions annuelles de GES a nécessité une augmentation de 20 % des coûts totaux du système, principalement pour accommoder le stockage électrique nécessaire (>1,5 heure de capacité de stockage de pointe PV) et une capacité solaire thermique accrue (200 m^2). Bien que ces valeurs numériques spécifiques dépendent des hypothèses de coûts sous-jacentes, les tendances concernant l'hybridation et le dimensionnement du stockage sont applicables à des typologies de quartiers similaires. En ce qui concerne le contrôle opérationnel, la mise en œuvre d'une nouvelle stratégie MPC a démontré un changement fondamental dans l'interaction avec le réseau. La stratégie MPC a permis une réduction de 4,2 % des coûts opérationnels par rapport à une commande basée sur des règles (RBC). Plus significativement, la stratégie MPC a amélioré le facteur de flexibilité du réseau de 33,8 %, transformant avec succès le système de chauffage urbain d'un actif contraignant pour le réseau en un actif de soutien au réseau, en découplant la production thermique des périodes de tarification de pointe de l'électricité.

Main findings (≪Take-Home Messages≫)

- A centralized High-Temperature District Heating network (combining heat pumps and solar thermal) proved 18 % more cost-effective than a Low-Temperature alternative with decentralized heat pumps, in the context of the analyzed office district. This suggests that centralizing generation can be economically superior to distributing it in certain urban typologies.
- The economic optimum favored downsizing heat pumps for baseload operation (running $>$ 6000 hours) while significantly increasing thermal storage capacity. This design strategy effectively smooths peak electrical loads without compromising heating reliability, directly addressing the winter electricity gap.
- A distinct trade-off exists between cost-optimized and environment-optimized designs. While standard renewable configurations are cost-competitive, achieving deep decarbonization within the analyzed residential district (e.g., a threefold emission reduction) requires approximately 20 % higher capital investment in technologies like batteries and solar thermal, highlighting the necessity for policy incentives to bridge this gap.
- Replacing standard rule-based controls with Model Predictive Control (MPC) transformed the district heating system from a grid-stressing into a grid-supporting asset. The implementation improved the Grid Flexibility Factor by 33.8 %, demonstrating that advanced control algorithms can shift significant thermal loads away from peak grid-stress periods.

Contents

Executive Summary

In order to achieve the goal of decarbonization, the Swiss Energy Strategy envisages a significant electrification of the heating sector. Moreover, the planned electrification of mobility will also substantially impact the electricity demand, particularly during winter months when grid emissions are at their highest. It is therefore imperative to limit the increase in winter electricity and energy demands within the building sector to a minimum. Besides other measures, like the consistent improvement of building envelope, this requires the implementation of highly efficient heat supply systems and their smart integration into multi-energy systems, thereby exploiting the synergies between the thermal and electrical sectors. Most recently installed heating systems rely on heat pumps that use ambient air or ground as a renewable heat source, each of which have their own shortcomings. This highlights the need for improvements and alternatives to these heating systems. The search for alternative solutions is more challenging in densely populated neighborhoods than in isolated individual buildings. However, the neighborhood scale offers opportunities to utilize synergies, for example via shared energy transformation and storage units.

In this context, the SolHOOD project pursued three primary goals: (1) Develop smart planning methods to achieve high-performance energy supply systems (heat and electricity) for neighborhoods, making optimal use of solar energy resources and using sector coupling synergies; (2) Provide alternatives to standard air and ground source heat pump systems, with low grid electricity demand in winter at the neighborhood scale; and (3) Develop an innovative advanced energy management (AEM) system based on model predictive control (MPC) to optimize the operation of complex energy systems in neighborhoods. These three goals aim to decarbonize Switzerland's energy supply systems, reduce winter electricity consumption and peak demand, provide greater grid flexibility and make efficient use of roofs and facades for solar energy harvesting.

To achieve these objectives, the project extended the open-source, Python-based optimization framework "optihood". The framework was applied to a representative neighborhood in Switzerland to evaluate and compare optimal system designs with a high degree of solar share. Moreover, the framework was applied to two case studies showing a variety of system design configurations and results, and demonstrating the effectiveness of the developed method on real cases. Additionally, the developed framework was also used to control a district heating system in order to quantify the benefits from using a smart control based on model predictive control against a standard rule-based control.

In terms of system design, the framework revealed that hybrid centralized solutions often outperform standard decentralized approaches. For a representative office district in Zurich, a centralized High-Temperature District Heating network powered by heat pumps and solar thermal collectors was identified as both the economic and environmental optimum. Compared to a standard decentralized ground-source heat pump alternative, this configuration achieved an 18 % reduction in total annualized costs while maintaining comparable emission levels. In the residential Eco-Thierrens case study, results highlighted the trade-off between economic and environmental goals: achieving the environmental optimum required a 20 % increase in investment (for electrical batteries and expanded solar thermal capacity) but yielded a threefold reduction in greenhouse gas emissions.

Regarding system operation, the developed MPC strategy was compared against a standard Rule-Based Control (RBC). The MPC successfully utilized thermal storage to decouple heat generation from electricity consumption, resulting in a 4.2 % reduction in operational costs. However, these savings are expected to be higher if the optimizer and digital twin models are aligned well. Crucially, the MPC transformed the system's grid interaction, improving the Grid Flexibility Factor by 33.8 %, effectively shifting loads away from peak pricing periods.

In conclusion, SolHOOD successfully developed an open-source framework for energy system optimization. The results demonstrate that through system design optimization and predictive control, the economic performance and grid flexibility of neighborhood energy systems can improve significantly, paving the way for a sustainable energy transition.

Kurzfassung

Um das Ziel der Dekarbonisierung zu erreichen, sieht die Schweizer Energiestrategie eine signifikante Elektrifizierung des Wärmesektors vor. Auch die geplante Elektrifizierung der Mobilität wird die Stromnachfrage erheblich beeinflussen, insbesondere in den Wintermonaten, wenn die Emissionen des Stromnetzes am höchsten sind. Es ist daher zwingend erforderlich, den Anstieg des Winterstrom- und Energiebedarfs im Gebäudesektor auf ein Minimum zu begrenzen. Neben anderen Massnahmen, wie der konsequenten Verbesserung der Gebäudehülle, erfordert dies die Implementierung hocheffizienter Wärmeversorgungssysteme und deren intelligente Integration in Multi-Energiesysteme, um so die Synergien zwischen dem Wärme- und dem Stromsektor zu nutzen. Die meisten kürzlich installierten Heizsysteme basieren auf Wärmepumpen, die Umgebungsluft oder Erdwärme als erneuerbare Wärmequelle nutzen, wobei jede dieser Technologien ihre eigenen Nachteile hat. Dies unterstreicht die Notwendigkeit von Verbesserungen und Alternativen zu diesen Heizsystemen. Die Suche nach alternativen Lösungen ist in dicht besiedelten Quartieren anspruchsvoller als bei isolierten Einzelgebäuden. Hingegen bieten sich auf der Quartiersebene Möglichkeiten zur Nutzung von Synergien, beispielsweise durch gemeinsame Energieumwandlungs- und Speicheranlagen. In diesem Zusammenhang verfolgte das Projekt SolHOOD drei primäre Ziele: (1) Entwicklung intelligenter Planungsmethoden zur Realisierung leistungsstarker Energieversorgungssysteme (Wärme und Strom) für Quartiere unter optimaler Nutzung solarer Energieressourcen und Einsatz von Sektorkopplungs-Synergien; (2) Bereitstellung von Alternativen zu Standard-Luft- und Erdwärmepumpensystemen mit geringem Netzstrombedarf im Winter auf Quartiersebene; und (3) Entwicklung eines innovativen, fortschrittlichen Energiemanagementsystems (AEM) auf Basis von Model Predictive Control (MPC), um den Betrieb komplexer Energiesysteme in Quartieren zu optimieren. Diese drei Ziele sollen dazu beitragen, die Energieversorgungssysteme der Schweiz zu dekarbonisieren, den Winterstromverbrauch und -spitzenlasten zu reduzieren, eine höhere Netzflexibilität zu gewährleisten und Dächer sowie Fassaden effizient für die Solarenergiegewinnung zu nutzen. Um diese Ziele zu erreichen, erweiterte das Projekt das open-source, Python-basierte Optimierungs-Framework „optihood". Das Framework wurde auf ein repräsentatives Quartier in der Schweiz angewendet, um optimale Systemdesigns mit einem hohen Solaranteil zu bewerten und zu vergleichen. Darüber hinaus wurde das Framework auf zwei Fallstudien angewendet, die eine Vielzahl von Systemkonfigurationen und Ergebnissen aufzeigten und die Wirksamkeit der entwickelten Methode an realen Fällen demonstrierten. Zusätzlich wurde das entwickelte Framework auch zur Steuerung eines Fernwärmesystems eingesetzt, um die Vorteile einer intelligenten Steuerung auf Basis der modellprädiktiven Regelung gegenüber einer standardmässigen regelbasierten Steuerung zu quantifizieren.

Im Bereich des Systemdesigns zeigte das Framework, dass hybride zentrale Lösungen oft besser abschneiden als standardmässige dezentrale Ansätze. Für ein repräsentatives Büroquartier in Zürich wurde ein zentrales Hochtemperatur-Fernwärmenetz, das durch Wärmepumpen und solarthermische Kollektoren gespeist wird, sowohl als das wirtschaftliche als auch das ökologische Optimum identifiziert. Im Vergleich zu einer standardmäßigen dezentralen Erdwärmepumpen-Alternative erzielte diese Konfiguration eine Reduktion der gesamten annualisierten Kosten um 18 % bei vergleichbaren Emissionswerten. In der Wohnquartier-Fallstudie Eco-Thierrens verdeutlichten die Ergebnisse den Zielkonflikt zwischen wirtschaftlichen und ökologischen Zielen: Das Erreichen des ökologischen Optimums erforderte eine Erhöhung der Investitionen um 20 % (für elektrische Batterien und eine grösseres Solarthermie-Feld), führte jedoch zu einer dreifachen Reduktion der Treibhausgasemissionen. Hinsichtlich des Systembetriebs wurde die entwickelte MPC-Strategie mit einer standardmässigen regelbasierten Steuerung (Rule Based Control – RBC) verglichen. Die MPC nutzte den thermischen Speicher erfolgreich, um die Wärmeerzeugung vom Stromverbrauch zu entkoppeln, was zu einer Reduktion der Betriebskosten um 4,2 % führte. Es wird jedoch erwartet, dass diese Einsparungen höher ausfallen, wenn die Modelle des Optimierers und des digitalen Zwillings gut aufeinander abgestimmt sind. Entscheidend ist, dass die MPC die Interaktion des Systems mit dem Stromnetz optimierte und den Netzflexibilitätsfaktor um 33,8 % verbesserte, indem Lasten effektiv weg von Zeiten mit Spitzenpreisen verschoben wurden.

Zusammenfassend lässt sich sagen, dass SolHOOD erfolgreich ein Open-Source-Framework für die Energiesystemoptimierung entwickelt hat. Die Ergebnisse zeigen, dass sich durch die Optimierung des Systemdesigns und die prädiktive Regelung die wirtschaftliche Leistung und die Netzflexibilität von Quartiersenergiesystemen signifikant verbessern lassen, was den Weg für eine nachhaltige Energiewende ebnet.

Résumé exécutif

Afin d'atteindre l'objectif de décarbonisation, la stratégie énergétique de la Suisse envisage une électrification significative du chauffage des bâtiments. De plus, l'électrification prévue de la mobilité aura également un impact substantiel sur la demande d'électricité, particulièrement durant les mois d'hiver lorsque les émissions du réseau sont les plus élevées. Il est donc impératif de limiter au minimum la croissance de les demandes d'électricité et d'énergie en hiver dans le secteur du bâtiment. Outre d'autres mesures, comme l'amélioration constante de l'enveloppe des bâtiments, cela nécessite la mise en œuvre de systèmes d'approvisionnement en chaleur hautement efficaces et leur intégration intelligente dans des systèmes multi-énergies, exploitant ainsi les synergies entre les secteurs thermique et électrique. La plupart des systèmes de chauffage installés récemment reposent sur des pompes à chaleur utilisant l'air ambiant ou le sol comme sources de chaleur renouvelable, chacune ayant ses propres désavantages. Cela souligne la nécessité d'améliorations et d'alternatives à ces systèmes de chauffage. La recherche de solutions alternatives est plus complexe dans les quartiers densément peuplés que pour les bâtiments individuels isolés. Toutefois, l'échelle du quartier offre les occasions d'utiliser des synergies, par exemple via des équipements partagés de transformation et de stockage d'énergie. Dans ce contexte, le projet SolHOOD a poursuivi trois objectifs principaux : (1) développer des méthodes de planification intelligentes pour obtenir des systèmes d'approvisionnement énergétique (chaleur et électricité) performants pour les quartiers, en faisant un usage optimal des ressources d'énergies solaires et en utilisant les synergies de couplage sectoriel ; (2) Fournir des alternatives aux systèmes standards de pompes à chaleur aérothermiques et géothermiques, avec une faible demande en électricité du réseau en hiver à l'échelle du quartier ; et (3) Développer un système innovant de gestion avancée de l'énergie (AEM) basé sur la commande prédictive par modèle (MPC) pour optimiser le fonctionnement de systèmes énergétiques complexes dans les quartiers. Ces trois objectifs visent à décarboniser les systèmes d'approvisionnement énergétique de la Suisse, réduire la consommation d'électricité hivernale et la demande de pointe, offrir une plus grande flexibilité au réseau et utiliser efficacement les toits et façades pour la production de l'énergie solaire. Pour atteindre ces objectifs, le projet a étendu le cadre d'optimisation open-source basé sur Python ≪ optihood ≫. Ce cadre a été appliqué à un quartier représentatif en Suisse pour évaluer et comparer des conceptions de systèmes optimaux ayant des rendements d'énergie solaire élevés. De plus, le cadre a été appliqué à deux études de cas illustrant une variété de configurations de conception de systèmes et de résultats, démontrant ainsi l'efficacité de la méthode développée sur des cas réels. En outre, le cadre développé a été également utilisé pour contrôler un système de chauffage urbain afin de quantifier les avantages de l'utilisation d'une commande intelligente basée sur la commande prédictive par rapport à une commande standard basée sur des règles.

Concernant la conception de système, le cadre a révélé que les solutions centralisées hybrides surpassent souvent les approches décentralisées standard. Pour un quartier de bureaux représentatif à Zurich, un réseau de chauffage urbain centralisé à haute température alimenté par des pompes à chaleur et des capteurs solaires thermiques a été identifié comme étant à la fois l'optimum économique et environnemental. Comparée à une alternative standard de pompes à chaleur géothermiques décentralisées, cette configuration a permis une réduction de 18 % des coûts totaux annualisés tout en maintenant des niveaux d'émissions comparables. Dans l'étude de cas résidentielle Eco-Thierrens, les résultats ont mis en évidence le compromis entre les objectifs économiques et environnementaux : atteindre l'optimum environnemental nécessitait une augmentation de 20 % de l'investissement (pour des batteries électriques et une capacité solaire thermique accrue) mais a permis une réduction par facteur de trois des émissions de gaz à effet de serre. Concernant le fonctionnement du système, la stratégie MPC développée a été comparée à une commande standard basée sur des règles (RBC). Le MPC a utilisé avec succès le stockage thermique pour découpler la production de chaleur de la consommation d'électricité, résultant en une réduction de 4,2 % des coûts opérationnels. De manière cruciale, le MPC a transformé l'interaction du système avec le réseau, améliorant le facteur de flexibilité du réseau de 33,8 %, déplaçant efficacement les charges hors des périodes de tarification de pointe.

En conclusion, SolHOOD a développé avec succès un cadre open-source pour l'optimisation des systèmes énergétiques. Les résultats démontrent que grâce à l'optimisation de la conception du système et à la commande prédictive, la performance économique et la flexibilité du réseau des systèmes énergétiques de quartier peuvent s'améliorer de manière significative, ouvrant la voie à une transition énergétique durable.

List of abbreviations

AEM	Advanced Energy Management
ASHP	Air-Source Heat Pump
CF	Carbon Footprint
CHP	Combined Heat and Power
COP	Coefficient Of Performance
DH	District Heating
DHW	Domestic Hot Water
FPC	Flat Plate Collector
GHG	Greenhouse Gas
GSHP	Ground-Source Heat Pump
GWP	Global Warming Potential
HP	Heat Pump
KPI	Key Performance Indicator
LCOH	Levelized Cost Of Heat
MILP	Mixed-Integer Linear Programming
MPC	Model Predictive Control
oemof	Open Energy Modelling Framework
PV	PhotoVoltaic
PVT	PhotoVoltaic-Thermal Solar Collector
RBC	Rule-Based Control
RC	Resistance - Capacitance
SH	Space Heating
SOC	State of Charge
STC	Solar Thermal Collector

1 Introduction

1.1 Context and motivation

Around 100 TWh, which represents 45 % of Switzerland's final energy consumption, can be attributed to the building stock. Approximately 75 % of this energy is utilized for heating purposes. At present, three-quarters of this energy is derived from fossil fuels. In order to achieve the goal of decarbonization, the Swiss Energy Strategy envisages a significant electrification of the heating sector. The planned electrification of mobility will also have a significant impact on electricity demand, particularly during the winter months, when grid electricity emissions are at their highest. This effect was estimated in a recent study by EMPA as shown in Rüdisüli et al. (2019). The results demonstrated that, in the event of the closure of nuclear power plants and with an installed photovoltaic capacity of 26.5 GWp, along with 75 % electrification of the heating sector and 20 % of transport, there would be a four and a half times greater deficit in electricity than the current level. Furthermore, over 70 % of this deficit would occur during the winter months (see Figure 1). This deficit would have to be covered by electricity imports, which already have a considerable impact on the CO_2 intensity of the Swiss electricity mix in winter, as documented in the EcoDynBat project[1]. As a result, the overall CO_2 emissions are hardly reduced in such a scenario. It is therefore imperative to limit the increase in the winter electricity and energy demand of the building sector to a minimum. Besides other measures, like the consistent improvement of building envelope, this requires the implementation of highly efficient heat supply systems and their smart integration into multi-energy systems, thereby exploiting the synergies between the thermal and electrical sectors.

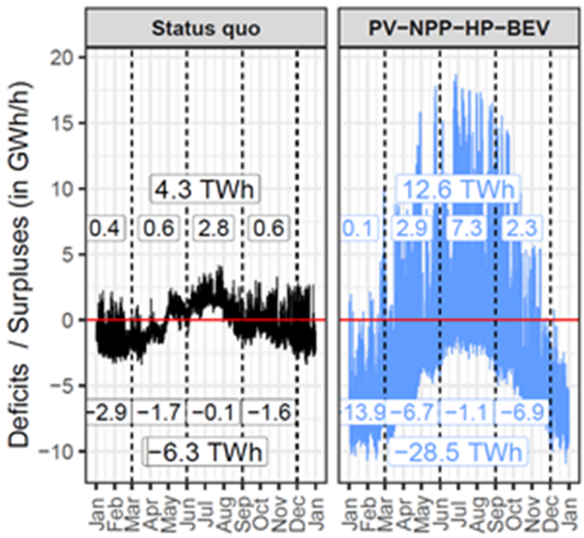

Figure 1: Deficits and surpluses in Switzerland's electricity supply, on the left for the status quo and on the right for a scenario without nuclear power plants, with 26.5 GWp PV, 80 % electrification of the heating sector and 20 % electric mobility. Source: Rüdisüli et al. (2019)

Most recently installed heating systems rely on heat pumps that use ambient air or ground as a renewable heat source. However, each of these variants are subject to certain shortcomings. Air source heat pumps have poor efficiency (high electricity consumption) in winter due to lower ambient temperatures. Furthermore, their operation can cause noise disturbances which can lead to social acceptance issues. Geothermal heat pumps offer high efficiency even in winter, but their installation costs are higher. Moreover, their installation is often restricted by water protection laws and the necessary space to drill boreholes can make them difficult to fit into

[1] https://www.aramis.admin.ch/Default?DocumentID=68220&Load=true

densely built-up areas. In addition, in areas with a high density of boreholes, the ground has to be regenerated by an additional heat source, which increases the system cost. This highlights the need for improvements and alternatives to these heating systems.

The search for alternative solutions is more challenging in densely built-up neighborhoods than in isolated individual buildings. This is due to the limited available area for solar installations. However, the neighborhood scale offers opportunities to utilize synergies, for example via shared energy transformation and storage units.

1.1.1 Purpose of the project

Solar energy technologies (thermal, photovoltaic, and PVT) are expected to play a significant role in the context of efficient heat supply solutions at the neighborhood scale. Solar heat can be used directly or serve as the source for a heat pump, for instance in conjunction with low-temperature (ice) storage units. Due to its ability to provide both heating and electricity, PVT has potential synergies with sustainable combined heat and power systems (with renewable fuels) that allow substituting grid electricity with own-produced low-carbon electricity during winter. Based on such synergies in connection with centralized or distributed storage systems, high-performance solar neighborhoods can be designed. However, an important prerequisite for this is the availability of suitable modelling and planning tools. A review on system modeling tools revealed a lack of usable tools for the neighborhood scale. Those that exist are difficult to use and further develop, because they are either developed within companies and hence disconnected from the open source community, or based on a commercial software (proprietary code). Nevertheless, some interesting collaborative platforms for the development of multi-energy systems exist, such as the Python-based "oemof". The project partners, SPF and IGT, previously collaborated on the development of an energy system optimization framework based on "oemof" within the project OPTIM-EASE[2], where the goal was to optimize the energy supply of building clusters connected electrically. SolHOOD has adopted to continue this development, while extending the optimization framework with additional features and tools necessary for answering the specific questions related to high solar fraction neighborhoods including thermal and electrical networks.

As stated previously, the transition to a low-carbon energy system needs support from modelling to find realistic pathways – technically and economically. The urgency has become very clear with the Paris Agreement, and if we aim at staying well below a temperature rise of 2 °C, there will only be a very tight carbon budget. Scenarios for Switzerland in 2050 already consider that CO_2 emissions will have to be negative by then. However, the transition path speed will have to be much faster than the current speed of changes if we want to achieve these ambitious goals. Decisions that affect the share of renewables in energy systems and the integration of new technologies for efficiency improvement are often taken at a regional/local level by local stakeholders. Planning tools such as the one proposed in SolHOOD will shorten the time it takes from analysing possible options to informing planners for implementing carbon free energy supply solutions. In particular SolHOOD will accelerate the growth and faster uptake of solar technologies and thermal storage solutions and their efficient use through flexibility options and sector coupling in the Swiss energy system. At the current stage, our main target stakeholder group are decision makers on the energy planning. However, the developed tools could be used in mid future for supporting policy makers to gain the necessary insights for implementing efficient policies with particular emphasis in the solar thermal field. Additionally, the choice of system configuration in the planning phase has a significant impact on the grid-electricity consumption. A well-designed combination of solar and storage systems could lead to a reduction in this consumption, which could support grid flexibility. In light of the growing competition between solar thermal and photovoltaic (PV) technologies for available roof space, particularly in the context of Switzerland's projected large-scale PV deployment in the future, PVT technologies will be of importance. With PVT, the collector output can almost double depending on whether the application is direct DHW heating or regeneration of geothermal probes (a source for heat pumps).

The consideration of energy systems on a neighborhood scale also presents opportunities regarding their operation strategies. With the help of smart control strategies, neighborhoods can achieve a high flexibility in terms of reaction to price and carbon footprint (CF) fluctuations. Model predictive control (MPC) algorithms

[2] https://www.aramis.admin.ch/Beteiligte/?ProjectID=48239

are a promising method, which will be applied and further developed in this project. MPC has been identified as a very powerful tool to activate energy flexibility and optimize system operation. MPC projects the behavior of the system in the future, and accordingly optimizes the system operation over a certain control horizon, for instance storing energy at times where it is more profitable, and releasing it later when needed. The lack of dynamics and anticipation of conventional Rule Based Controls (RBC) are therefore clearly surmounted by MPC. For individual buildings, MPC approaches outperform RBC in terms of annual operation cost, efficiency and comfort. The tools for implementing such advanced energy management (AEM) strategies will be closely related to the tools developed for the system design optimization.

The methods developed in SolHOOD, therefore, will benefit the planning process and the setup of operation strategies for newly-built neighborhoods and refurbishment projects. Figure 2 illustrates the importance of the planning phase in the development of a project. Small additional efforts in the planning phase potentially lead to great reductions in cost and environmental impacts, since planning essentially involves the initial assessments and decision making. In contrast, during the construction and operation phases, changes to the energy system and AEM will be more time-consuming and costly, with lower benefits.

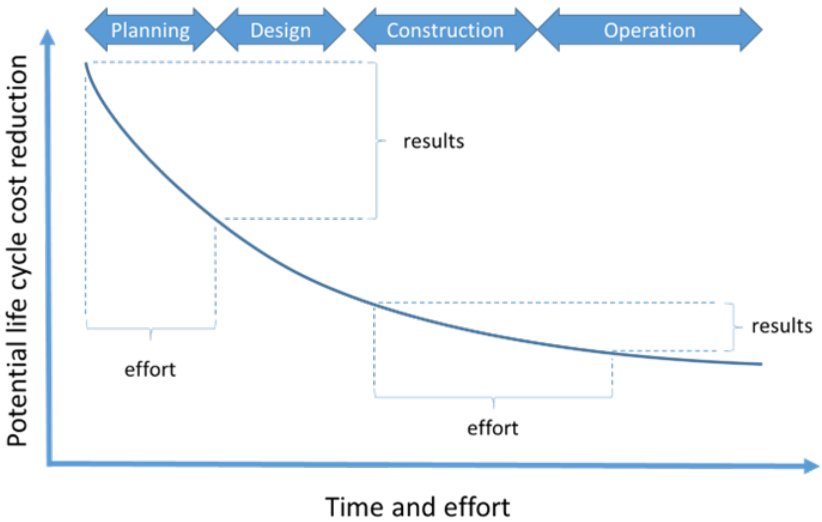

Figure 2: Potential life cycle cost reduction during the development phase of a project in relation the time and effort to achieve each phase.

1.1.2 Review on existing modelling tools

A lot of work has been conducted across Europe on the modelling of energy systems. The used models consider different sectors (electricity, heat, transport, gas, etc.) and their interdependence. The main differences between those models lie in the spatial resolution (EU, national, regional) and the temporal scales (from minutes to years). The selection of these key aspects depends on the type of questions one wants to answer. For the very large spatial scale (EU) as well as for the medium-scale (country), there exist many packages, most of them based on MILP optimization. Some of the examples are TIMES (and all its variants customized for individual countries, TIMES-DK, TIMES-PT, or for Europe JRC-EU-TIMES), Balmorel, EnergyPlan, Dispa-SET, EnergieScope, Calliope. Most of these models are meant to be used to create and analyze scenarios with a large projection on time. They offer the possibility to solve with more or less detail all energy sectors with a tendency to treat the heating sector in a similar way to electricity, i.e. simplified to the degree of being independent of temperature levels. Moreover, the spatial resolution targeting a large region does not usually allow to easily consider several units of the same type, i.e. these models consider that the whole country uses one single unit such as seasonal storage, heat pump, etc. This degree of simplification of the problem makes these tools unsuitable for the neighborhood scale, in which we are interested. Other open source tools exist that target specific energy sectors. For example, pandapower and PyPSA are python-based tools for power system modelling, analysis and optimization. A similar tool to pandapower called pandapipes, was developed to solve stationary and quasi-stationary gas and district heating sectors. However, these tools were not developed to consider sector-coupling in an easy way and thus, are not suitable for our needs.

What is needed for the neighborhood scale is an energy modelling framework that would allow consideration of an energy system in a more detailed manner. In this regard, the number of existing open source frameworks is much lower, and they usually have a very small user community, which strongly limits their collaborative development and the availability of good documentation. Existing simulation frameworks at the neighborhood scale that we know of are described in the following paragraphs.

CitySim is an urban energy modelling tool that considers the simulation scene as a complex urban environment, where the energy fluxes interact with each other. Several works that present the main features of the tool are published, as well as the physical model behind it. However, the model is not shared in GIT openly, so it does not seem possible to extend/improve the models and the whole framework used and thus, it does not fulfill our requirements. Moreover, CitySim focuses on the modelling of the building physics to predict their energy demands, which is of lesser interest in this project.

The Holistic Urban Energy Simulation (HUES) is an open-source framework of computational resources to support distributed energy system design and control. This platform is composed of a bunch of models that cover very different aspects, components and models written in many different languages and by different people, from PhD students to established researchers. Thus, it is very difficult to know what can be used and how to link all these individual packages.

The HUES platform also offers the Ehub Modeling Tool, an open-source tool for optimizing the design and operation of distributed multi-energy systems at the level of buildings and districts. It consists of a set of Matlab scripts for creating, executing and visualizing the results of an energy-hub model for a given case study and a set of technologies using Aimms. The fact that Ehub depends on Matlab and Aimms, two commercial softwares, is already a big barrier. Moreover, the main developers run a company called Sympheny that further develops the concept within the company. Thus, following this path would not be an alternative as well since no more developments and support could expected in near future.

The FINE python package provides a framework for modelling, optimizing and assessing energy systems based on pyomo. With the provided framework, systems with multiple regions, commodities and timesteps can be modelled. Target of the optimization is the minimization of the total annual cost while considering technical and environmental constraints. However, the model descriptions were not easily found in the documentation.

Open Energy Modelling Framework (OEMOF) is a framework for energy systems that addresses current and future challenges in energy system as it can be cross-sectoral, multi-regional, time-step-flexible, modular, open-source and community-driven. OEMOF is not a model in itself but provides a framework based on pyomo from which libraries can be based on. For example the library oemof.thermal accounts for thermal energy components and DHNx for district heating network optimization. The oemof.thermal considers only four components that could be theoretically reused by us. However some are way to simplified (Carnot efficiency with fix efficiency reduction for a heat pump) and many others such as PVT, seasonal sensible and latent (ice) storages or heat sources such as ground are not available. Thus, it is clear that further extensions will be necessary for it to be usable for us.

From our perspective, both CitySim and HUES were not found useful to answer the research questions of SolHOOD. This is because we cannot further develop them, and would therefore be limited to what already exists within these tools. The two open-source frameworks based on pyomo, FINE and OEMOF, presented interesting alternatives. OEMOF, being community-driven, well-documented and actively-maintained, was chosen as a basis to develop the optimization framework (co-developed within OPTIM-EASE project) which will be used within this project.

1.2 Project objectives

The overarching objectives of the SolHOOD project are to develop:

Obj. 1 Smart planning methods to achieve high-performance energy supply systems (heat and electricity) for neighborhoods, making optimal use of solar energy resources and using sector coupling synergies.

Obj. 2 Alternatives to standard air and ground source heat pump systems, with low grid electricity demand in winter at the neighborhood scale.

Obj. 3 Innovative advanced energy management (AEM) system based on model predictive control (MPC) to optimize the operation of complex energy systems in neighborhoods, using forecasts of the electrical and thermal demands, weather data, dynamic electricity tariffs and environmental impacts of grid electricity.

These three goals aim to decarbonize Switzerland's energy supply systems, reduce winter electricity consumption and peak demand, provide greater grid flexibility and make efficient use of roofs and facades for solar energy harvesting. They will be measured against the following Key Performance Indicators (KPI):

- Obj. 1 provides a method for finding optimal solutions and quantifying their advantages over more conventional solutions. This benefit is qualitative and no target value can be set for it. The goal is reached, if the developed methods are operational and can be usefully applied to real case studies.
- The benchmarks for Obj. 2 in terms the KPIs to be defined (e.g. seasonal performance factors at neighborhood scale) will be the reference solutions with air and ground source heat pumps. Alternative solutions have to be found, that reach at least competitive performance values.
- The benchmark for Obj. 3 is based on results from existing MPC solutions for heat pump systems. Compared with standard rule based approaches, not reacting to external electricity price signals, they should allow to lower energy costs by 15%. At least similar cost reductions should be reached at the neighborhood scale. The potential of the AEM for reducing CO2 emissions and improving grid flexibility will be evaluated in the course of the project.

2 Approach and methodology

The methodology followed in SolHOOD is based on using optimization tools for planning, design and operation. A holistic approach is adapted, such that tools used for planning can be reused with small modifications for real operation. Both, planning and operation are foreseen to be approached with optimization algorithms. The way to use them, i.e. the target functions (e.g. in operation strategies investment costs are not important anymore) and time horizons differ. Thus, a well-thought development of the framework is necessary, in order to maximize synergies of design/planning and operation strategies. The optimization tools will be based on mixed integer linear models (MILP). The methodology to achieve the final goals is the following.

The overall boundary conditions (energy demands, weather data, etc.) for the problems to be solved will be defined. For these, "typical" neighborhoods as well as KPIs with special emphasis on grid flexibility and dynamic consideration of the CO_2 emissions of the electricity grid will be identified.

An existing simulation framework will be further developed and extended, where planning and operation will be considered. The simulation framework will consider pre-processing and post-processing of data. Using the extended framework, the optimization studies will be carried out on the identified reference neighborhoods in order to find optimal configurations of energy systems as a function of specific targets, focusing on environmental impact, grid flexibility and cost. Finally, the framework developed will be adapted to solve operational strategies using Model Predictive Control (MPC). The idea is that the models used for the MPC will be the same but the approach to use them will be different. At operational level, typically a one-to-two-day time horizon will be simulated, and optimizations will be carried out every 15 or 30 minutes to take control decisions. These MPC models will be coupled with TRNSYS which will emulate the real system in a co-simulation framework developed in python. This coupling is the first step to developing an MPC that can later be implemented in a real controller, since it does the same functions of acting on specific devices such as valves, pumps, and manages heat pump operation.

The developed frameworks will be applied to real situations, by considering two case studies, in order to analyze the potentials, practicability, and usability of the proposed methods. The case studies are mainly intended to test the powerfulness of the tools. Recommendations and lessons learned will most of all be beneficial to similar future neighborhood developments. Nevertheless, recommendations for minor adaptations of the system design as well as recommendations regarding the system operation might already flow into these concrete projects.

2.1 Optihood framework

Optihood is an open-source optimization framework developed within the project OPTIM-EASE[3], based on the python package oemof (**o**pen **e**nergy **mo**delling **f**ramework) presented by Hilpert et al. (2018), for the modelling and optimization of energy systems. Using oemof, one can define energy systems as combinations of linear component models namely, energy sources, sinks (or demands), transformers (conversion technologies) and storages. Furthermore, buses (representing energy flows) are used to connect these different components together. Oemof then formulates a MILP (mixed-linear integer programming) optimization problem with a set of decision variables, parameters, optimization constraints and target, using pyomo, an open-source optimization modelling language. This optimization problem, in turn, can be solved with a number of different solvers. Currently, we use the commercial solver gurobi, which offers a free academic license. Other solvers like cbc, glpk, etc. which are supported by pyomo, may be used as well. In the context of an optimization problem, the objective is to identify a solution within a defined region of the parameter space (specified by a set of constraints) that minimizes or maximizes a target function. The target function could relate to costs, CO_2 emissions or energetic efficiency, as an example. The optihood framework extends oemof by defining energy systems for groups of buildings, where each building could have a set of components. Therefore, the basic construct of oemof is modified in a sense that the components (sources, transformers, storages and

[3]https://www.aramis.admin.ch/Beteiligte/?ProjectID=48239

sinks) are assigned and grouped by buildings and the results (time-series of energy production/consumption, costs, emissions, etc.) can be obtained per building. Moreover, optihood enables a simplified definition of the optimization scenario/problem using either a configuration (or config) text file or an Excel file. Within this project, we have used and further extended the optihood framework. Furthermore, Optihood was published as an open-source python package on GitHub[4], together with an online documentation available on ReadTheDocs[5].

Formulation of an optimization problem

The first step when formulating an optimization problem is to define the scenario (available components, inputs, parameters, etc.) for optimization. The optimization scenario defines all the available components (sources, sinks, storages and transformers), their parameters (e.g. tilt of PV panels), and the connections between them (for e.g. PV can supply electricity to a heat pump). Optihood uses either a configuration (or config) text file or an Excel file as an input to define this scenario. Therefore, all the possible energy conversion/storage technologies, resources and the buildings to which they belong should be listed within this input file. This input file also specifies a few basic optimization constraints such as the minimum/maximum allowed capacities of a component. Furthermore, several additional properties for different component models are also defined within this file, for example efficiencies, cost/emission assumptions, etc.

Optimization

The optimization procedure uses a predefined, but not necessarily constant, time resolution. All the input time-series data such as the weather and the energy demand profiles need to be provided in the specified time resolution. The space heating demand of a building could be presented either as a fixed profile or modelled dynamically using a linear RC (Resistance - Capacitance) building model implemented within the framework. The optimization then tries to match the available energy resources to the demands in each hour (using energy conversion and storage technologies). If it fails to do so, the problem is declared as infeasible and an error message is displayed. Optihood offers two modes for optimization. In the *dispatch mode*, the capacities of the components are fixed, and the optimizer tries to find the optimal scheduling of their operation, which minimizes the target function, e.g. costs. In the *investment mode*, the optimizer, in addition to optimizing operation, also finds the capacities of the components that minimize the target function. This mode is suitable for determining the optimal choice between alternative technologies while sizing the selected components.

It is further possible to run a multi-objective optimization, i.e. where one tries to minimize two or more target functions at once, and to find the corresponding Pareto front, with the help of the epsilon constraint method. If, for instance, the two target functions are costs and CO_2 emissions, the procedure is as follows. First, the optimizer executes separately a cost optimization and a CO_2 emission optimization. These two results provide the end points of the Pareto front, the case with the minimum cost and the one with minimum carbon footprint. The resulting domain is then resolved successively by a number of cost optimizations while constraining the CO_2 emissions to different values between the values at the end points.

2.2 Extensions to optihood within this project

The optihood framework was extended and improved, in order to realize the goals of this project. The following subsections describe the extensions made with respect to different types of components in optihood.

2.2.1 Energy conversion technologies

This section described the energy conversion technology models implemented within optihood for this project. The models for other technologies, including PV, were already implemented in the framework (documentation available[6]).

[4] https://github.com/SPF-OST/optihood
[5] https://optihood.readthedocs.io/
[6] https://optihood.readthedocs.io

Solar thermal collector (STC)

The model for solar thermal collector was based on the flat plate collector module in oemof.thermal package[7]. The total irradiance on the collector plane is obtained using pvlib (Holmgren et al. (2018)) based on the azimuth and the tilt angle of the collector.

The thermal output $\dot{Q}$ of a flat plate thermal collector can be determined based on the incident solar irradiation $(G \cdot A)$, the ambient air temperature (T_{amb}) and the mean temperature of the collector fluid (T_m), as expressed by the following equation:

$$\frac{\dot{Q}}{A} = G \cdot \eta_o - a_1(T_m - T_{amb}) - a_2(T_m - T_{amb})^2 \tag{1}$$

where, A is the gross area of the collector surface, η_0 is the nominal efficiency of the collector, a_1 is the linear heat loss coefficient and a_2 is the quadratic heat loss coefficient of the collector.

The efficiency of collector η_c can, therefore, be calculated as:

$$\eta_c = \frac{\dot{Q}}{G \cdot A} = \eta_0 - a_1 \cdot \frac{(T_m - T_{amb})}{G} - a_2 \cdot \frac{(T_m - T_{amb})^2}{G} \tag{2}$$

here, $(T_m - T_{amb})$ could be expressed as $T_{c,in} + \Delta T_n - T_{amb}$. $T_{c,in}$ and ΔT_n denote the collector inlet fluid temperature, and the temperature difference between the collector's mean and inlet fluid temperatures, respectively.

Therefore, depending on a given inlet fluid temperature $T_{c,in}$, we can obtain different collector efficiencies depending on the chosen ΔT_n. The collector's heat output is then calculated based on the following relation:

$$\dot{Q} = \eta_c \cdot G \cdot A \tag{3}$$

The label *SolarCollector* was added to the energy conversion technology processing function in optihood, to allow the definition of a STC in the input scenario Excel/config file.

Heat pump (HP) model

The performance of heat pump was modeled using a bi-quadratic polynomial fit of the condenser heating power $\dot{q}_c$ and the electrical power consumption of the compressor $\dot{w}_{cp}$ as proposed by Afjei and Wetter (1995).

$$\begin{aligned} \dot{q}_c &= bq_1 + bq_2 \cdot \bar{T}_{e,in} + bq_3 \cdot \bar{T}_{c,out} \\ &+ bq_4 \cdot \bar{T}_{e,in} \cdot \bar{T}_{c,out} + bq_5 \cdot \bar{T}_{e,in}^2 + bq_6 \cdot \bar{T}_{c,out}^2 \end{aligned} \tag{4}$$

$$\begin{aligned} \dot{w}_{cp} &= bp_1 + bp_2 \cdot \bar{T}_{e,in} + bp_3 \cdot \bar{T}_{c,out} \\ &+ bp_4 \cdot \bar{T}_{e,in} \cdot \bar{T}_{c,out} + bp_5 \cdot \bar{T}_{e,in}^2 + bp_6 \cdot \bar{T}_{c,out}^2 \end{aligned} \tag{5}$$

where $T_{e,in}$ is the fluid inlet temperature in the evaporator and $T_{c,out}$ the fluid outlet temperature in the condenser. The normalized temperature $\bar{T}$ is defined as $\bar{T} = T$ [°C]/273.15. The polynomial coefficients

[7] `https://oemof-thermal.readthedocs.io/en/latest/solar_thermal_collector.html`

bq_i and bp_i are calculated from the catalog heat pump data using the multidimensional least square fitting algorithm of Scipy (Jones et al. (2001)) in Python.

The condenser fluid outlet temperature $T_{c,out}$ was fixed to 35 °C for space heating and to 65 °C for domestic hot water production to approximate and interpolate the datasheet values. This bi-quadratic polynomial fit model defined by Eqs. (4) and (5) was implemented within optihood for both air-source and ground-source heat pumps. In case of an air-source heat pump (ASHP), $T_{e,in}$ represented the ambient air temperature, while it would denote the ground temperature for ground-source heat pump (GSHP). The fitted coefficients, bq_i and bp_i, for the ground-source and air-source heat pumps are given in Appendix A. In the present implementation of GSHP, the ground source is highly simplified and implemented as a temperature profile with sinusoidal seasonal variation (Appendix A).

The heat pump model, in the optihood framework, therefore was implemented with a single required input energy flow ($\dot{w}_{cp}$) and a single required output flow (produced heat or $\dot{q}_c$). The output heat flow was calculated based on the input electricity flow and the COP (calculated using Eqs. (4) and (5)).

$$\dot{w}_{cp} = \frac{\dot{q}_c}{COP} \tag{6}$$

In addition to the required input energy flow ($\dot{w}_{cp}$), the heat pump model also supports the definition of an optional second input energy flow to represent the low temperature heat source on the evaporator side of the HP. This enables a simplified representation of a low-temperature thermal grid with decentral HPs within the optihood framework. The magnitude of the low temperature heat input of the heat pump, $\dot{q}_e$, is evaluated based on the law of energy conservation:

$$\dot{w}_{cp} + \dot{q}_e = \dot{q}_c \tag{7}$$

Furthermore, the heat pump model could also have more than one output heat flows at different temperature levels or $T_{c,out}$, with a different COP for each temperature level. In reality, a heat pump could produce heat at only one temperature level at a time. However, since we consider an hourly timestep within simulations, the heat pump model could produce both space heat (at 35 °C) and domestic hot water (at 65 °C) within the same timestep. In reality, this would mean that within one hour, the heat pump could produce heat at two different temperature levels (but not at the same time).

The labels *ASHP* and *GSHP* were added to the config-file/excel-file-processing function in optihood, in order to interpret them as air-source and ground-source heat pumps, respectively, during the formulation of optimization problem. This would enable the user to specify the technology label as *ASHP* for example, in the input scenario file, to use the air-source heat pump model.

PVT collector model

`PVT` class was implemented within the energy converters module in optihood. The collector output is modelled based on the characteristic curve model reported in the SwissEnergy-sponsored project PVT Wrap-Up (Zenhäusern et al. (2017)). The thermal output of a PVT collector, $\dot{Q}$, highly depends on the surrounding environment and the operating conditions. The most significant influencing factors are the solar irradiation per collector surface area (G), ambient air temperature (T_{amb}) and the mean temperature of the collector fluid (T_{m}). The characteristic equation for the thermal output of the PVT collector resembles that of a flat plate collector (see Eq. (1)), but includes an additional term to account for the electrical power output:

$$\frac{\dot{Q}}{A} = \left(G - \frac{P_{el}^{DC}}{(\alpha\tau)\cdot A}\right)\cdot\eta_o - a_1(T_m - T_{amb}) - a_2(T_m - T_{amb})^2 \tag{8}$$

Here, the additional term $\frac{P_{el}^{DC}}{(\alpha\tau)\cdot A}$ accounts for the electrical output of the PV cells, effectively reducing the solar irradiance available for the generation of thermal energy. P_{el}^{DC} stands for the DC electrical output of the collector and $(\alpha\tau)$ is the transmission absorption product of the collector.

A corresponding label *PVT* was added to the energy conversion technology processing function, to allow the definition of a PVT collector in the input excel/config file while preparing the optimization problem.

Electric heating rod to cover peaks

Electric heating rods were implemented as a back-up technology to cover the peaks in the space heating and domestic hot water demands (if needed). It was observed in some situations that in the absence of back-up electrical heating rods, the optimizer selects one centralized heat pump along with individual heat pumps (of very small capacities) in each building to cover peak load. Therefore, adding the option for electrical rods as a back-up could in such cases result in cheaper and more ecological (if we include embodied emissions) solutions. This was achieved by implementing a constraint that allows investment in electrical rods only as a back-up system when a heat pump is selected as the main technology. The constraint limited the total allowed capacity/size of electrical heating rods, to ensure that it does not exceed the total heating capacity of the installed heat pumps in the optimal solution.

$$\sum_{buildings} S_{el,rod} \leq \sum_{buildings} S_{ASHP} + \sum_{buildings} S_{GSHP} \tag{9}$$

where, $S_{el,rod}$, S_{ASHP} and S_{GSHP} are the installed capacities of electric heating rod, ASHP and GSHP, respectively, within a specific building in the optimal solution.

The label *ElectricRod* was included in the input scenario file processing function, to represent the electric heating rod technology (for covering peaks in demand).

2.2.2 Energy storage technologies

Layered thermal energy storage and discrete temperature levels

A discretized thermal energy storage with several predefined discrete temperature levels was implemented within optihood. In addition, the implementation of heat production technologies such as heat pumps, solar thermal collectors, etc. was extended to allow multiple output flows (at different temperature levels). The heat production technologies could have a predefined efficiency curve (hourly) related to each temperature level. As an example, the efficiency of solar collector would depend on the weather profile (irradiation and ambient air temperature), but also the temperature level at which the collector is providing output heat. The number of discrete temperature levels is parameterized and can be defined in the input scenario excel file.

A class `ThermalStorageTemperatureLevels` was developed to represent a discretized-multi-temperature-level thermal energy storage. This storage model is a combination of dual-temperature-zone storages from oemof.thermal python package (Hilpert et al. (2018)).The total storage volume V_{stor} was calculated as the sum of volumes of individual layers (v_i), as follows:

$$\sum_{i=1}^{n} v_i = V_{stor} \tag{10}$$

where n denotes the number of discrete temperature levels.

Furthermore, a constraint was developed to implement the following capacity rule on the total storage volume:

$$V_{stor,min} \leq V_{stor} \leq V_{stor,max} \tag{11}$$

where $V_{stor,min}$ and $V_{stor,max}$ represent the minimum and the maximum limits for the storage volume.

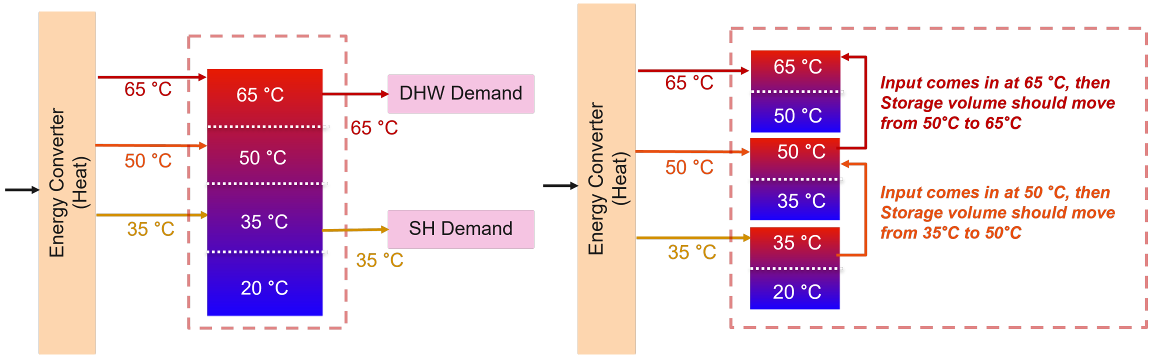

Figure 3: Graphical representation of a layered thermal energy storage model with four discrete temperature levels at 35°C, 50°C, 65°C and 20°C (return temperature).

Figure 3 shows a graphical representation of a layered thermal energy storage with four discrete temperature levels. The DHW demand is met using the topmost temperature level at 65 °C i.e. highest temperature, while the temperature level at 35 °C is used to cover the SH demand. As mentioned previously, each layer is modelled using the dual-temperature-zone storage model from oemof.thermal[8]. We implemented a rule for charging the multi-layer thermal storage which is also illustrated in Figure 3 on the right. The energy inflow at a given storage layer (except the lowest layer), equals the energy outflow from the preceding storage layer. Therefore, in order to supply thermal energy at 50 °C to the storage, the volume added at the 50 °C layer should be displaced from layer below, i.e. from the 35 °C layer. This means that the energy conversion technologies can heat water from 35 °C to 50 °C and from 50 °C to 65 °C, in that order. It should be noted that the temperature difference (ΔT) between the subsequent storage layers should be identical (in the example shown it is 15 °C).

Moreover, the dual-temperature-zone storages from oemof.thermal include predefined calculations for losses from the top/bottom and lateral surfaces. While the lateral surface losses are preserved for the storage layers at each temperature level, the top and bottom surface losses should only be considered for the topmost (i.e. at the highest temperature level) and the lowest (i.e. at the lowest temperature) layers. Moreover, the fixed one-time investment cost of the discretized thermal energy storage should be added to the objective function only once (instead of being added for each layer separately). These functionalities were implemented within the `ThermalStorageTemperatureLevels` class.

Ice storage

The `IceStorage` class was implemented within the storages module of optihood. The formulation of the ice storage model is based on the solution of the energy conservation law applied as per Carbonell et al. (2015). The equation is essentially the same as the energy conservation law for hot water storage with the inclusion of the latent heat term for ice formation $\frac{h_f}{V}\frac{\partial M_{ice}}{\partial t}$:

$$\rho c_p V \frac{\partial T_{stor}}{\partial t} = -(UA)_{tank} \cdot (T_{stor} - T_{amb}) + \frac{h_f}{V}\frac{\partial M_{ice}}{\partial t} + \sum_{i=1}^{n} \dot{Q}_{hx-port}(i) \tag{12}$$

where, ρ and c_p are the density and specific heat capacity of water, respectively. V is the storage volume, T_{stor} is the average temperature of water in the storage, T_{amb} is the ambient-air temperature, $(UA)_{tank}$ is

[8]https://oemof-thermal.readthedocs.io/en/latest/stratified_thermal_storage.html

the product of overall heat transfer coefficient and the external area of the storage tank, M_{ice} is the mass of ice and h_f the latent heat of fusion. $q_{hx-port}$ are the heat fluxes between the heat exchanger and the direct ports, and can be represented as:

$$\sum_i \dot{Q}_{hx-port}(i) = \sum_i \dot{Q}_{in}(i) - \sum_i \dot{Q}_{out}(i) \tag{13}$$

here $\dot{Q}_{in}$ and $\dot{Q}_{out}$ are the heat inflows and outflows to/from the ice storage tank, respectively.

The term for heat of solidification and melting appearing in Eq. 12 can be discretized as:

$$\dot{Q}_{lat} = h_f \frac{M_{ice}^{t+1} - M_{ice}}{\Delta t} \tag{14}$$

The complete discretized equation for ice storage model is, therefore, represented as:

$$\rho c_p V \frac{T_{stor}^{t+1} - T_{stor}^t}{\Delta t} = -(UA)_{tank} \cdot (T_{stor}^t - T_{amb}^t) + h_f \frac{M_{ice}^{t+1} - M_{ice}}{\Delta t} + \sum_{i=1}^{n} \dot{Q}_{hx-port}(i)^t \tag{15}$$

In order to solve this equation one can split the formulation in two parts. One considering only the sensible part where the $M_{ice} = 0$ kg and a second formulation for the latent part assuming $T = 0$ °C. The equation with ice formation is reduced to:

$$0 = (UA)_{tank} \cdot T_{amb}^t + h_f \frac{M_{ice}^{t+1} - M_{ice}}{\Delta t} + \sum_{i=1}^{n} \dot{Q}_{hx-port}(i)^t \tag{16}$$

In addition, the following constraints were implemented within the ice storage model. The constraint to set up the initial conditions such as initial storage temperature and initial ice fraction is given by:

$$\begin{bmatrix} T_{stor}^0 \\ f_{ice}^0 \end{bmatrix} = \begin{bmatrix} T_{stor}^{init} \\ f_{ice}^{init} \end{bmatrix} \tag{17}$$

The constraint defining the range of water temperature inside the storage (during the operation of ice storage) is given by:

$$0 \leq T_{stor}^i \leq 90 \quad \forall\, i \in t \tag{18}$$

The ice fraction, also known as ice packing factor, f_{ice}^t, is calculated as follows:

$$f_{ice}^t = \frac{M_{ice}^t}{M_{water,max}} \tag{19}$$

where, $M_{water,max}$ denotes the overall amount of water and ice in the storage tank.

The constraint on the maximum allowed value of f_{ice}^t within the storage is represented as:

$$f_{ice}^t \leq f_{ice,max} \tag{20}$$

Depending on the ice storage design, the value of $f_{ice,max}$ can be in the range of 0.5 to 0.8.

2.2.3 Energy demand

Building model

Within the optihood framework, energy demands are generally represented as fixed time-series profiles, for example for electricity, space heating and domestic hot water consumption. A building's space heating demand could also be represented dynamically using a resistance capacitance (RC) building model. This allows the optimizer to use the building's inertia to shift the space heating demand during optimizations. Since optihood uses a MILP formulation to define the optimization problem, all the optimization constraints as well as component models need to be linear. Therefore, the detailed and non-linear building models used in the simulation frameworks such as TRNSYS are not adequate in this case. A linear 3R3C (three-resistance-three-capacitance) model describing the thermal behavior of a building was implemented into the optihood framework to replace the static heating demand profiles. The schematic representation of the RC building model is given in Figure 4. The implemented building model has been proposed and validated by Péan et al. (2019).

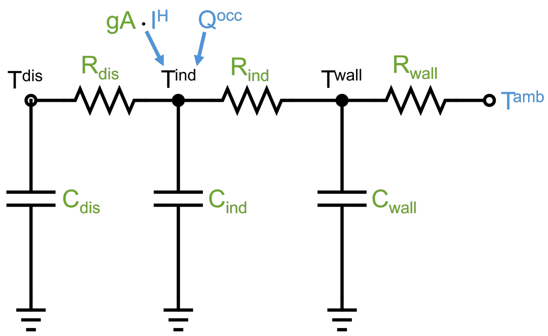

Figure 4: Schematic representation of the RC building model.

A building is characterized by three thermal elements: distribution system, walls (including building mass) and indoor air mass. Each element has two associated configuration parameters, thermal resistance (denoted by R) and thermal capacity (denoted by C). For example, the thermal resistance between the indoor air and the walls, and the thermal capacity of the indoor air mass are denoted as R_{ind} and C_{ind}, respectively. At a given time step, each thermal element is at a certain temperature, which results from the optimization. An acceptable comfort range needs to be defined for the indoor air temperature, beyond which the optimizer should not shift the heating demand. The weather data (ambient temperature and irradiation) and the internal gains due to occupancy serve as exogenous inputs to the model. The implemented building model is described further in Appendix A.

This 3R3C building model was implemented within the optihood framework by defining a new component class `SinkRCModel` and its associated constraint group. The default comfort range for indoor air temperature was defined as 19°C-23°C. These values can be modified, if needed. A new column "building model" was added within the demand sheet of the input scenario Excel file to specify whether the building model should be used by the framework during optimization. If set to 'Yes', the component class for RC building model is used. Otherwise, the framework uses fixed demand profiles for space heating.

A comfort violation indicator variable, ε_t^{ind}, was introduced to allow a (penalized) violation of the predefined comfort temperature range. This was done to reach optimization feasibility in unavoidable cases. The indoor comfort temperature rule is represented by the equation:

$$T_{min}^{ind} - \varepsilon_t^{ind} <= T_t^{ind} <= T_{max}^{ind} + \varepsilon_t^{ind} \tag{21}$$

where T_t^{ind} denotes the indoor air temperature (°C) at time t, and $[T_{min}^{ind}, T_{max}^{ind}]$ is the defined comfort temperature range.

In order to keep the indoor air temperature within the range $(T_{min}^{ind}, T_{max}^{ind})$ whenever possible, the value of ε_t^{ind} chosen by the optimizer should be as low as possible. To account for this, we introduced a penalty factor (δ) linked to ε_t^{ind} in the objective function of optimization. This penalty factor (δ) should be defined when formulating the optimization problem. As a general recommendation, the chosen δ should be considerably higher than the cost of providing heating energy to the building i.e. it is more expensive to violate the indoor temperature range than to provide the necessary heat to the building.

Furthermore, the building model class `SinkRCModel` allows both heating and cooling. Cooling is implemented as a possibility of heat rejection, for example by means of a chiller with a fixed efficiency. The building model currently does not implement user behavior and therefore, opening of windows if the rooms heat up too much in summer is not modelled. This could lead to a violation of the indoor air temperature range in summers, if there is no possibility for the building to reject heat. The state space equation corresponding to the heat distribution temperature of the building model, which reflects heating and cooling power, is given as:

$$C_{dis} \cdot \dot{T}^{dis} = \frac{1}{R_{dis}}(T^{ind} - T^{dis}) + Q_t^{heat} - Q_t^{cool} \tag{22}$$

where R_{dis} and C_{dis} denote the thermal resistance (in K/kW) and heat capacity (in kWh/K), respectively, of the heat distribution system. T^{dis} and T^{ind} are the temperatures of the heat distribution system and indoor air space, respectively, in °C. Q_t^{heat} and Q_t^{cool} represent the heating power and the cooling power (in absolute terms) of the distribution system, respectively, in kW at time t.

Fitting of building model parameters

In order to use the building model, it is essential to define its parameters, including the thermal resistances and capacities for each of the three thermal elements. The parameters R_{wall} and C_{wall} are dependent on the building's insulation properties and can therefore be calculated for a particular building. Among these parameters, $U_{building}$, the building's overall thermal transmittance (expressed in kW/K), exerts the most significant influence on the energy balance. It is defined by the following relation:

$$\frac{1}{U_{building}} = \frac{1}{U_{ind}} + \frac{1}{U_{wall}} \tag{23}$$

here, U_{ind} and U_{wall} denote the thermal transmittance of the indoor air mass, and of the wall and building mass, respectively.

A simplified fitting method was implemented to determine the U_{ind} parameter for a given building. This method utilizes the following equation to calculate the heating power, Q_t^{heat} (in kW), at time t:

$$Q_t^{heat} = U_{dis}(T^{dis} - T^{ind}) = U_{building} \cdot (T^{ind} - T^{amb}) - gA \cdot I_t^H - Q_t^{occ} \tag{24}$$

where T^{dis}, T^{ind} and T^{amb} denote the distribution system, indoor air mass and ambient air temperatures, respectively, in °C. The term gA represents the product of transmittance of glass, the lumped factor for considering window surfaces at different orientations, and the total aperture area of the windows in m^2. I_t^H and Q_t^{occ} are the total horizontal solar irradiation (kW/m^2) and heat gain from occupancy (people, electrical equipment, lights, etc.) in kW, respectively, at time t. U_{dis} is the thermal transmittance of the distribution system in kW/K.

The effective thermal transmittance of a building $U_{building}$ is determined by fitting the heating demand calculated by Eq. (24) to the actual heating demand of the building using the minimization method of Scipy (Jones et al. (2001)) in Python.

An approximation of the parameter C_{ind} can be derived from empirical values, scaled by the energy reference area of a given building. Similarly, R_{dis} and C_{dis} primarily depend on the type of distribution system, allowing for the use of empirical approximations.

All these model parameters need to be predefined and provided while formulating an optimization scenario.

2.2.4 Additional developments

Thermal and electrical links

In order to allow buildings to share electricity, space heat and domestic hot water production, a new `Link` component was implemented within optihood. Figure 5 illustrates a schematic representation of this component for space heating energy flows. The dashed lines denote the alternative connections (where buildings cannot share the produced space heat), in case the optimizer does not choose to connect a building to the link. The `Link` component connects all the relevant input/output flows of a specific type (electricity, space heat or domestic hot water) between the buildings, using the following relation:

$$\sum_{i=1}^{b}(E^f_{i,link} \cdot \beta^f_{i,link}) = \sum_{i=1}^{b} E^f_{link,i} \tag{25}$$

where, b denotes the number of buildings, $E^f_{i,link}$ is the energy flow from the building i to the link component for flow type f (e.g. space heating), $E^f_{link,i}$ is the energy flow from the link component to the building i for flow type f, and $\beta^f_{i,link}$ is a conversion factor (used to represent losses) between the building i and the link.

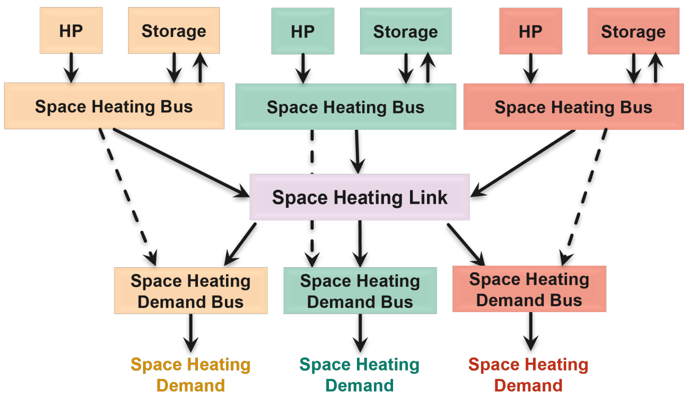

Figure 5: Schematic representation of the implementation of the space heating link between three buildings (each having a heat pump, a hot water storage and a demand sink). Each building is denoted by a different color (yellow, green and red)

The implementation of links, however, adds complexity to the optimization problem and as a result, affects the run-time. When the optimizer needs to decide whether to connect the buildings using links (and which ones to connect), each output of a link adds a binary variable to the optimization problem. This increases the computation time exponentially as the number of buildings (i.e. number of binary variables) and the types of links (electrical, space heating, domestic hot water) increase. In order to improve the optimization speed, an option to merge the respective buses or energy flows (electricity, space heating and domestic hot water) of all the buildings was added into the framework. Figure 6 presents an example with a merged space heating bus for the scenario with three buildings (shown earlier in Figure 5). This option can be used to perform optimization in two steps. In the first step, the implementation of links shown in Figure 5 is used, which allows the optimizer to select whether connecting the buildings is the best solution or not (although takes longer). Once it has been established that connecting the buildings is the best solution, the new option to merge buses (Figure 6) is used to produce additional optimizations results faster.

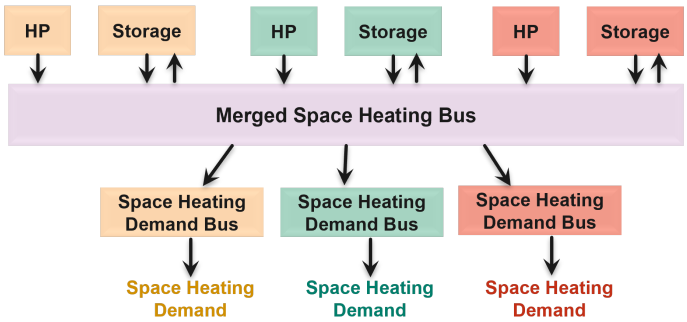

Figure 6: Schematic representation of the option to merge space heating buses of three buildings. Each building is denoted by a different color (yellow, green and red).

Input config file

We implemented an alternative to the existing Excel input file (see section 2.1) in order to simplify the formulation of an optimization problem. The Excel file offers a large degree of flexibility in problem formulation. As an example, the Excel input file could define different available technologies for different buildings, different parameters for a given technology in different buildings and provide various possibilities to connect the components together. However, as the number of buildings increase, formulating an optimization problem using an Excel file could become rather cumbersome and error-prone. For example, if each building has an identical list of available technologies, this would require the same row to be repeated over and over again for every building within the Excel file. In order to address this, a configuration (or config) text file was introduced as an alternative method (less flexible but more intuitive) to formulate an optimization problem.

In a config file, one could provide the same information as in the input Excel file but for a case where all the buildings have an identical setup (technologies, limits on capacities, cost assumptions, etc.). Figure 7 shows an example of a config file where grid electricity is used as a primary energy source and heat is produced using air-source and ground-source heat pumps (ASHP and GSHP). Each building would have the same available energy sources and technologies. Paths to the weather file, electricity impact and demand profiles are also specified within this config file. Moreover, the connections between energy sources, conversion and storage technologies and demands are fixed to default system connections (shown in Figure 8). Note that the specific connections would realize only when the corresponding technologies/sources/sinks are selected in the optimal solution. As an example, the connection between natural gas resource and CHP would be realized only if the optimizer chooses CHP as a solution within the optimization results.

A new method was implemented in optihood to read a config text file and produce the equivalent Excel input file based on the default system component connections. It is worthwhile to note that this method could still be used to prepare a first version of the Excel file even when the system components for all the buildings are not identical. The prepared Excel file could then be modified later on instead of creating it from scratch.

```
##############################################################
# CONFIG FILE TO CREATE THE INPUT SCENARIO EXCEL FILE  #
##############################################################

# NOTE: UNITS FOR ALL PARAMETERS ARE IN PER KW

[CommoditySources]
# Set True or False for each possible commodity source
# The sources which are set to True should have an associated secti
# Weather data path is also set here
electricityResource=True
naturalGasResource=False
WeatherPath=.\data\weather.csv

[electricityResource]
# CO2 impact and cost per kW should be defined here
# Either a constant value or a path to the time series could be def
Cost=0.204
Impact=.\data\electricity_impact.csv
FeedinTariff=0.09
```

```
[naturalGasResource]
Cost=0.087
Impact=0.228

[Demands]
# The program expects all the three demands (EL, SH and DHW) to be
# Path to demand profiles and whether demand profiles are fixed or
# Fixed is set to 0 if building model is used for space heating (1
# The path should contain all the demand profiles (all buildings)
Fixed=1
Path=.\data\profiles_noSH_summer_25DHW

[Transformers]
# Set True or False for each possible transformer (energy conversio
# The transformers which are set to True should have an associated
CHP=False
ASHP=True
GSHP=True
GasBoiler=False
ElectricRod=False
```

Figure 7: Example of a configuration file or config file for optimization problem definition.

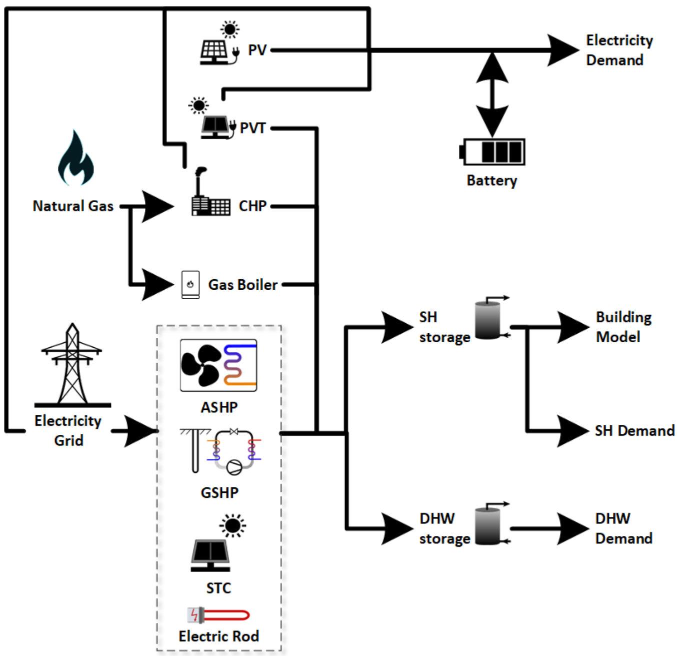

Figure 8: Default connections between different system components when a config file is used for optimization problem definition.

Model predictive control (MPC) functionality

The optihood code was updated with respected to the latest upgraded version of the oemof.solph package (i.e. v0.5.0). The v0.5.0 of oemof.solph supports non-convex investment flows and therefore, constraints such as the minimum up and downtime, the minimum and maximum output power flows of an energy conversion technology. The following main updates were made to the optihood code to allow MPC functionality:

- The output flows of energy conversion technologies were defined as non-convex output flows, in order to activate the constraints related to the minimum up/ downtime, etc., when needed. In the previous version of oemof.solph, a combination of non-convex flows with investment optimization was not possible.
- A constraint to avoid the production of both SH and DHW at the same time step by a heat pump was added. If one works with long time intervals (e.g. hours or longer), then this constraint might not be needed. However, for control optimization (i.e. MPC), where one needs to work with smaller

time intervals, it is necessary. This constraint was formulated based on the `limit_active_flow_count` constraint from the upgraded oemof.solph version.

- The changes corresponding to the renaming and restructuring of modules within the oemof.solph v0.5.0 were made.

2.3 Solar radiation processing

The inclusion of technologies such as photovoltaic (PV), solar thermal (ST), and photovoltaic-thermal (PVT) systems into energy system optimization frameworks poses challenges, particularly due to the inherently nonlinear nature of solar energy generation processes. Factors such as the tilt and azimuth angles of solar surfaces directly influence the incident solar radiation, thereby affecting the energy output. These nonlinear dependencies cannot be directly incorporated into mixed-integer linear programming (MILP) optimization frameworks, such as the optihood framework used in the SolHOOD project. To address this challenge, a pre-processing step has been adopted to determine optimal solar surface configurations prior to the main MILP-based optimization. This "solar pre-processing" step simplifies the nonlinear aspects of solar energy modeling by calculating several configurations of tilt, azimuth and layout for solar surfaces (PV, ST, and PVT systems) in a given geographical and architectural context and selecting only those that offer the maximum solar yield related to their surface or the maximum annual coverage of the energy demand. These optimized configurations ensure that the solar components considered in the subsequent optimization assure maximum efficiency while remaining computationally tractable within the linear optimization framework.

To enable the implementation of the solar preprocessing step, two new Python classes were developed. The first, the "weather class," focuses on processing meteorological data, including clustering techniques for generating representative weather profiles. The second class calculates the feasible number of solar panels that can fit on a rectangular roof based on specified tilt, azimuth, and panel layout configurations. Together, these classes provide the foundational tools necessary for accurately modeling solar energy potential within the pre-processing routine.

The *weather* class

One of the main set of data required for energy system optimization is made by meteorological information (i.e, typically: pressure, temperature and humidity of outdoor air, global, diffused and direct solar irradiance, direction and speed of the wind). To formulate an optimization scenario in SolHood, in fact, one has to define the source for meteorological data in the input configuration file, on the "profile" tab of the Scenario file. The *weather* class added to the optihood framework allows one to download these type of information from the PVGIS website[9] or to compile user-provided data into the format required by the optimization processing. In an attempt to reduce computational complexity, the *weather* class was equipped with clustering analysis

Figure 9: Panel arrangement for an east-west structure (left image), according to portrait layout (center image) and for the case of a slanted roof (right pane).

features. The user can either provide a list of clusters or use the embedded subroutine to compute a user

[9] https://pvgis.com/es

defined number of clusters. This latter can be done by applying the *kmeans* method to the daily average values or, together with euclidean distance, to the 24 hour profiles of the variables of choice. Appendix A provides further details on the *weather* class and on the preliminary validation results for the adopted clustering strategy. It is to be confirmed that clustering of metereological and energy demand data yields acceptable results when compared to unclustered data treatment in the optihood framework.

Once the meteorological data have been processed, either by downloading them or by formatting the user-provided data, they are used to optimize the solar surfaces to be adopted in the energy system. Given the high-non linearity affecting the solar optimization process, a "brute-force" approach is implemented. By using a second python class added to the framework (class *Calepinage*), the number of solar panels (PV, ST or PVT) that fit a rectangular flat or slanted roof can be computed for several configurations by the *weather* class before-hand. Among the multiple pre-computed solar configurations, the class then selects only the solutions that offer the best return in terms of specific solar yield or specific energy demand coverage (both in $[\frac{kWh}{m^2y}]$) and writes them to the scenario file, in order for them to be included in the optimization process as possible components of the optimal energy system configuration.

The list of pre-computed cases is made of the following configurations:

- case of a **flat** roof
  - solar surface oriented on a *portrait* arrangement (left pane in Figure 9)
    - 3 types of panel alignment
      - panel aligned to the short side of the building roof;
      - panel aligned to the long side of the building roof;
      - panel aligned to the south;
    - Several types of tilt optimization:
      - *tilt* optimization: the surface's optimal tilt is queried to the PVGIS website for the building location and for the panel azimuth, while the distance between panel rows is computed by avoiding inter-shadowing;
      - *max4dist* optimization: the surface's tilt is computed based on a distance between panel rows which equals a user provided minimum value while avoiding inter-shadowing;
      - *tilt+10* and *tilt+20* optimization: the queried optimal tilt is increased by 10° and 20°, respectively, while, for each case, the distance between panel rows is computed by avoiding inter-shadowing;
  - solar surface installed on a fixed tilt *East-West* structure (center pane in figure 9)
    - 3 types of structure alignment (to the short and long side of the building roof or with the east-west structure aligned to the South azimuth).
- case of a **slanted** roof (right pane in figure 9): panels are superposed to each side of a slanted roof (i.e., the panel tilt is the same of the roof tilt) and the number is computed based on user-provided minimal distance between panel rows without any shadowing.

As an example, table 10, 10, 10 and 10 show the solar configuration cases compiled by the *weather* class for a 10 m by 20 m flat roof oriented -30° South-East (i.e.,according to the convention for which South is 0°, West is +90° and East is -90°). Based on the resulting specific production and the specific demand coverage, 2 configurations for each arrangement (i.e., portrait or east-west) are selected to be written in the "solar" worksheet of the scenario file, where all of the main technical and economical parameters of the technology solution are set. In the case of *portrait* layout, the configuration with optimal tilt and south alignment offers the highest specific production, while the one offering the best potential coverage of the energy demand is the configuration featuring panel alignment on the building long side an tilt assuring minimal row inter-distance, maximum roof area utilization, and, incidentally, also the largest installed solar surface and capital cost. Computed results, like the ratio between the solar surface area and the total roof area, are then used in the following optimization process to estimate the solar yield of the corresponding solar configuration.

The *Calpinage* class

The "calepinage" class serves the purpose of determining the optimal number of solar collectors that can be accommodated on a rectangular roof with arbitrary orientation. It allows considering different aspects like the location, the size of the roof of a building and its orientation, in order to optimize the distance between adjacent collector strings, lower reciprocal shadowing and adjust the collector placement to adapt correctly to the available space. Leveraging the capabilities of the Python package "Shapely," tailored for set-theoretic analysis and manipulation of planar features, the projection of the reference panel onto the horizontal plane is employed. This projection dynamically populates the specified geometry until further placement of panels is precluded by the geometric constraints defined by reciprocal shadowing distances and roof features, such as orientation, latitude, and safety distances to the roof edge. This method ensures an efficient and optimized arrangement of panels within the given spatial constraints, maximizing solar collector coverage on the roof. Upon completion of the computations, the class provides the maximum number of panels that can be accommodated on the provided rectangular-shaped roof, factoring in the assumed orientation and tilt. In each of the cases listed in section 2.3, the class outputs several KPIs that can be used to rank different solutions. In the case of the *weather* class, it adopts the solar configurations that assure the maximum value of specific solar yield of the solar surface or the maximum coverage ratio that the input roof can assure for the energy demand linked to the scenario input file. For a more in-depth understanding of the "Calepinage" class and its functionalities, additional details are outlined in the Appendix A, together with a use-case example.

Tilt optimization: max4dist Tilt that minimize inter-row distance avoiding inter-shadowing for location (47.39152138,8.173695099) **Panel alignment**: short side **Panel layout:** portrait	**Tilt:** 7° **Panel azimuth:** + 60° W **Row inter-distance:** 0.6 m **N. of 2 m-by-1 m panels:** 36 **Solar footprint ratio:** 0.57 m$^2_{solar}$/m$^2_{roof}$ **Specific yield (PV):** 242 kWh$_e$/m^2/y **Specific self-consumption:** 138 kWh$_e$/m$^2_{roof}$/y	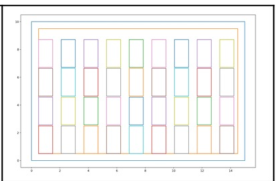
Tilt optimization: optimal tilt by PVGIS Tilt that maximize solar yield with the distance to avoid inter-shadowing for location (47.39152138,8.173695099) **Panel alignment**: short side **Panel layout:** portrait	**Tilt**: 28° **Panel azimuth:** + 60° W **Row inter-distance:** 1.1 m **N. of 2 m-by-1 m panels:** 28 **Solar footprint ratio:** 0.44 m$^2_{solar}$/m$^2_{roof}$ **Specific yield (PV):** 247 kWh$_e$/m^2/y **Specific self-consumption:** 110 kWh$_e$/m$^2_{roof}$/y	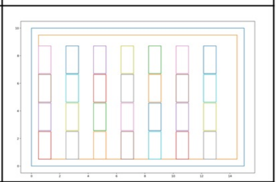
Tilt optimization: optimal tilt by PVGIS increased by 10° and no shadows for location (47.39152138,8.173695099) **Panel alignment**: short side **Panel layout:** portrait	**Tilt**: 38° **Panel azimuth:** + 60° W **Row inter-distance:** 1.38 m **N. of 2 m-by-1 m panels:** 28 **Solar footprint ratio:** 0.44 m$^2_{solar}$/m$^2_{roof}$ **Specific yield (PV):** 244 kWh$_e$/m^2/y **Specific self-consumption:** 108 kWh$_e$/m$^2_{roof}$/y	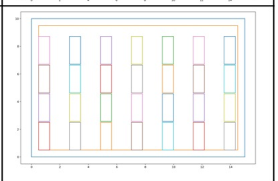
Tilt optimization: optimal tilt by PVGIS increased by 20° and no shadows for location (47.39152138,8.173695099) **Panel alignment**: short side **Panel layout:** portrait	**Tilt**: 48° **Panel azimuth:** + 60° W **Row inter-distance:** 1.67 m **N. of 2 m-by-1 m panels:** 24 **Solar footprint ratio**: 0.38 m$^2_{solar}$/m$^2_{roof}$ **Specific yield (PV):** 237 kWh$_e$/m^2/y **Specific self-consumption:** 90 kWh$_e$/m$^2_{roof}$/y	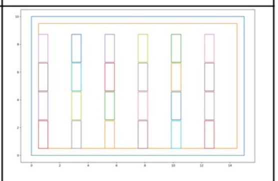

Figure 10: Cases compiled by the *weather* class for portrait layout and panel alignment to the short side of the building.

Tilt optimization: max4dist Tilt that minimize inter-row distance avoiding inter-shadowing for location (47.39152138,8.173695099) **Panel alignment**: long side **Panel layout:** portrait	 **Tilt:** 7° **Panel azimuth:** - 30° E **Row inter-distance:** 0.6 m **N. of 2 m-by-1 m panels:** 36 **Solar footprint ratio:** 0.57 m^2_{solar}/m^2_{roof} **Specific yield (PV):** 243 $kWh_e/m^2/y$ **Specific self-consumption:** 139 $kWh_e/m^2_{roof}/y$	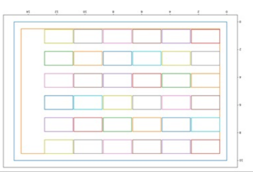
Tilt optimization: optimal tilt by PVGIS Tilt that maximize solar yield with the distance to avoid inter-shadowing for location (47.39152138,8.173695099) **Panel alignment**: long side	**Tilt**: 33° **Panel azimuth:** - 30° E **Row inter-distance:** 1.23 m **N. of 2 m-by-1 m panels:** 24 **Solar footprint ratio:** 0.38 m^2_{solar}/m^2_{roof} **Specific yield (PV):** 251 $kWh_e/m^2/y$ **Specific self-consumption:** 96 $kWh_e/m^2_{roof}/y$	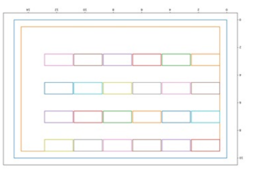
Tilt optimization: optimal tilt by PVGIS increased by 10° and no shadows for location (47.39152138,8.173695099) **Panel alignment**: long side **Panel layout:** portrait	**Tilt**: 43° **Panel azimuth:** - 30° E **Row inter-distance:** 1.53 m **N. of 2 m-by-1 m panels:** 24 **Solar footprint ratio:** 0.38 m^2_{solar}/m^2_{roof} **Specific yield (PV):** 246 $kWh_e/m^2/y$ **Specific self-consumption:** 94 $kWh_e/m^2_{roof}/y$	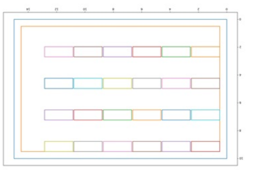
Tilt optimization: optimal tilt by PVGIS increased by 20° and no shadows for location (47.39152138,8.173695099) **Panel alignment**: long side **Panel layout:** portrait	**Tilt**: 53° **Panel azimuth:** - 30° E **Row inter-distance:** 1.8 m **N. of 2 m-by-1 m panels:** 24 **Solar footprint ratio**: 0.38 m^2_{solar}/m^2_{roof} **Specific yield (PV):** 237 $kWh_e/m^2/y$ **Specific self-consumption:** 90 $kWh_e/m^2_{roof}/y$	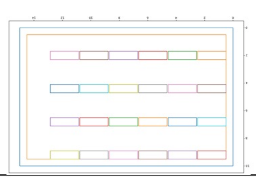

Figure 11: Cases compiled by the *weather* class for portrait layout and panel alignment to the Long side of the building.

Tilt optimization: max4dist Tilt that minimize inter-row distance avoiding inter-shadowing for location (47.39152138,8.173695099) **Panel alignment**: facing South **Panel layout:** portrait	 **Tilt:** 7° **Panel azimuth:** 0° S **Row inter-distance:** 0.6 m **N. of 2 m-by-1 m panels:** 30 **Solar footprint ratio:** 0.47 m^2_{solar}/m^2_{roof} **Specific yield (PV):** 245 $kWh_e/m^2/y$ **Specific self-consumption:** 117 $kWh_e/m^2_{roof}/y$	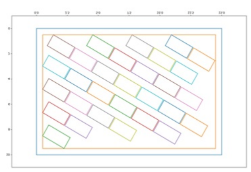
Tilt optimization: optimal tilt by PVGIS Tilt that maximize solar yield with the distance to avoid inter-shadowing for location (47.39152138,8.173695099) **Panel alignment**: facing South **Panel layout:** portrait	**Tilt**: 36° **Panel azimuth:** 0° S **Row inter-distance:** 1.32 m **N. of 2 m-by-1 m panels:** 23 **Solar footprint ratio:** 0.36 m^2_{solar}/m^2_{roof} **Specific yield (PV):** 258 $kWh_e/m^2/y$ **Specific self-consumption:** 94 $kWh_e/m^2_{roof}/y$	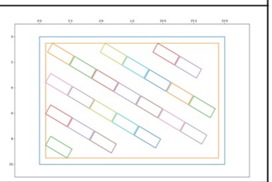
Tilt optimization: optimal tilt by PVGIS increased by 10° and no shadows for location (47.39152138,8.173695099) **Panel alignment**: facing South **Panel layout:** portrait	**Tilt**: 46° **Panel azimuth:** 0° S **Row inter-distance:** 1.62 m **N. of 2 m-by-1 m panels:** 22 **Solar footprint ratio:** 0.35 m^2_{solar}/m^2_{roof} **Specific yield (PV):** 253 $kWh_e/m^2/y$ **Specific self-consumption:** 88 $kWh_e/m^2_{roof}/y$	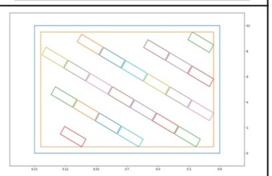
Tilt optimization: optimal tilt by PVGIS increased by 20° and no shadows for location (47.39152138,8.173695099) **Panel alignment**: facing South **Panel layout:** portrait	**Tilt**: 56° **Panel azimuth:** 0° S **Row inter-distance:** 1.9 m **N. of 2 m-by-1 m panels:** 21 **Solar footprint ratio:** 0.33 m^2_{solar}/m^2_{roof} **Specific yield (PV):** 243 $kWh_e/m^2/y$ **Specific self-consumption:** 80 $kWh_e/m^2_{roof}/y$	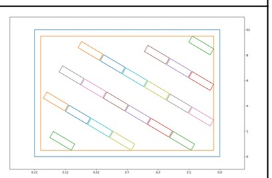

Figure 12: Cases compiled by the *weather* class for portrait layout and panel alignment to the south.

Tilt optimization: max4dist Tilt that minimize inter-row distance avoiding inter-shadowing for location (47.39152138,8.173695099) **Panel alignment**: long side **Panel layout:** East-West structure	 **Tilt:** 7° **Panel azimuth:** 0° S **Row inter-distance:** 0.6 m **N. of 2 m-by-1 m panels:** 30 **Solar footprint ratio:** 0.47 m^2_{solar}/m^2_{roof} **Specific yield (PV):** 245 $kWh_e/m^2/y$ **Specific self-consumption:** 117 $kWh_e/m^2_{roof}/y$	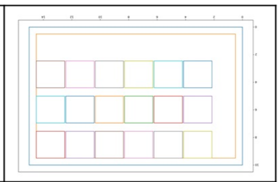
Tilt optimization: optimal tilt by PVGIS Tilt that maximize solar yield with the distance to avoid inter-shadowing for location (47.39152138,8.173695099) **Panel alignment**: facing South **Panel layout:** East-West structure	**Tilt:** 36° **Panel azimuth:** 0° S **Row inter-distance:** 1.32 m **N. of 2 m-by-1 m panels:** 23 **Solar footprint ratio:** 0.36 m^2_{solar}/m^2_{roof} **Specific yield (PV):** 258 $kWh_e/m^2/y$ **Specific self-consumption:** 94 $kWh_e/m^2_{roof}/y$	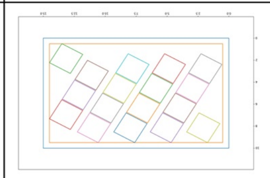
Tilt optimization: optimal tilt by PVGIS increased by 10° and no shadows for location (47.39152138,8.173695099) **Panel alignment**: short side **Panel layout:** East-West structure	**Tilt:** 46° **Panel azimuth:** 0° S **Row inter-distance:** 1.62 m **N. of 2 m-by-1 m panels:** 22 **Solar footprint ratio:** 0.35 m^2_{solar}/m^2_{roof} **Specific yield (PV):** 253 $kWh_e/m^2/y$ **Specific self-consumption:** 88 $kWh_e/m^2_{roof}/y$	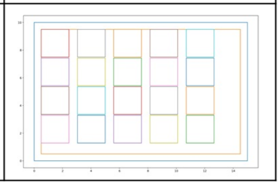

Figure 13: Cases compiled by the *weather* class for East-West layout and for the 3 types of panel alignment.

.

2.4 Optimization target

An optimization target function, or objective function, is a mathematical function that quantifies the goal of an optimization problem. It defines the quantity to be minimized or maximized. By systematically adjusting the decision variables (in our case, the invested capacities of technologies and the energy flows between components), the optimization process seeks to identify the optimal solution that yields the best possible value for the target function. The optimization results would, therefore, directly depend on the chosen target function. Within this project, we want to minimize both the cost and the carbon emissions which leads to the definition of two functions.

2.4.1 Cost minimization

The system is optimized economically by minimizing the total annualized cost (Z) in CHF/year. The total annualized cost consists of three components: CAPEX, OPEX and feed-in revenue. CAPEX refers to the annualized capital investment cost to install a given technology. The investment cost for each technology is defined as the sum of a "base" investment cost (constant or independent of the capacity), and a "cost per unit capacity" (proportional to the installed capacity). The costs for installation and planning are also considered as percentages of the CAPEX. The second component, OPEX, is the operation cost or the cost related to the use of energy inputs/resources, for example, grid electricity cost to drive a heat pump. Additionally, OPEX also includes the maintenance cost for each technology selected by the optimizer. The third component is the feed-in revenue, which includes the revenues earned from feeding in surplus electricity (if any) to the grid.

The target function, $f(x)$, in this case can be expressed as:

$$f(x) = minimize \quad Z = \sum_b \sum_t [X_{b,t} \cdot (CAPEX_{b,t} + OPEX_{b,t})] - \sum_f (Tariff_f \cdot E_f) \tag{26}$$

with,

- b, t and f refer to buildings, technologies and feed-in energy flows, respectively.
- $X_{b,t}$ is a binary variable, which is 1 if the technology t is installed in building b in the optimum solution, and 0 otherwise.
- $CAPEX_{b,t} = \left(Cost_t^{base} + Cost_t^{capacity} \cdot S_{b,t}\right) \cdot CRF$
  Here, $S_{b,t}$ is the installed capacity of the technology t in building b and CRF is the capital recovery factor for calculating the annuity (expressed as $CRF = \frac{r \cdot (1+r)^n}{(1+r)^n - 1}$, r being the interest rate, and n the lifetime of the technology). We consider an interest rate r of 5% for calculating the annuity.
- $OPEX_{b,t} = \sum_i \sum_h \left(Cost_i^h \cdot E_{i,b,t}^h\right) + Cost_t^{maintenance}$
  Here, i and h denote the energy inputs and the time-steps, respectively. $Cost_i^h$ is the cost of the energy input i at time h and $E_{i,b,t}^h$ is the energy flow related to the input i for operating the technology t in building b at time h.
- $Tariff_f$ and E_f are the feed-in tariff and the total energy fed into the grid, respectively.

2.4.2 Environmental impact minimization

In order to evaluate the optimum system configuration from an environmental perspective, we minimize the annual environmental impact (Y) in kgCO_2eq/year of each technology and input. The environmental impact is evaluated based on the Global Warming Potential (GWP) from IPCC, which quantifies the greenhouse gas emissions to the atmosphere as kilograms of equivalent CO_2 effect on the global warming potential over a period of 100 years.

The target function, $f(x)$, in this case is given by:

$$f(x) = minimize \quad Y = \sum_b \sum_t \left[X_{b,t} S_{b,t} \cdot \frac{Emission_t}{n})\right] + \sum_i \sum_h \left(Emission_i^h \cdot E_{i,t}^h\right) \tag{27}$$

Here, the first term of the equation corresponds to the impact from the installation of technologies and the second term denotes the impact from the operation of the system.

2.4.3 Multi-objective optimization

The optimization goal could be either to minimize a single objective function (cost using Eq. 26 or emissions using Eq. 27) or to perform multi-objective optimization by considering a combination of the two. In multi-objective optimization, we run a series of optimizations to obtain a pareto front curve between the cost and environmental optimum using epsilon constraint method (Mavrotas (2009)). The first and the second optimizations determine the two extremes of the curve where the cost-alone and the emissions-alone are minimized. The remaining optimizations (or solutions on the pareto front curve) perform cost minimization with a constraint on the permissible emissions.

2.5 Optimization constraints

Optimization problems often involve constraints, which are limitations or restrictions on the values that the decision variables can take. These constraints define the feasible region, i.e. the set of all possible solutions that satisfy the problem's requirements. Several required constraints, such as the minimum/maximum allowed capacity of a technology or epsilon constraint method for multi-objective optimization, were already implemented in optihood (either from the base package oemof or from previous developments). The additional constraints implemented for this project are described with the respective technology in section 2.2. Apart from the ones already described, the available roof area limit constraint was implemented to respect the maximum installation size of solar technologies (STC, PV and PVT).

2.5.1 Available roof area limit

Following the optimization, more than one type of solar installation can be adopted for a same roof. Either multiple same-technology solutions are selected, or more than one technology needs to find space on the roof. As a consequence, a roof area constraint has been incorporated into the optimization model. to limit the total installed capacity of solar technologies by considering the physical footprint of each technology on the roof area. Specifically, the constraint calculates the total occupied roof area by multiplying the investment decision variables (capacity) with a coefficient representing the area required per unit of capacity for each technology. The sum of these values must not exceed the total available roof area for the corresponding building in the neighborhood. This ensures that the selected combination of solar technologies fits within the actual spatial limits of the investigated rooftops, promoting realistic and implementable solutions.

2.6 Cost and Emission assumptions

This section summarizes the cost and emission assumptions for the different technologies and energy inputs considered within the scope of this project. These cost and emission assumptions were used in the target functions defined by Eq. (26) for cost minimization and Eq. (27) for environmental impact minimization. Table 1 summarizes these assumptions for different energy conversion and storage technologies considered within this project. The cost functions for PVT collectors were derived based on the offers for surfaces between 1 m^2 to 50 m^2. The offers included the costs of installation and planning, transport and the accessories. Installation costs included labor to install all the components (accumulator, expansion vessels, etc.), the cost of the electrical connection and the cabinet, hydraulics, and commissioning. Operation and maintenance costs of PVT collectors are similar to those of PV panels, an average annual cost of 2 % of the CAPEX is taken into consideration. The environmental impact data for PVT collectors is retrieved from the KBOB 2021 database. The GHG emissions for the production of a PVT system with a photovoltaic efficiency of 0.167 kWp/m^2 is 370 gCO_2eq/m^2 or 2.220 gCO_2eq/kWp, the installation including the panels, inverter, mounting system, exchanger and pipes. The linearized cost function for seasonal thermal energy storage was taken from project IceGrids (Carbonell et al., 2024). It is valid for seasonal storage up to a capacity of 37,000 m^3. The GHG emissions for the production of seasonal thermal storage were considered similar to those of short-term hot water storage. The assumptions for remaining technologies were obtained from the project OPTIM-EASE (Jobard et al. (2022)).

Furthermore, grid electricity as an energy input would have an associated cost and GHG emissions. Other energy inputs like ambient heat or solar irradiation energy do not incur any costs or emissions and therefore, will not be discussed in this section. For the cost of grid electricity, we consider different scenarios (fixed tariff and dynamic prices) which will be described in the respective sections later. A fixed tariff of 9 c/kWh is considered for feeding in electricity to the grid. Moreover, the optimizations employ a dynamic carbon footprint of grid electricity, which is described in the following section.

2.6.1 Carbon footprint of the Swiss grid

The Swiss electricity mix for at hourly time step is generated with the electricity system modeling tool EcoDyn-Elec[10] that was built in the EcoDynBat project. It is based on ENTSO-E data for modeling the exchanges and productions on the European grid at the hourly and sub-hourly timescale. Swiss consumption mix modeling is refined with additional data from Swissgrid (imports and exports) and from the Swiss Federal Office of Energy (losses, correction to missing productions in ENTSO-E data). The GHG emission profile of the low voltage

[10] https://github.com/LESBAT-HEIG-VD/EcoDynElec

Table 1: Summary of cost and GHG emissions for different energy conversion and storage technologies.

	CAPEX [CHF]	$Cost^{maintenance}$ [% CAPEX/y]	Lifetime [y]	GHG emission [gCO_2eq]
Energy Conversion Technologies				
PV	17950 + 1103/kWp	2	30	1131/kWp
STC	5500 + 820/m^2	0.5	30	127/m^2
PVT	7128 + 1066/m^2	2	30	370/m^2
ASHP	16679 + 2152/kW	2	20	280.9/kW
GSHP (including BHE)	22257 + 3052/kW	2	20	772/kW
Energy Storage Technologies				
Battery	5138 + 981/kWh	0	20	28.66/kWh
Hot water storage	2132 + 6.88/L	0	20	0.49/L
Seasonal thermal storage	292628 + 0.059497/L	0	20	0.49/L

electricity Swiss consumption mix is shown for 2020 and 2021 in Figure 14. This output is used to assess the GHG emissions of building electricity consumption.

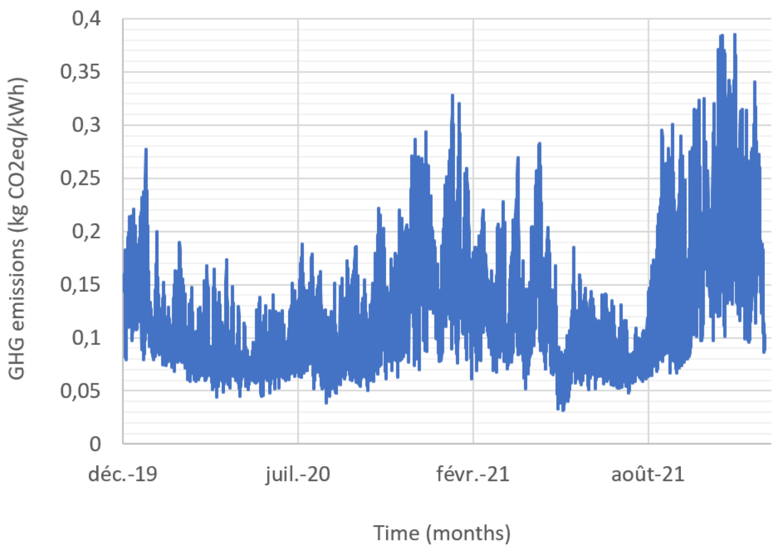

Figure 14: Hourly step GHG emissions of the Swiss electricity consumption throughout 2020 and 2021.

The following influential aspects in the temporal determination of GHG emissions of the swiss electricity mix have been identified:

- The national (uncontrollable) production of photovoltaic panels and wind turbines is only determined by local weather variables (radiation, temperature and wind velocity).

- The national hydroelectricity production has a controllable part with lake reservoir plant and uncontrollable part with run-of-river plant. The water stock in reservoir and productivity is subjected to seasonal influences from precipitation and snow melting.
- Pumped storage hydro power plant is controllable and often used during peak demand.
- The national demand of electricity is the aggregated regional demands, respectively highly influenced by their local weather conditions (radiation, temperature and wind velocity).
- The national demand is also influenced by the economic activity of the day. The demand is higher during weekdays than weekend days and holidays.
- Following an offer-demand principle that ensure equilibrium of the grid at the European scale, the controllable production technologies and the exchanges (imports and exports) are activated to meet the residual demand (i.e. the demand minus the uncontrollable production).
- Due to the high amount of exchange between Switzerland and its neighboring countries, the previous aspects in those countries also affect the final consumption mix in Switzerland, especially regarding exchanges with Germany and France.
- All the previous aspects interact and are reflected with the price of electricity in many different ways and temporal horizons (long-term, day-ahead, infra-day).
- The installed production capacities evolve each year due to new and closed production facilities.

EcoDynElec is a tool to generate and analyze the electricity mix profiles of historical year. If those historical profiles are jointly used for building assessment with climate data from other historical year, it induces temporal and physical inconsistencies. Depending on the application of such method, this inconsistency can have more or less importance in the reliability of the results. The optimization of building energy systems consist in controlling the production and storage in response to variability in the demand with the objective to minimize GHG emissions. An inconsistency between the building needs calculation and the impacts of electricity should be avoided as it would affect each time step of the optimization process, thus leading to less reliable CO2-optimal control. Furthermore, in a real time application such as predictive control, it is necessary to jointly predict local climate conditions and the global electricity system in which the building takes part. A coupled modeling of the dynamic interactions in the electricity system could be a solution for the price of highly complex efforts in terms of collecting data and building a reliable and robust mathematical model.

A much simpler and straightforward statistical approach is adopted in this work to use correlated climate and electricity mix data in building performance assessment. It is based on the historical data generated with EcoDynElec and the Typical Meteorological Year (TMY) used in building performance simulation. TMY are standardized weather data sets defined for a given location and used in building performance simulation. They contain hourly time-series that are statistically selected among a bank of data from a period of at least 10 years to represent the most frequent climatic condition. The goal and deliverable of this task is to create a similar "Typical Electricity Year" (TEY) that represent hourly GHG emissions profiles that are sufficiently representative and realistic in terms of temporal variability to be reliably used in building performance assessment.

While the end result and the field of application are similar for TMY and TEY, the logic behind TMY design can't be directly translated to electricity mix due to the geographical and temporal interactions occurring in an electricity system between weather, electricity demand and production. Several specificities of the studied systems have to be noted:

- Both the demand and production components of an electricity system are heavily influenced by local weather conditions.

- Geographical scope: while TMY are defined for local conditions based on regional weather observations, the GHG emission of electricity at the grid is considered to be the same at any place in Switzerland[11]. Hence, our TEY is defined at national scale.
- Due to the interactions between the national grid and many local weather conditions across the country, the TEY must be built according to the 24 TMY-related weather stations covering Switzerland. The advantage is that a unique TEY can be used jointly with any of the 24 TMY used in the process.
- Unlike weather data, a 10-years average approach to construct a typical electricity mix is not relevant because older years are obsolete due to the rapid evolution of the installed capacities, especially for the case of photovoltaic in Germany that directly affects the exported electricity mix to Switzerland. (This statement is valid when considering physical average mix, but not necessarily when considering marginal mix. Marginal mix is related to production technologies that are identified by they merit order, the latter does not evolve in the same manner than the national installed capacities.)

The method to produce TEY is described as follow. TEY time-series has been synthesized for a given historical year by associating each meteorological day from a Typical Meteorological Year (TMY) [12] with a corresponding day from the historical year of an electricity mix data. The selection is operated by minimizing the difference in weather and other conditions according to the parameters given below. The TMY and weather data for the chosen historical year is retrieved form Meteonorm. The electricity mix data are retrieve from EcoDynElec for the years 2021 and 2022.

The historical hourly GHG emission profiles according to each selected day are then assembled to form the TEY, an artificial hourly profile, statistically compatible with the 24 swiss TMY and representative of the conditions of the electricity system in a given year. This approach allows us to construct an artificial profile for one year of the hourly GHG emissions of the grid, maximizing their correlation with the weather patterns of the TMY. The principle is illustrated with this example. For a typical 5$^{\text{th}}$ January and the weighted weather conditions over Switzerland according to 24 TMY data, the day with the closest historical conditions in 2021 is identified to be the 2$^{\text{nd}}$ February. Hence, in the TEY, the hourly GHG emissions of the electricity mix is set to be the historical GHG emission profile of the 2$^{\text{nd}}$ February 2021 from EcoDynElec. The methodology is explained in Figure 15:

1. Load historical meteorological for the chosen year and the 24 weather stations according to the SIA 2028.
2. Compute daily averages on the following variables: air temperature, global horizontal solar radiation, wind speed, relative humidity, and water reservoir levels.
3. Load TMY data from the 24 weather stations and compute daily averages of the same weather variables.
4. Matching: this calculation is performed for each weather station. For each day of the TMY, a vector containing the distance values to each day of 2021 is calculated. The distance is defined as the weighted sum of differences between each meteorological variable.
5. Weighting: For each day, the weighted sum of distances over the 24 weather stations is calculated. A distance is weighted by the population of each canton the weather station belong to. If multiple stations are in the same canton they are weighted based on the population of the district where they are located (an administrative division between the municipality and the canton).
6. A typical year based solely on a mixture of days from 2021 is synthesized by selecting the day that has the minimum distance over all the weather stations. The "nearest day of 2021" to the weather and electric system conditions of a day mutual to all 24 weather stations.
7. Load hourly GHG emissions of a kWh of electricity from the chosen year (from EcoDynElec).

[11] according to the physical approach and national security of supply adopted in EcoDynElec modelling
[12] Generated using Meteonorm 8.2 between 2000 and 2020

8. Associate the identified nearest day (bullet point 6) with the corresponding day in the chosen year and its hourly GHG emissions.

9. Finally, a TEY with hourly values of GHG emissions of the swiss electricity mix is generated as a recombination of historical days from the chosen year. The TEY is consistent with weighted average conditions of 24 TMY data over Switzerland and compatible with those TMY data.

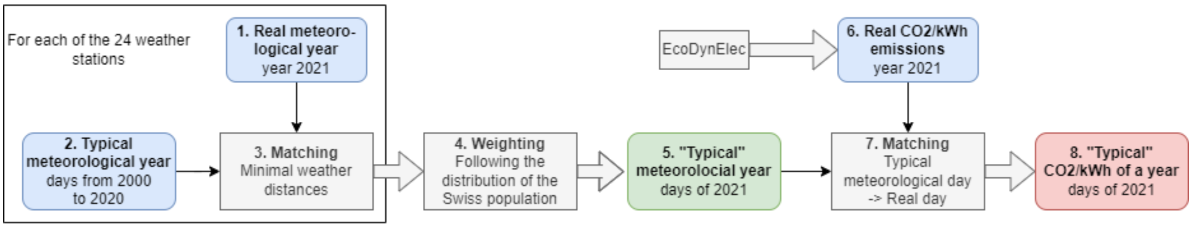

Figure 15: Algorithm established to synthesize 'typical' years of GHG emissions related to electricity consumption in Switzerland.

Figure 16 displays the results obtained as a hourly profile of GHG emissions of the electricity consumed in Switzerland. The red curve represents the synthesized profile, selecting the closest day (in terms of weather conditions) from 2021 for each day of the typical meteorological year. The gray interval corresponds to an uncertainty interval set between the min and max profiles over a given number of closest days-profiles. The number of closest days-profiles that are selected is determined to match the same range of uncertainty observed in the historical years from EcoDynElec. The observed historical variations to the 6-year average of the annual average GHG emissions of the electricity mix between 2016 and 2022 is approximately -20% to +20% .

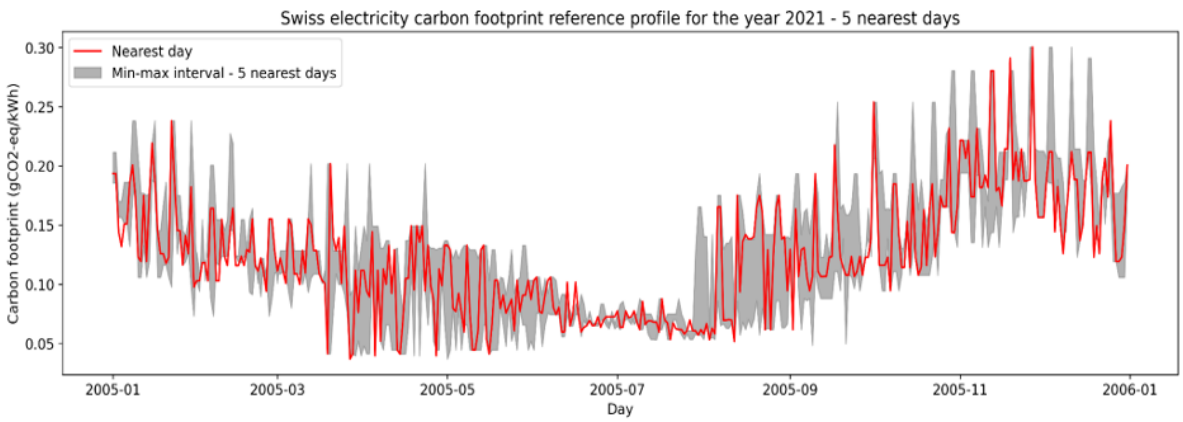

Figure 16: Typical hourly profile synthesized from the typical meteorological year and the days of 2021.

The decision to choose *the* nearest day was made to ensure the preservation of extreme values, which would not have been retained by methods like "averaging the nearest N days". In order to assess the uncertainty of the calculated values, we also consider a range representing the minimum and maximum greenhouse gas emissions, derived from the five closest days of a chosen typical day. This selection allows for an annual average GHG emissions range of -18 % to +25 % around the "nearest days" GHG emissions profile, which is close to the observed historical variations around the 6-year average of annual average GHG emissions of the electricity between 2016 and 2022, as shown on Figure 17.

It is worth noting that a TEY is highly linked to a chosen historical to represent the electricity system conditions. For example, the year 2022 is not similar to the year 2021, with events such as the Ukraine war and the low availability of French nuclear power plants that have altered electricity production and exchange patterns

gCO2eq/kWh of swiss electricity, consumer mix	2021		2022	
	Annual average	% difference of annual average to "Nearest"	Annual average	% difference of annual average to "Nearest"
Nearest TEY	124	-	141	-
Min TEY (min GHG value from 5 Nearest days)	101	-18%	120	-15%
Max TEY (max GHG value from 5 Nearest days)	153	+23%	166	+18%

Figure 17: Annual average GHG emissions of the TEY profiles generated: Nearest profile, min profile and max profile selected among 5 nearest days selected in the process.

throughout Europe. These differences are visible on Figure 18 which represents the real GHG emissions profiles of 2021 and 2022 : the carbon footprint in March, April and during the summer of 2022 are significantly higher than in 2021.

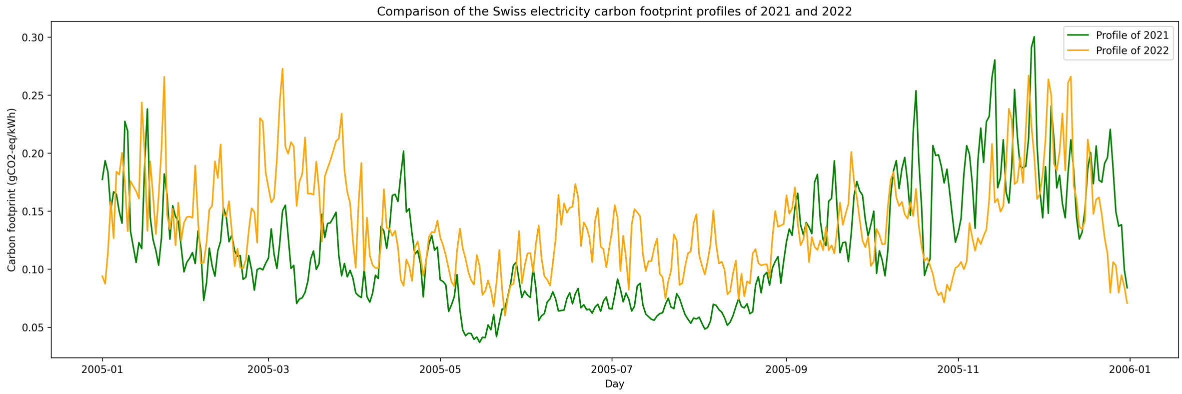

Figure 18: Comparison of the Swiss electricity carbon footprint profiles of 2021 and 2022

2.7 Key Performance Indicators (KPI)

In order to assess and compare different solutions from energy system optimization, key performance indicators (KPIs) need to be defined. In Yang et al. (2020) several KPIs for comparing energy systems are validated and ranked based on statistical measurements for a scientific purpose, the most important indicators being: energy efficiency, environmental impact, availability factor, ramp rate, and energy and equipment cost. In the report Siemens Industry (2014) a list of the most important KPIs for energy systems are compared for an industrial purpose with energy costs and greenhouse emissions as the most important strategic KPIs, and onsite connectivity and energy control as the most important site-specific KPIs. Faria et al. (2121) highlight the importance of using indicators that represent the total lifetime cost of the system, but focus also on reliability-related objectives to validate the local power grid of the system regarding interruption frequency and duration. A comprehensive list of KPIs for assessing the flexibility of a local energy grid is given in Lund et al. (2015). Another flexibility KPI is given in Péan et al. (2019) that focuses on the ability to shift electricity use for heating purpose during the day to benefit from cheaper or low-emission periods. Based on these references, the KPIs are defined and presented next.

The selection, design, and operation strategy of an energy supply system for a neighborhood depends on various decision factors. Hence, a comprehensive list of KPIs is required in order to evaluate and compare different system variants. In optihood, KPIs can be implemented as target functions for the optimization. The default goal of the optimization in optihood is to determine optimal solutions based on costs and environmental impact. The two default KPIs to quantify these two aspects are the annual net present value and the global warming potential (GWP). Additional KPIs for the economic viability, environmental impact, energy quality and flexibility as well as system performance can be used, to further distinguish the obtained solutions or optimize their operation strategy. In the following paragraphs we present the definitions of the two basic KPIs plus a selection of additional relevant KPIs.

2.7.1 Economic viability

System Electricity Costs: The price for electricity from the power grid is an important input parameter for designing an energy system. However, the real price for electricity used in the system depends also on the local production via technologies like photovoltaic. The price per kWh of electricity will be therefore considered based on the share of self-produced electricity in the total electricity demand with the use of the levelized costs (defined in Eq (31) as the cost per kWh) of the set of electricity generating units $u =$ [CHP, PV, PVT] and the grid electricity price:

$$p_{\text{system, elec}}(t) = \frac{p_{\text{grid, elec}}(t) \cdot E_{\text{Grid}}(t) + \sum^{U} (C_{\text{LC}}(u) \cdot E_{\text{prod}}(u,t))}{E_{\text{Grid}}(t) + \sum^{U} E_{\text{prod}}(u,t)} \qquad \forall t \tag{28}$$

with:
- $p_{\text{system, elec}}(t)$: Electricity price for the energy system in time-step t
- $p_{\text{grid, elec}}(t)$: Electricity price from the power grid in t
- $C_{\text{LC}}(u)$: Levelized costs for the installed technology u
- $E_{\text{Grid}}(t)$: Electricity purchased from the power grid in t
- $E_{\text{prod}}(u,t)$: Electricity produced by unit u in t

For time steps with no electricity consumption we set the system electricity cost to the grid price.

Annual Net Present Value (ANPV): The net present value is defined as the sum of all costs associated with the energy technology minus the revenues over the projects lifetime calculated as a present value (see Yang et al. (2020)). The total cost of the technology u over its lifetime is given as the sum of the investment costs $C_{\text{inv}}(u)$ and its total operation costs $C_{\text{oper}}(u)$:

$$C_{\text{anpv}}(u) = (C_{\text{inv}}(u) + C_{\text{oper}}(u)) \cdot a(u) \qquad \forall u \tag{29}$$

$$a(u) = \frac{i}{1-(1+i)^{-lt(u)}} \qquad \forall u \tag{30}$$

with:
- $C_{\text{anpv}}(u)$: Annual net present value for technology unit u
- $C_{\text{inv}}(u)$: Total investment costs for u
- $C_{\text{oper}}(u)$: Total operational costs for u
- i: interest rate
- $lt(u)$: Lifetime of technology unit u in years

By adding the annualization factor $a(u)$ for each technology unit u as a function of the interest rate i and the lifetime $lt(u)$ of the technology, the annual net present value is calculated. The ANPV defines a single annual value that inherently accounts for the full operational lifetime of each technology and therefore, streamlines the aggregation of costs associated with different technologies.

Levelized cost of energy: This is obtained by dividing the the annual net present value by the annual heat and electricity production. The levelized costs (see Hoffmann et al. (2020)) represent the costs of the selected technology in the considered solution to generate one kWh of heat and/or electricity, respectively.

$$C_{\mathsf{LC}}(u) = \frac{C_{\mathsf{anpv}}(u)}{\sum_{t=0}^{8760} H(u,t)} \tag{31}$$

with: $C_{\mathsf{LC}}(u)$: Levelized costs for technology unit u
$H(u,t)$: Heat (and/or electricity) production of unit u in time-step t

A back-up unit has therefore often far higher levelized costs compared to units operating on a base load level, since the installation cost is independent of its operation.

2.7.2 Environmental Impact

To evaluate the environmental impacts, LCA data of each energy vector and technology are evaluated. The main life cycle impact assessment method considered is the Global Warming Potential (GWP) over 100 years from IPCC (Stocker et al. (2013)). It quantifies greenhouse gases (GHG) emitted to the atmosphere as kilogram of CO2 equivalent effect on global warming potential over 100 years (kg CO2-eq.). The GHG emissions of a technology is calculated for a year accounting for the manufacturing, the use stage and the recycling/disposal at end-of-life. The use stage is calculated by summing the hourly energy vectors consumptions and productions over a year. The impacts of manufacturing and end-of-life are added and yearly amortized by the infrastructure's lifetime. The GHG emissions are defined for the system as well as per technology. The LCA data energy vectors, converters and storage are retrieved from the Swiss LCA database KBOB Ökobilanzdatenbestand DQRv2:2022 KBOB et al. (2022). This database follows the quality requirements of UVEK DQRv2-2022 and is based on ecoinvent v2.2 cut-off system model Frischknecht et al. (2007).

Electric system GHG emissions: In a similar manner to the system electricity price, the GHG emissions induce by the production and use of electricity $GHGE_{\mathsf{system,\ elec}}(t)$ is calculated for each time step t. The local production of electricity is determined based on the share of all electricity generation sources including the power grid and the set of all local installed units U and their GHG emissions:

$$GHGE_{\mathsf{system,\ elec}}(t) = \frac{GHGE_{\mathsf{grid,\ elec}}(t) \cdot E_{\mathsf{Grid}}(t) + \sum^{U} (GHGE_{\mathsf{tec}}(u) \cdot E_{\mathsf{prod}}(u,t))}{E_{\mathsf{Grid}}(t) + \sum^{U} E_{\mathsf{prod}}(u,t)} \qquad \forall t \tag{32}$$

with: $GHGE_{\mathsf{system,\ elec}}(t)$: GHG emissions of the electricity supply of the energy system in t
$GHGE_{\mathsf{grid,\ elec}}(t)$: GHG emissions of the power grid in t
$GHGE_{\mathsf{tec}}(u)$: GHG emissions of installed technology unit u

The system GHG emissions are important to evaluate the correct impact of the whole system if electricity is required as input for heating technologies as heat pumps or electric rods.

Technology GHG emissions: The GHG emission of each technology is the sum of all direct and indirect emissions appearing during the life cycle of the technology. All technologies are subjected to indirect emissions due to the construction, transportation, installation and recycling/disposal at end-of-life. In addition some technologies also emit direct emissions by combustion of fuels or operation of electric devices as pumps. The GHG emissions of the consumption of natural gas can be considered as fix, but the impact of electricity varies over time.

$$GHGE_{\text{tec}}(u) = Q(u) \cdot GHGE_{\text{indir}}(u) + (\sum^{U} GHGE_{\text{system, elec/gas}}(t) \cdot E_{\text{cons}}(u,t)) \tag{33}$$

with:

$GHGE_{\text{tec}}(u)$:	GHG emissions of u
$Q(u)$	Installed capacity of u
$GHGE_{\text{system, elec/gas}}(t)$	GHG emissions of the electricity or gas supply to the energy system in t
$E_{\text{cons}}(u,t)$:	Energy (fuel or electricity) consumed to operate technology unit u in t

2.7.3 System Performance

Self-Sufficiency: The self-sufficiency of an energy system determines how much a system depends on the power grid. It can be defined either as an energy balance over time or as the ratio (adjusted based on Hoffmann et al. (2020)) between all electricity generation (CHP, PV and PVT in this case) minus the injection into the grid and the total consumption in the considered period. The ratio is calculated for different time periods t, which can relate to an hour, a month or a year, depending on how large the time period t is selected.

$$SR(t) = \frac{(\sum^{U} El_{\text{prod}}(u,t)) - El_{\text{excess}}(t)}{El_{\text{grid}} + (\sum^{U} El_{\text{prod}}(u)) - El_{\text{excess}}(t)} \qquad \forall t,\ \forall u \in \text{U} = \text{[PV,PVT]} \tag{34}$$

with:

$SR(t)$:	Self-Sufficiency ratio for time step t
$El_{\text{prod}}(u,t)$	Electricity produced with unit u in t
$El_{\text{excess}}(t)$	Excess electricity sold to the grid in t

Grid Flexibility Factor : For an energy system to operate properly, the power supply and demand in the electric grid needs to be in balance at each point of time. The heat and electricity system should be capable to deal with uncertainty and variability in both demand (e.g. natural gas and electricity) from the public grid and supply (e.g. heat and electricity) to the consumers. The variation of the electricity cost and the environmental impact of the electricity used in the system is considered as important in this project. The ability of the system to react to these two variations of the power grid is used to determine the grid flexibility factor of the considered energy system, as defined in on Péan et al. (2019). The electricity price and environmental impact of the system defined in Equation 28 and 32 are divided into low and high value periods for the whole year (see Figure 19). The categorization of high and low value periods has been implemented based on the recommended methodology given by Péan et al. (2017), with a 24h time period of value analysis and using the 40 % highest values during this 24h as high period and the 40 % lowest values as low period.

The flexibility factor (FF) between the electricity used during high and low value periods gives an indication of the flexibility.

$$FF_p = \frac{\int_{lp} E_{\text{cons, total}}(t)\ dt - \int_{hp} E_{\text{cons, total}}(t)\ dt}{\int_{lp} E_{\text{cons, total}}(t)\ dt + \int_{hp} E_{\text{cons, total}}(t)\ dt} \tag{35}$$

with:

FF_p:	Flexibility factor
lp, hp	low value periods and high value periods
$E_{\text{cons, total}}(t)$	Electricity consumed for heating purpose in the energy system in t

A ratio of 1 means the energy system is very flexible towards the selected parameter (cost or environmental impact), a ratio of -1 on the other hand a very inflexible system.

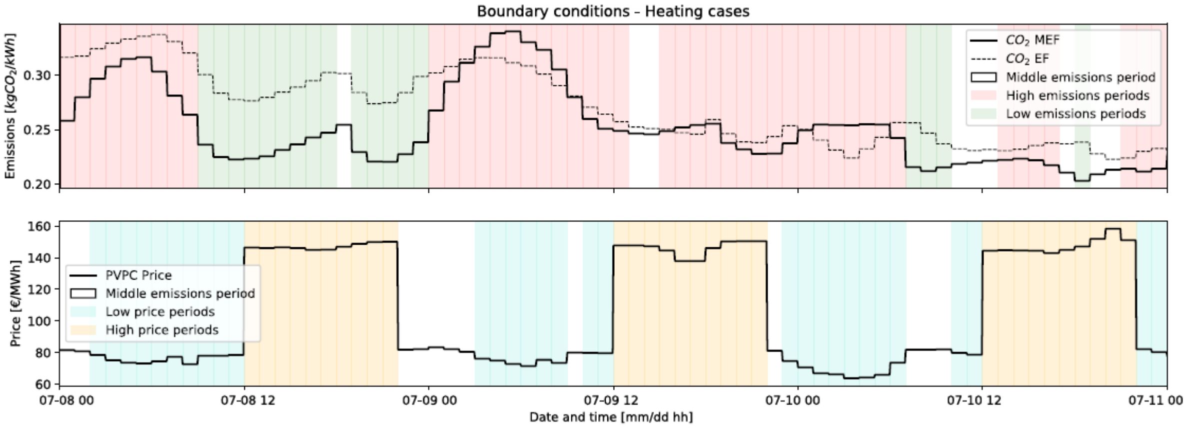

Figure 19: Example for defining low and high value periods from Péan et al. (2019)

3 System design optimization

System design optimization for energy systems is a comprehensive process focused on determining the most efficient and effective configuration of system components to achieve specific objectives, such as minimizing costs and environmental impacts.

Within Solhood project, these two objectives—cost and environmental impact—serve as the primary optimization criteria guiding the design workflow. To identify a representative district to serve as a reference case, a statistical analysis of Swiss districts was undertaken and it identified a representative district to serve as a reference case, forming the basis for a "base case" that defines the district's baseline energy demand and system characteristics.

This base case is optimized using the Optihood framework: by benchmarking against the selected district and its typical energy system, the project ensures that its optimization process remains both practical and effective. External boundary conditions affecting the adoption of solar technologies are also addressed to further enhance this practical approach, allowing to include, ex.g.,legal constraints in the Python tools used to determine how many panels one can install on a given rectangular roof.

3.1 Representative neighborhood typologies

Several typologies of grid connected neighborhoods exist in Switzerland, each adapted to its local reality. Categorizing them and studying the distribution of their main features allows focusing on aspects which are common across different parts of the country and might contribute to defining an archetype district to be studied in detail.

In order to derive a significant insight into the characteristics of district and hoods, the cases studies from the "Site 2000 Watts" certification scheme have been analyzed together with other data-sets taken from a variety of data sources, standards and norms.

In fact, as it is not a straightforward task to define representative typologies of energy systems at the level of districts or neighborhoods in Switzerland, a double approach was chosen to gain a deeper view on the subject. On one hand, a number of databases concerning sustainable districts and buildings were studied, while, on the other hand, the most relevant standards for sustainable districts were reviewed (see Katrin et al. (2021) for a comprehensive list).

Table 2 shows the list of building databases analyzed together with the relevant feature information retrieved, in particular concerning physical and geometrical aspects of interest useful to model the energy system and its interactions with its surroundings (orientation, height, external surface, etc..).

Table 3, instead, shows the list of standards and norms which have been reviewed, together with the relevant information retrieved from them. In fact, labels and certifications provide reference values and targets for consumption, space allocation, energy production systems, etc. They may include voluntary or compulsory requirements, as e.g. in the case of the Minergie standard (Minergie (2011)) and the MoPEC2014 (EnDK (2008)), respectively. A number of features and parameters of interest were selected in this way to define the energy system at the neighborhood level and facilitate the definition of case studies or application examples (see Figure 20).

An analysis of the projects certified under the scheme "Site 2000 Watts" and Minergie, together with the information included in the building cadaster of the Swiss confederation (RegDB), was performed to identify the features of interest when characterizing an energy system at a district level. The key findings from this study are reported below.

Table 2: List of databases and sources consulted to identify district features of interest.

Database	Collected Entries	Focus	Features of interest
Site 2000 Watts	41 entries	district	parcel surface; number of buildings; norm / label
Minergie buildings	20714 entries (2015 - 2022)	building	building use / allocation; Reference Energy Area
RegBL	ca 3M entries	building	building footprint; number of floors
MonToitSolaire / MaFacadeSolaire	ca 1M entries	building	orientation; roof tilt; surface available on roof or facades.

Table 3: List of standards and norms consulted to collect insight on typical district features of interest.

Type of standard / label	Denomination	Features of interest
Technical norms	SIA2040 - SIA Energy Efficiency Path	design rules, typical generating system layout, typical consumption
	SIA2032 - Embodied energy of buildings	typical energy content (transmission network)
	SIA2039 - Mobility - energy demand depending on the building location	typical consumption values for mobility
	SIA380/1 - heating requirements	technical installation features
Energy and performance governmental prescriptions	MoPEC2014	energy consumption targets
Volunteer building standard	Minergie	energy consumption targets
Sustainability label	Seed (one Planet Living), DGNB	space use, roof availability, soft requirements

Identified key features

Parcel surface area: The surface area of the parcel over which a district/neighborhood project typically extends has a median value of about 30000 m^2 (see Figure 21). This was established from 41 of the reviewed "Site 2000 watts" certified sites.

Most common building standard: If the most common standard adopted for new buildings is of the Minergie family, the most followed technical norms are SIA2040 (concerning energy efficiency) and SIA2039 (concerning mobility). Labels at the district level are more and more common, in particular those of the labeling schemes DGNB, SNBS and Seed, with requirements that go beyond energy efficiency or mobility planning, particularly including other voluntary initiatives to assess the living standard assured by the project.

Space allocation within a district: The buildings composing the districts can have a single or multiple use. Among those studied, districts are usually composed by several buildings with mixed usage and space allocation. Diverse building space allocation is in fact one of the requirements commonly found in labels and certification schemes related to the sustainability of a district. If districts are usually mixed, the same cannot

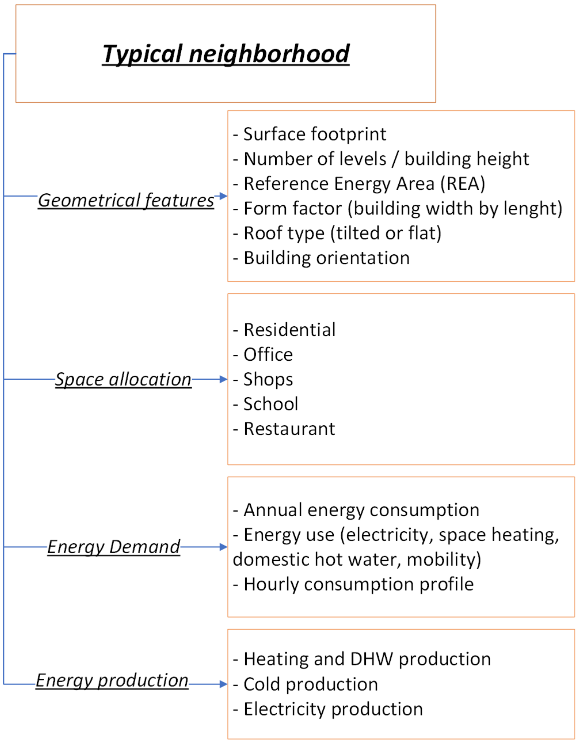

Figure 20: Several features of interest have been selected to describe a district with sufficient detail and be modeled in the context of the current project.

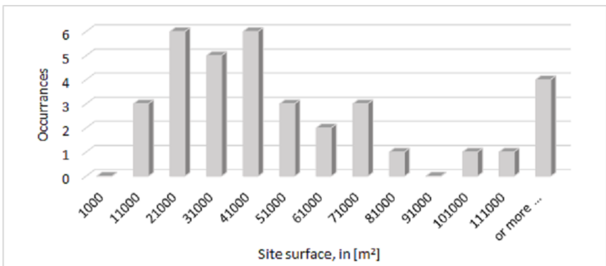

Figure 21: District parcel area distribution among 41 of the "Site 2000 watts" certified sites.

be said for the individual buildings composing the district. Across an available sample of 17000 Minergie buildings studied for the current project, the space use, in 75 % of the cases, is of the single type and the most common allocations by energy reference area are the following:

- Multi-family house (75 %);
- Offices & Warehouses (11 %);
- School (2.3 %);
- Shops & restaurants (0.5 %);
- Others (Sport facilities, Hospitals, Indoor swimming pools, special constructions - 11.2 %);

Number of building floors: Upon inspecting the Minergie entries and the RegBL database, it has been possible to group the available statistics in order to derive some information about the building geometry. The number of floors, in particular, supply useful information as the building height is a multiple of it. From Table 4, which shows the median value of number of floors and the Reference Energy Area (REA) among buildings based of their use category, it can be inferred that taller buildings have usually a variety of uses. The median value of the number of floors and the REA can be taken as references for the typical buildings of a representative district.

Table 4: Median value of number of floors and Reference Energy Area (REA) among buildings based on their use category.

Building Use Category	1 use; median REA [m^2]	1 use; median floors	2 uses; median REA [m^2]	2 uses; median floors	n+ uses; median REA [m^2]	n+ uses; median floors
Multi-family dwelling	1189	4	4619	5	22303	6
Warehouse	1499	3	678	4	3539	4
Single-family dwelling	255	2	567	3	302	4
Offices	2198	3	868	4	5883	5
Restaurant	627	1	587	4	1572	5
School	1040	2	1652	4	4126	4
Industry	2912	2	2499	3	19871	4
Shop	1353	2	1361	5	3184	6

The energy production system: In our statistical approach, we have evaluated that heat pumps, either equipped with geothermal probes (25 % of cases) or using groundwater (16 % of cases), are the most widespread heating generator type, followed by district heating which is used in 25 % of the cases. As expected, the cold production system in 40 % of the cases is absent, while the most widespread solution, when present, is based on geo-cooling and free-cooling. The electricity supply system, typically, is based on PV panel electricity production covering a variable fraction of the district consumption, together with origin certificates assuring the environmental quality of the electricity drawn from the grid to complement the latter. RCPs (Regroupement pour la Consommation Propre – i.e. producers / consumers consortia able to access the grid with their own MT infrastructures) are present in less than 10 % of the reviewed cases.

3.1.1 Identification and optimization of a typical representative district

The identification of features typical among district projects labeled for sustainability and efficiency has allowed the definition of a typical neighborhood or district which is representative of the Swiss building parc and which can be adopted as a benchmark or case study in the current project. Table 5 shows the main characteristics of a representative district, with features defined both at district and building levels. Consumption expectations drawn from EnDK (2008) for each type of building use and application are also shown. These results can be used to create an idealized typical district or to select a case of interest out of the real districts which have been investigated and which approach an idealized neighborhood. By using the latter approach, the project "Iam Lenz" has been considered as a show case to benchmark our numerical optimization approach. Given the large extent of the IamLenz district, made of 16 buildings, our idealized neighborhood considers only 10 of them, in order to increase the similarity with typical district described in section 3.

District Im Lenz The district Im Lenz is located in Lenzburg (AG) and it has received the 2000-Watt site certification. The 61500 m^2 site comprises around 500 Minergie-standard apartments, while also having a mixed space allocation, with significant areas for commercial activities and nursing homes. Composed by 17 buildings, the district adopts biomass to cover 100 % of its heat energy needs (90 % wooden chips; 10 % bio-gas) while origin certified hydro-electricity drawn from the grid satisfies the district electricity consumption.

Table 5: The identification of features typical among district projects labeled for sustainability and efficiency has allowed the definition of a typical neighborhood or district which is representative of the Swiss building parc.

District level	***Parcel surface***	Mid-sized: 30000 m²			Large: 60000 m²			
	Number of building	10						
	Usage	Mixed (61% Multi-family housing; 17% Warehouse; 7% single family housing; 3.6% offices; 3% Restaurant; 2% School; 2% industry; 2% shops)						
	Typical label	Minergie / SIA2040						
	Heating production system	Heat Pumps with 50% geothermal probes and 50% underground water						
	Cold production system	50% geothermal probes and 50% underground water						
	Thermally connected building	Yes if more than 500 MWh/ha						
	Electricity production system	PV production and labeled electricity from the grid						
Building level	***Usage type***	***Multi-family***	***Office***	***Industry***	***Shops***	***School***	***Restaurant***	***Units***
	REA	1189	2198	2912	1353	1039.5	1039.5	m^2
	N° of floors (single use)	4	3	2	2	2	2	-
	Max N° of floors (multiple use)	6	5	5.5	7	5	5	-
	Footprint	297	733	1456	677	520	520	m^2
	Roof type	flat	flat	flat	flat	flat	flat	-
	Form factor (facteur d'enveloppe)	1.3	0.8-1.8	1.8	1	1.2	1.5	-
	annual weighted energy cons. limit	35	40	20	40	35	45	kWh/m^2
Energy needs (Mopec2014)	***Heating***	13	13	10	7	14		kWh/m^2
	DHW	16	2		2	3	59	kWh/m^2
	Cold	0	18		48	10	36	kWh/m^2
	Ventilation (elec.)	1	4		5	4	11	kWh/m^2
	Auxiliary	13	19		6	5	50	kWh/m^2
	Lighting	2	7		30	5	49	kWh/m^2

As shown in Figure 22 for the district "Iam Lenz", it is possible to retrieve all information needed to create a case study centered around a mid-sized district heating, thanks to the data made available by open access tools, as those developed in the context of the OPEN initiatives "MonToitSolaire" and "MaFacadeSolaire" (https://www.uvek-gis.admin.ch/BFE/sonnendach/?lang=fr), or from the publicly accessible database of the Swiss building cadaster (RegBL). Once collected, data can be compiled as in Table 5 and used to model the district for the optimization process.

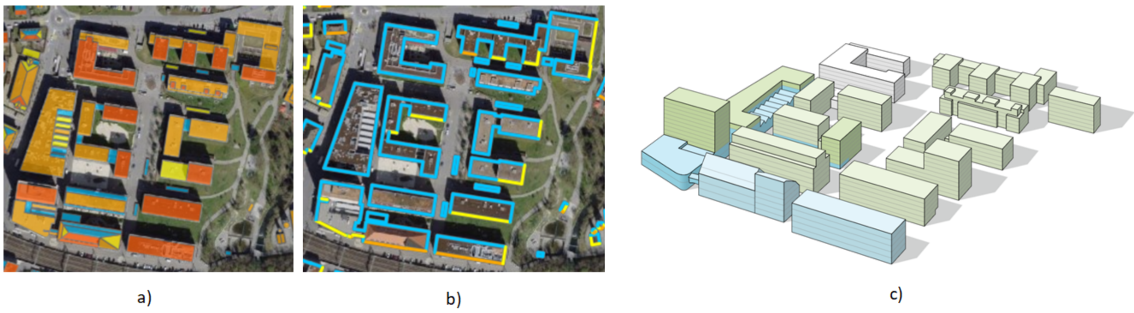

Figure 22: Layout of the district Iam Lenz: a) and b) show the useful solar roof and facade surfaces, respectively, while c) shows the location and shape of the district buildings.

An idealized Swiss district The typical Swiss neighborhood has been defined in section 3 based on different approaches. Based on the features listed in table 5 and some of the main characteristics of the district of IamLenz, an idealized district has been defined as a benchmark for the current analysis. The base-case, in particular has the following features:

- The parcel on which the district is built has an extension of about 30000 m^2.
- The district is made of 10 buildings.
- Each building features a single use/allocation.
- 8 buildings have a multi-residential use and 2 buildings are used as offices
- The main energy production system is based on a district heating network, supplied by ground-water source or geothermal heat pumps.
- The district features mainly flat roofs and one building with slanted roof.
- An internal electricity network allow the district buildings to share consumption and PV production (if present);
- No solar surfaces are installed on the roofs, but certified electricity is bought from the grid.
- Electricity is fed from the grid under normal tarif fares, including energy, transportation and taxes.

Figure 23 shows a 3D representation of the buildings included in the analysis, produced with the help of City Energy Analyst, an open-source tool for urban design and energy system engineering (see []). The input table to be included in the "Hood" tab of the OptiHood Excel scenario file in order to provide the main geometrical features used in the optimization, is shown in Figure 24. Values which are input are the following:

- Building orientation (i.e., direction of the building short side; expressed based on the convention that North is 0°, East is 90°, South is 180° and West is 270°).
- latitude and longitude of the center of the roof;

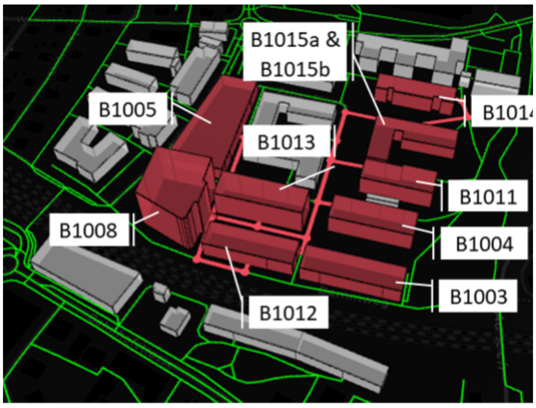

Figure 23: 3D representation of the benchmark district.

	A	B	C	D	E	F	G	H	I	J	K	L	M
1	building	latitude	longitude	bld_orientation	short_side	long_side	busy_area	pv	solarCollector	pvt	Roof_tilt	Roof_Ridge	Bld. ID
2	1	47.3915	8.1737	120	40	85	250	1	1	1	0	S	B1005
3	2	47.3909	8.1735	190	40	40	300	1	1	1	0	S	B1008
4	3	47.3905	8.1752	190	15	65	300	1	1	1	0	S	B1003
5	4	47.3909	8.1753	190	17	57	50	1	1	1	0	S	B1004
6	5	47.3915	8.1753	110	15	39	50	1	1	1	0	S	B1015
7	6	47.3915	8.1758	190	15	39	50	1	1	1	0	S	B1015
8	7	47.3906	8.1741	190	19	60	150	1	1	1	40	L	B1012
9	8	47.3909	8.1742	190	19	60	50	1	1	1	0	L	B1013
10	9	47.3912	8.1755	190	17	50	50	1	1	1	0	L	B1011
11	10	47.3919	8.1756	190	11	58	150	1	1	1	0	L	B1014

Figure 24: Scenario file input tab for hoods.

- The building short-side and long-side length, in [m];
- The "busy area" (expressed in [m^2]), which identifies the roof extension which cannot be used for panel installation.
- A boolean value specifying if the building adopts PV, ST and/or PVT technology on its roof.
- The building roof tilt (0 for flat roof, roof tilt for slanted roof).
- The roof ridge direction, along the long side of the roof (L) or the short one (S), needed to identify the roof rafter orientation and to identify on which side of a slanted roof to install panels (neglected for a flat roof).

The indication of which solar technology is available for each building, allow the solar pre-processing tools to create the different scenarios of solar technology deployment, which are then written in the "Solar" tab of the input scenario file to be included in the optimization process.

3.2 Boundary conditions for the use of solar technologies

The adoption of solar technologies depends, among other things, on the regulatory framework and roof space availability. The roof area is contended for several conflicting uses and the available surface is constrained by several factors. To identify the constraints imposed on the adoption of solar technology, we again referred to the prescriptive models included in MoPEC2014 but also to the voluntary initiatives foreseen in the context of the sustainability labels issued by various organizations. Safety constraints derived from the SUVA guidelines for professional activities on building roofs were also taken into consideration.

Competition for the solar resource on roofs

Regulation for the adoption of energy supply solutions based on photovoltaic panels or thermal collectors has improved over the years. Several initiatives exists at the federal and cantonal level to promote the adoption of solar technologies, as a regulation imposed by some of the cantons to install a minimum of 10 W per m^2 of REA in new building constructions (EnDK (2008)), or to offset a certain fraction of own electricity consumption by renewable energy production.

Yet, the increase in solar installations, together with the increasing adoption of roof gardening solutions in new environmentally-friendly districts, has augmented the competition for installation space at the roof level. Roof gardens and solar installations need to be combined on top of the buildings (see Figure 25) as more and more cantonal authorities are imposing them for new buildings (as in Neuchatel) or even during renovation (as in Bale, Bern, Zurich, Lucerne, St.Gallen, etc.).

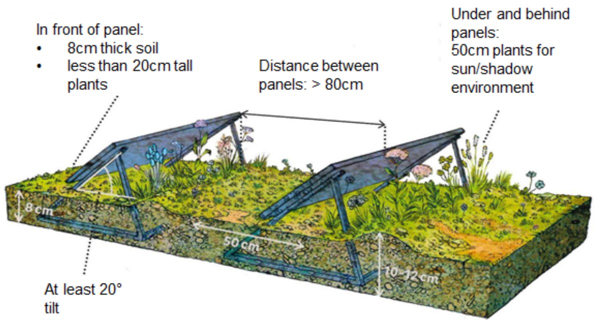

Figure 25: Garden and solar installations can be combined on building roof to satisfy local regulations (SPADOM).

This has to be further combined with the restrictions on the available surfaces imposed by the work-place safety, which requires, e.g., minimum escape distances from roof entrances, minimum passageways for maintenance or surfaces reserved for individual or collective protection (see SUVA et al. (2022) and SUVA (2022)). All these elements contribute in reducing the space available for the installation of solar fields on building roofs, and they need to be taken into account when estimating the maximum available area for the installation of solar panels on a given building (e.g, see Figure 26, taken from SUVA et al. (2022)).

The python class "weather" and "calepinage", developped in the framework of the project to pre-process building data, can take into account the possible coexistence of gardens and solar installations on building roofs, through the input parameter "busy area" of the "hood" tab in the scenario file. This type of constrain reduce the available space for installation, while safety distances and inter-rows pathways are established according to the best practices foreseen by the branch.

Heating networks availability and solar thermal energy

The availability of heating networks servicing the buildings in a district depends on several factors, encompassing both economical and technical aspects. In fact, even if the installation of a thermal network connecting all the buildings of a same district could seem beneficial to improve the efficiency of the energy system, the same initiative could be detrimental (or simply unrealistic) from the economical point of view. It is clear, then, that some indicator has to be derived to differentiate those cases where a district heating network is unrealistic or uneconomical from those for which DHN solutions are feasible. To achieve the latter goal, we consider the urban DHN to be economical if the local customer base features a minimum density of more than 500 MWh/$(y \ \ ha)$ of energy needs (Quiquerez (2017)). This limit figure can also used to check if a district heating based solution is feasible for a given project to confirm the soundness of the optimization results.

If a district heating network is feasible, or present, then it might also be interesting to consider solar district

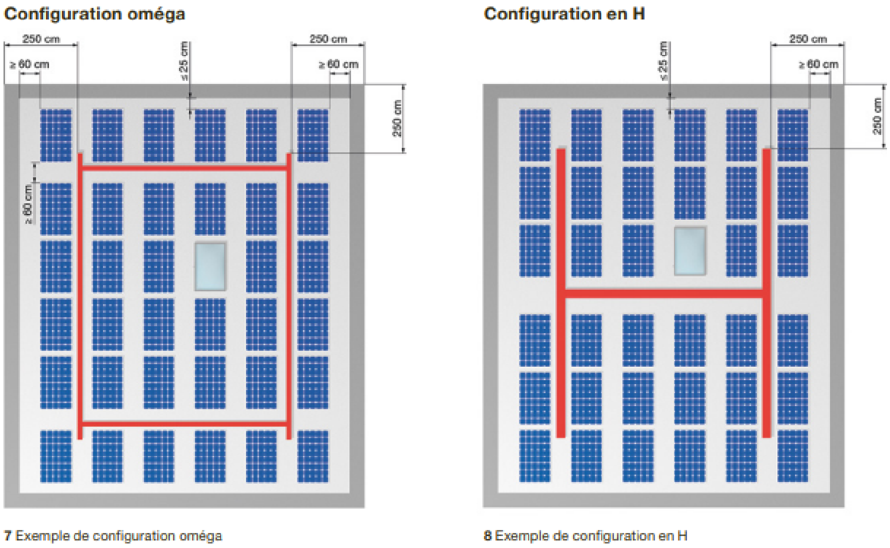

Figure 26: For a given building roof, a portion of the available space has to be reserved for maintenance and safety issues (image taken from SUVA et al. (2022))

heating as a possible type of integration of the solar energy at the district level. Based on previous work (see Diane et al. (2021)), solar district heating can be considered a viable solution to supply renewable heat to the district if, e.g., conditions similar to the followings are met:

- summer energy needs are larger than 17 MWh/y;
- the DHN features temperatures lower than 90°C;
- the viable distance between solar field and DHN is less than:
  - 170 m for fields with surfaces up to 500 m^2;
  - 500 m for fields of more than 1500 m^2.

Boundary conditions on roofs

The increase in solar installations, together with the increasing adoption of roof gardening solutions in new environmentally-friendly districts, has augmented the competition for installation space at the roof level. Roof gardens and solar installations need to be combined on top of the buildings (see Figure 25) as more and more cantonal authorities are imposing them for new buildings (e.g. Neuchatel) or even during renovation (e.g. Bale, Bern, Zurich, Lucerne, St.Gallen, etc.).

This has to be further combined with the restrictions on the available surfaces imposed by the work-place safety, which requires, e.g., minimum escape distances from roof entrances, minimum passageways for maintenance or surfaces reserved for individual or collective protection (see SUVA et al. (2022) and SUVA (2022)).

The features and characteristics of flat roofs have been revisited in order to derive a condensed table providing the most important indications relating to the combination of PV panels and garden surfaces on building roof. The resulting features are shown in Figure 27.

	PV on flat roof	PV integrated on garden roof
Inter-distance between panel rows	Based on row inter-shadowing at noon on winter solstice.	Based on living space required by garden roof vegetation.
Distance to roof edge	> 60 cm (if pathways) > 25 cm (if no circulation / pathway)	
Panel tilt	Free (at least > 1% to enhance rain cleaning).	> 20° (to leave vital space for plants)
Ballast	Ballast or roof hooks computed accoring to SIA 261.	Roof garden soil (8 cm in front of PV, 10-12 cm on the back, >50 cm in width) – assessment with SIA261 required.
Operating costs	2-6 ctsCHF/kWh$_e$	For garden roofs: add 0.5 ctsCHF/kWh$_e$ [x]
Vegetation heights	n.a.	< 20 cm in front; <50 cm on the back.

[x] «Couts d'exploitation des installations photovoltaïques», Suisse énergie, Article Numéro 805.523.F

Figure 27: Main features to be taken into account in the planning phase of a flat roof solar installation with or without vegetation or gardening.

4 Operation optimization

Smart operation strategies could help in optimally utilizing the synergies between the buildings in a neighborhood. Such strategies incorporate flexibility by allowing the energy systems to react to the fluctuations in price and carbon emissions. To analyze the potentials of this approach, we use a model predictive control (MPC) combined with a digital twin of the energy system. This digital twin represents the real performance of the neighborhood and it has been implemented in pytrnsys using TRNSYS as the computational engine.

Overall, all systems (real or simulated) that have some kind of control algorithm follow a basic scheme: the environment provides status variables (mainly temperatures when it comes to thermal systems) and the control makes some decisions that are then applied to the system via some actuators (valves, pumps, machines, etc.). This scheme can be applied to an MPC too.

The following section will introduce the model that has been used as system representation in TRNSYS. After that, the base case scenario control strategy (the rule-based control) will be explained. Finally, the section concludes with a description of the developed Model Predictive Control (MPC) approach.

4.1 System representation in TRNSYS environment

The model that has been implemented in TRNSYS aims to represent the real behavior of the system; it will work as a digital twin of the system whose performance optihood will optimize. These TRNSYS simulations have been conducted by making use of the open-source python-based package called pytrnsys[13]. This package allows the user to automate and simplify the preparation and post-processing of TRNSYS simulations.

The pytrnsys package also includes a visual interface in which the user can represent the hydraulic connections of the main components of the system. In Figure 28, a snapshot of this interface illustrating the hydraulic diagram of the considered district heating system is shown. The system that will be used to test the operation optimization is a district heating system with three buildings and includes a centralized solar collector field and an ice storage.

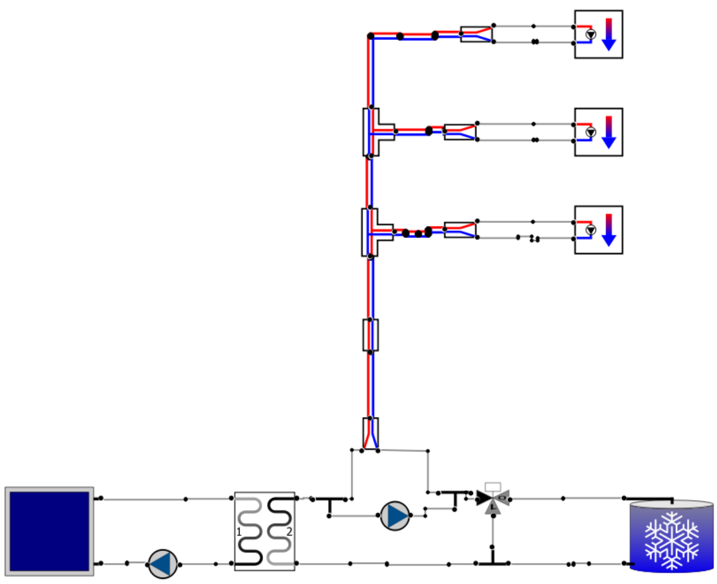

Figure 28: Hydraulic diagram of the district heating system.

[13]https://github.com/SPF-OST/pytrnsys

The centralized solar collector field (on the bottom left-hand side) is the heat source for the whole system. The ice storage (which is centralized, as well), that can be seen on the bottom right-hand side of the diagram, works as a seasonal storage. The ice storage is located in the coldest point of the system (the return of the district heating network) and offers a higher specific storage capacity compared to sensible water since it exploits the latent heat of water. The three squares on the top represent the three buildings. The lines that connect the components denote the pipes. The red/blue connections represent the double buried pipes (flow/return) for the DH. The centralized systems works on brine.

For the buildings, even though a single symbol is visible in Figure 28, each box represents the whole heating system of a building, which include the SH and DHW production systems. The heating system of these buildings consists of a brine-source heat pump connected to the district heating network, two hot water tanks (for SH and DHW) connected to the outlet of the heat pump and a radiant floor (which will heat up the building itself). Furthermore, the electric system of each household has a PV system for electricity generation and a battery for storage.

A schematic representation of the hydraulic system of each building is shown in Figure 29. Each building has a compression heat pump that raises the temperature of the water coming from the district heating network. The evaporator of those heat pumps (the heat source) is connected to this network, while the condenser (the heat sink) supplies heat to the water tanks.

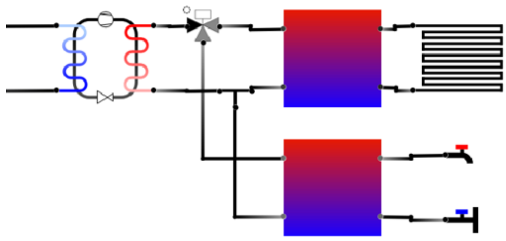

Figure 29: Hydraulic diagram of the buildings.

To summarize, the district heating network has a heat source (the solar collectors), a storage (the ice storage) and heat sinks (the three buildings). The heat produced by the collectors can be delivered to the buildings and/or accumulated in the ice storage. When there is not enough radiation, the demands will extract heat from the storage.

The ice storage is meant to be a seasonal heat storage in the context of this district heating network (DHN). That is, it will accumulate heat coming from the solar collectors in summer months. When the heating season comes, heat will be extracted from the storage in order to fulfill the demands of the three buildings. In this process of heat extraction, at a certain point, ice will be formed inside the storage. When the heating season is over, the ice storage gets regenerated (melted) again by the heat coming from the solar collectors, closing the cycle. The ice storage, even though it is sized to work as a seasonal storage, is, of course, able to provide heat for smaller fluctuations: for example, it stores heat during daytime and provides energy at nighttime.

Overall, a system simulation like the one that is being presented consists of two main parts: the modeling of the components and the control algorithm that decides how these components should operate. In TRNSYS, the mathematical models are included in "types": encapsulated binary files that reflect the performance of a specific component. In 4.1.1, an explanation of these components has been presented.

The definition of the control algorithms will be introduced in sections 4.1.2 and 4.1.3. In the former, the base case scenario will be defined (the rule-based control); whereas in the latter, the novel model predictive control (which makes use of the optimizer) will be presented.

4.1.1 System components

As mentioned, the district heating system that has been simulated consists of three main components: the solar collectors, the ice storage and the buildings. When talking about the buildings, we are referring to their thermal (space heating (SH) and domestic hot water (DHW) demands) and electric performance.

The solar collectors have been modeled by making use of the type 1 of TRNSYS. This model is based on a quadratic efficiency curve with three coefficients for the constant, the linear and the quadratic terms. The solar collector area is sized considering the total thermal demand of the system, which is in the order of 320 MWh. By applying a factor of 2 m^2/MWh, the total solar collector area has been sized to a value of 640 m^2. With this amount of solar collectors, no other auxiliary sources (as electric rods in the water tanks) are necessary to fulfill the SH and DHW demands of the buildings.

For the ice storage, a self-made type has been implemented; introduced in Carbonell et al. (2018). Mass and energy conservation laws are applied for the formulation of this storage. The coupling to the ground is also considered in the model using the approach followed in Carbonell et al. (2016b). The ice storage has a volume of 200 m^3, a sizing decision that is based on the total thermal demand of the system, since a factor of around 0.6 m^3/MWh has been used.

Another self-made type (the type 977) has been used to model the heat pumps. The model was introduced in Carbonell et al. (2016a) and it basically consists of two pairs of second-degree polynomial equations, as shown in 36 and 37.

$$Q_{cond} = a_0 + a_1\overline{T}_{evap} + a_2\overline{T}_{cond} + a_3\overline{T}_{evap}\overline{T}_{cond} + a_4\overline{T}^2_{evap} + a_5\overline{T}^2_{cond} \tag{36}$$

$$COP = b_0 + b_1\overline{T}_{evap} + b_2\overline{T}_{cond} + b_3\overline{T}_{evap}\overline{T}_{cond} + b_4\overline{T}^2_{evap} + b_5\overline{T}^2_{cond} \tag{37}$$

with:
- $\overline{T}_{evap}$: Normalized temperature in the evaporator
- $\overline{T}_{cond}$: Normalized temperature in the condenser
- Q_{cond}: Delivered heat in the condenser
- COP: COP of the heat pump
- $a_{0...6}$: Coefficients to calculate the delivered heat in the condenser
- $b_{0...6}$: Coefficients to calculate the COP of the heat pump

Connected to the condenser of this heat pump, we can find the two water tanks: the one for DHW and the one for SH. The heat pump delivers hot water to one of the thermal energy storages by making use of a diverging three-way valve. The model that has been used for these tanks can be found in Carbonell et al. (2016a) and it is an extension of the plug flow model, which considers stratification.

The SH tank supplies water to the radiant floor (type 1792), which is the heat distribution method that has been selected for the simulations. The radiant floor is at the same time connected to a thermal model of a building. For the simulations that have been carried out in SolHood, type 5998 is used to represent the thermal behavior of the buildings. This type is based on ISO 13790 and considers a thermal equivalent circuit of the building, with two capacitors and five resistances.

In Iturralde et al. (2019), the thermal demands of two multifamily buildings were described. One of them has a yearly demand of 90 MWh/m^2 for a central European climate like Zurich; while the other one (with better insulation), has a demand of 30 MWh/m^2. The coefficients of the previously mentioned buildings have been implemented, as well as another one whose thermal performance is in between the other two.

The first building has a total yearly SH demand of 127 MWh, the second one 87 MWh and the third one 44 MWh. The three buildings have the same DHW demand profile of 17.4 MWh. Due to the differences in demands for SH, the sizing of the heat pumps differs from building to building leading to nominal capacities of 110 kW, 82 kW and 33 kW respectively.

The buildings have 200 m^2 of the roof area dedicated to PV panels for self-consumption purposes, which gives a PV installation with a nominal power of 35 kW. The type 194 from TRNSYS has been used to model the PV performance. Alongside the PV panels, the buildings have an electric battery to store the excess of electricity that is produced but not consumed instantaneously.

In Table 6 and in Table 7, the most important parameters of the main components of the system have been presented as a summary. In the first table, the main parameters of the centralized components and the parameters that are common for all buildings appear. In the second, one specific parameters that are building-dependant can be seen.

Table 6: Summary of the main parameters of the system.

Component	**Parameter**	**Value**	**Unit**
Solar collectors	Area	640	m^2
Ice storage	Volume	200	m^3
DHW tank	Volume	1.25	m^3
SH tank	Volume	10	m^3
PV panels	Peak power	35	kW
Battery	Nominal capacity	50	kWh
Electricity demand	Yearly demand	18 913	kWh

Table 7: Summary of the main parameters of the buildings.

	Building 1	Building 2	Building 3
Yearly SH demand (MWh/m^2)	108.7	71.80	36.41
Heat pump nominal capactiy (kW)	109	86	40

4.1.2 Rule-based control

Rule-based controls are based on relatively simple if-then conditions. When those conditions are fulfilled, the controller activates (or deactivates) a certain response in an actuator. With regard to our hydraulic system, those actuators will be pumps, three-way valves and the activation (on/off) of the individual heat pumps. Specifically, these are the actuators present in the system:

- The pump of the centralized solar collectors
- The three-way valve of the centralized ice storage
- The activation and deactivation of the brine-source heat pumps (x3)
- The three-way valves that choose the connection of the outlet of the heat pumps to the one of the tanks (x3)
- The bypass valves between the district heating connection point and the tanks (x3)

Next, the rules that define the functioning of each element will be defined. As mentioned, under this kind of control, the actuators are controlled by if-then conditions or rules.

The pump of the solar collectors considers two conditions for its activation: the horizontal solar irradiation must be higher than 100 W/m^2 and the outlet temperature of the collectors must be 5 K higher than the inlet temperature of the demand side of the heat exchanger. Both conditions must be met at the same time to activate the pump.

The ice storage has a maximum ice fraction of 0.8. That is, when the mass of ice inside the tank covers more than 80 % of the total mass, the three-way valve bypasses the ice storage, which is usual practice to avoid damaging the vessel due to the ice expansion. If that is not the case, the ice storage is always connected to the return of the district heating network.

The brine-source heat pumps inside the individual buildings consider the temperatures of the SH and DHW tanks. For SH, the set-point temperature change from building to building. The building with the highest SH demand has a set-point of 40 °C, the intermediate one 35 °C and well-insulated one 30 °C. For DHW, the three buildings have a set-point of 55 °C.

With a dead-band of ± 1 K for these temperature set-points, the controller activates or deactivates the heat pump. That is, for example, when the temperature at the DHW tank goes below 54 °C, the heat pumps starts working and the three-way valve is connected to the corresponding tank. When the temperature surpasses 56 °C, it stops. The same principle is applied to the SH tank. When both demands happen at the same time, the system prioritizes the production of DHW.

When solar irradiation is high and the thermal demand of buildings is low, such as during summer, the district heating water may reach temperatures sufficient to bypass the heat pump. During these periods, solar availability is abundant, and space heating demand is negligible, leading to elevated temperatures in the district heating network. Consequently, when the inlet temperature of the heat pump reaches the set-point for domestic hot water, the heat pumps are deactivated and bypassed, allowing the district heating water to be directly supplied to the thermal energy storages.

The PV panels will generate electricity that will supply the electricity demand of the household in the first place. Afterwards, the electricity consumed by the compressor of the heat pump and the circulation pumps will be targeted. The connection to the electricity grid will make sure that the demand is covered when the electricity coming from the PV panels is not enough. At the same time, when there is surplus of PV production, it will be stored in the battery for later consumption by the household.

4.1.3 Model predictive control

The MPC that has been designed and implemented in SolHood is a more advanced technique to control the system. It no longer considers individual components separately, but the system as a whole with a concept schematically represented in Figure 30. At this point, it is important to remark one of the key features of this scheme: the difference in the time steps for both software environments. The simulation in TRNSYS has a time step of 2 minutes, which is considered to be an appropriate value for yearly simulations for thermal systems. Smaller time steps would slow down the simulation; whereas bigger ones would cause divergences from the real system we are depicting and may cause potential convergency problems within the TRNSYS simulation.

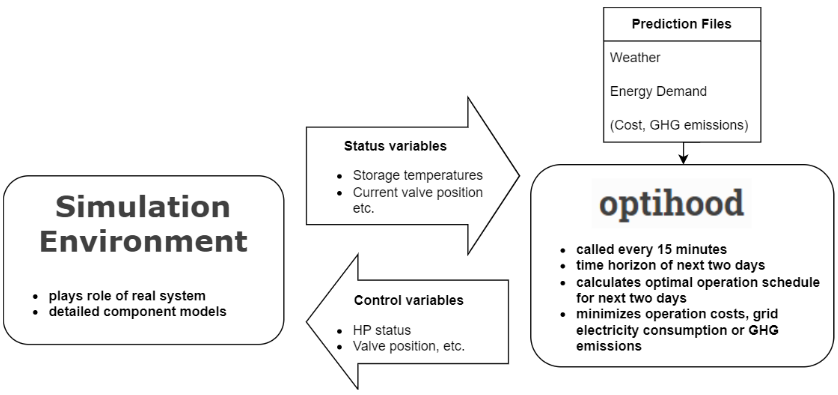

Figure 30: Schematic representation of the MPC framework.

The detailed TRNSYS environment would invoke optihood framework every 30 minutes to run an optimization in dispatch mode with a forecast horizon of 24 h. From a theoretical point of view, the longer the horizon, the better the results of the optimizer will be. However, forecast horizons longer than a day are not realistic, since the electricity price forecast is not possible due to the functioning of the electrical market. Also, the weather forecast uncertainties increase with the time horizons.

The goal of the optimization could be to minimize the operation costs, grid electricity consumption or GHG emissions. However, in the framework of SolHood, the system will be optimized to minimize only costs. The operation costs would arise from the use of primary energy sources for the production of electricity/heat. For example, use of grid electricity would incur higher operation costs in contrast to using PV electricity. In general, the operational costs and emissions are linked to one another. Renewable technologies such as PV and solar thermal benefit from cost-free operation, and likewise produce zero emissions during operation. Whereas, using natural gas or grid electricity adds to the operation cost and also to operational GHG emissions.

For this matter, the simulation environment would need to formulate the optimization problem for optihood, including definition of boundary conditions (cost, impact, weather and energy demand). For the initial simulations, we consider perfect predictions of the weather, energy demand and grid electricity impacts. This is an idealization and the improvements in KPIs due to MPC will, hence, represent the maximum possible improvement. Additionally, the status variables of technologies, e.g. storage temperature, would also need to be exchanged between optihood and the simulation environment. Once the optimization is complete, the results from optihood are used to set the control variables within the simulation environment acting as a digital-twin.

The optimizer (optihood) returns the control variables (as shown in Figure 30), based on which the simulation environment decides how the system should be operated in the next time step until new control decisions are provided, that is, after 30 min. Some key aspects which could be adapted when optimizing the operation of an energy system in a neighborhood are listed below:

- Heat pump management
  - Operate heat pumps when PV electricity is available or grid electricity is cheaper (or comes with low emissions). Such systems can then also react to variable electricity tariffs (or CO_2 impacts). This operation is possible if thermal energy storages capabilities are present.
  - Operate heat pumps when they are efficient, i.e. when the source temperature is higher.
- Thermal energy storage management
  - Avoid charging the storages with a heat pump if the demand prediction doesn't require it and/or if PV or solar thermal energy production is expected soon. This way one can reduce use of grid electricity, storage energy losses and increase the PV self-consumption.
- Room temperature management. This feature is not used in SolHood.
  - If the MPC is used also for controlling the indoor room temperature, then the required flow temperature to the heating distribution system can be controlled better, thanks to the anticipation of the heating loads.
  - One can also relax the comfort constraints and allow the room temperature to be in a larger range. This allows the optimizer to optimally shift loads using the building thermal inertia as an extra (and cost free) storage capacity and thereby reduce costs or emissions.
- Battery management
  - Use electricity from the battery when grid electricity is expensive or has high CO_2 emissions.
  - If the tariff or the CO_2 impact of grid electricity is low, then the MPC can decide to charge the battery with grid electricity (if PV production is not anticipated) and use it later when the tariff is higher.
  - Store PV electricity in battery when the demand is less than the PV production. The optimizer could choose whether to feed in the overproduction from PV or to store it in the battery for later use.

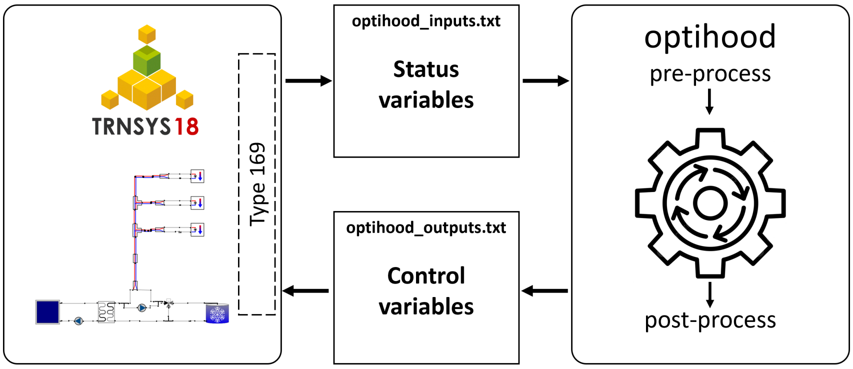

Figure 31: Block diagram of the connection between TRNSYS and optihood

As it can observed, the optimizer only takes care of the energy flows through the components of the three individual buildings; the centralized solar collectors and the ice storage are not part of the optimization process. This decision can be justified by the nature of the ice storage itself. In our system, the ice storage works as a inter-seasonal storage. That is, the thermal energy that is stored during warm seasons is then consumed in the heating season (when the temperature of the tank drops and it freezes). However, due to the limited forecast horizon of the optimizer (1 day), optihood cannot foresee this effect. Theoretically, if the inter-seasonal nature of the ice storage wants to be exploited by the optimizer, much longer forecast horizons would be needed. Nevertheless, stretching the horizon to such extremes is not at all realistic: it is not feasible to forecast the weather conditions, the electricity price or the heating demands for more than a few days.

Thus, for the control of the centralized heat production and storage, the previously implemented rule-based control will be used.

4.2 Co-simulation framework

The co-simulation framework between TRNSYS and optihood is a central feature of the simulation framework that has been used during this project. As mentioned previously, the TRNSYS simulation represents the real behavior of the system. The role of optihood is to optimize the performance of the system to provide the control decisions for the upcoming timesteps.

The fundamental concept of this connection is illustrated in Fig. 31. To explain the integration between the two software environments and further elaborate on the block diagram, the specific connection type employed will first be introduced, as it inherently determines the connection method. Subsequently, the connection will be analyzed from the perspective of optihood, followed by a discussion of the implementation and modifications made in python.

4.2.1 Type 169 in TRNSYS

The connection between optihood and TRNSYS is made using type 169, which is part of the main TRNSYS library (i.e., it is not a self-made development). This type creates a connection with python with two intermediate files that are used to exchange information between the two environments. The basic inner structure of the type is as follows (applied to the project and its objectives):

1. Write `optihood_inputs.txt` with the status variables
2. Run the python file that performs optimizations using optihood and saves the results
3. Read `optihood_outputs.txt` for obtaining the control variables

4.2.2 Optimization setup for optihood

The other part of the co-simulation framework (optihood with its corresponding pre- and post-processing stages) requires a more coding-intensive approach. First of all, it must be considered that optihood needs the so-called "scenario file" to optimize (described previously in Section 2.1). In this scenario file, we define the system itself: the components that are present, how they are connected to each other, their sizing and their initial state (e.g. initial storage SOC). If a single optimization is desired, a unique definition of this scenario file is sufficient. The user defines this input file and optihood optimizes the energy flows between the components over a pre-defined time window.

However, in the operation optimization workflow, optihood is called multiple times in intervals of 30 minutes to optimize the system. During each optihood call, the state of the system changes and the scenario file must be updated accordingly. Once the scenario file is updated, the optimization could then be carried out. The optimizer calculates the optimum energy flows between the components for the next 24 h (also called horizon) in order to minimize the cost. As a result, it gives a matrix of these energy flows at an hourly time resolution with the selected horizon. Due to the use of simplified linear models within the optimizer, the real behavior of the system (represented by the TRNSYS simulation) will never exactly match the optihood predictions. Because of these differences, the optimizer is called every 30 minutes, which results in only the first time step of the matrix to be considered.

The results of the optimization include the energy flows between components. These energy flows, however, cannot be directly applied to the TRNSYS simulation. Just like any other simulation, the model that is implemented in TRNSYS requires control variables. Thus, a post-processing of the results is necessary to convert these energy flows into variables for the actuators of the system. Also, it must be considered, that optihood does not recognize temperature values for tanks: they must be converted into State of Charge (SOC) values by the following equation:

$$SOC_{tank} = \frac{T - T_{min}}{T_{max} - T_{min}} \tag{38}$$

with:

SOC_{tank}:	SOC of a sensible water tank
T:	Actual temperature of the water tank
T_{min}:	Temperature level at which the water tank is considered empty
T_{max}:	Temperature level at which the water tank is considered full

In summary, the Python interface script invoked by TRNSYS executes to the following workflow:

1. **Import State:** Read the system status variables from `optihood_inputs.txt`.
2. **Pre-processing:** Process the status variables.
3. **Scenario Update:** Update the input scenario configuration for optihood.
4. **Optimization:** Run operation optimization using optihood.
5. **Post-processing:** Extract the relevant optimization results.
6. **Export Control:** Write the derived control variables to `optihood_outputs.txt`.

5 Results and discussion

5.1 System design optimization

Meteorological data and energy demand profiles

Together with the geometrical features of the buildings included in the idealized district under analysis, the meteorological data and the energy demand profiles have to be generated. For the base case, the data of the weather station of Buchs-Aarau is chosen, since it is, according to the SIA2028, representative of the climatic region 4, central plateau. The historical weather data are combined and the hourly profiles for the Typical Meteorological Year are obtained. Moreover, the energy demand profiles have to be included in the analysis. To derive the profiles for the reference district, City Energy Analyst is employed: the energy demand for electricity, space heating and domestic hot water production is computed for each building based on details for building geometry, use and construction standard; the effect of surrounding buildings; local meteorological conditions and occupancy schedules based on SIA2028. By combining the energy demand profiles of each building, the aggregated profiles for the district can be derived, as shown in Figure 32 for the total district energy demand due to electricity consumption for appliances and lighting, 33 for the total electricity demand for auxiliary and , and 34 for the aggregated space heating and domestic hot water preparation. The table shown in Figure **??** details the specific energy demand of each building considered in the current analysis, together with the reference energy area, the type of use, the number of floors and the envelope standard of each building. This latter parameter is used to to specify the constructive features that have an impact on the energy performance of the district buildings (See [The CEA team (2024)]). For the current analysis, the construction year of the selected buildings was used to derive the correct building envelope standard to adopt in each case.

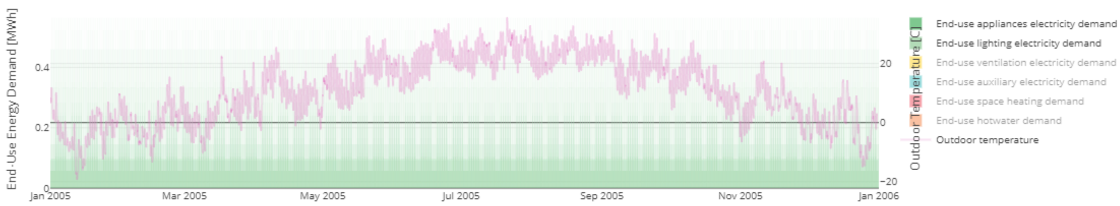

Figure 32: Aggregated load curve for the district electricity demand due to lighting and appliances .

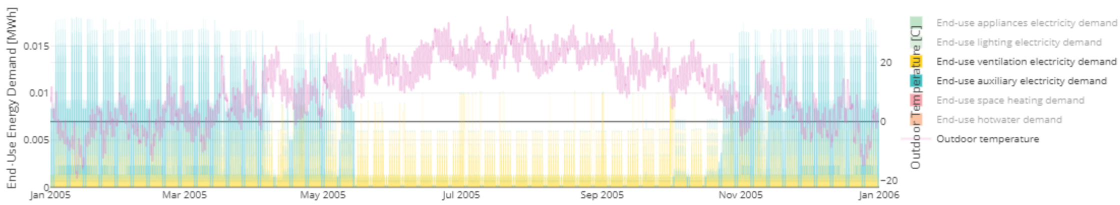

Figure 33: Aggregated load curve for the district electricity demand due to ventilation and auxiliary services.

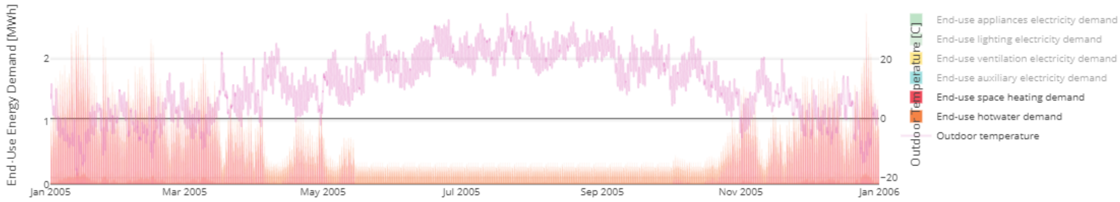

Figure 34: Aggregated load curve for the district energy demand due to space heating and domestic hot water preparation.

Table 8: Building characteristics, energy demand, and envelope classification.

Bld. ID	**Use**	**Bld. envelope class**	**N. of Floors**	**Energy reference area (m^2)**	**Specific electricity demand (kWh/m^2)**	**Specific SH demand (kWh/m^2)**	**Specific DHW demand (kWh/m^2)**
B1005	Multi-residential	Standard2	3	10200	21.5	37.5	19.5
B1008	Multi-residential	Standard5	13	20800	21.9	27.5	20.5
B1003	Office	Standard6	5	4875	59.3	0.5	3.2
B1004	Multi-residential	Standard5	6	5814	22.7	28.3	21.3
B1015	Multi-residential	Standard5	4	2340	25.1	32.2	23.5
B1012	Office	Standard5	5	5700	46.9	16.4	2.5
B1013	Multi-residential	Standard5	8	9120	20.9	27.1	19.5
B1011	Multi-residential	Standard5	6	5100	21.5	28.6	20.1
B1014	Multi-residential	Standard6	5	3190	28.1	10.5	26.5

Optimization of a centralized district energy system

As mentioned, the typical heat generator found in districts recently built in Switzerland are mainly based on heat pump technology. Depending on the existence of a heating network linking the district buildings, the installed energy system solution is usually based on air-source-heat pumps, in the case without heat distribution network, or groundwater/geothermal heat pumps, if a district heating is present. This is mainly due to the fact that the heating capacities featured by large commercial air-source heat pumps are still limited to about 400 kW. Moreover, groundwater/geothermal heat pumps, even if more expensive than the air-source type, feature a larger COP. The higher price of the technology can be better justified in the case of large installations, for which the advantage in COP has a sizable impact, rather than in cases requiring smaller capacities. The costs of the low temperature energy source, moreover, has a stronger impact on smaller systems than on the larger ones.

A base case scenario is assumed as reference, in which an internal district heating network supplied by a geothermal heat pump is the only district heat generator. In this case, the energy system has been assumed to be equipped with a stratified storage tank sized by the optimizer for cost. No solar installations are present and an internal grid gather the district buildings in a consumption community, enabling the district to access the electricity tariff reserved for commercial consumers (or, in other cases not covered in the current study, access directly the electricity market trough their own electrical infrastructure). Table 9 shows the energy balance of the district buildings and heat generator, while table 10 presents the annual key values for the base case. These values can be adopted as benchmark values for the evaluation of the optimization results.

Table 9: Energy demand and production for the base case with district thermal and electrical grids.

Entity	SH	DHW	Electricity	Unit
Building 1	382819	198669	219476	kWh/y
Building 2	33604	84630	89513	kWh/y
Building 3	571365	425549	455426	kWh/y
Building 4	2251	15708	289024	kWh/y
Building 5	164627	123647	131944	kWh/y
Building 6	75311	54919	58659	kWh/y
Building 7	75311	54919	58659	kWh/y
Building 8	93557	14457	267381	kWh/y
Building 9	246829	178262	190672	kWh/y
Building 10	146065	102636	109473	kWh/y
District end-use consumption	1791741	1253397	1870228	kWh/y
GWHP	1791741	1258646	1383802	kWh/y

Table 10: Summary values for the base case of the district supplied by a GSHP on a district network.

Parameter	Value	Unit
GWHP Heat Production	3,051,809	kWh/y
GWHP seasonal COP	2.21	-
GWHP capacity	1,108	kW
District SH end-use	1,791,741	kWh/y
District DHW end-use	1,253,397	kWh/y
District electricity consumption	3,254,030	kWh/y
TES capacity	256,229	lt
Electricity cost	750,544	CHF/y
Investment cost	477,400	CHF/y
Env. Impact of electricity consumption	451,168	$kgCO_2$ / y
Env. Impact of GWHP	21,532	$kgCO_2$ / y
Env. Impact of Storage	6,278	$kgCO_2$ / y
Tot env. impact	478,978	$kgCO_2$ / y

The district energy system optimization is performed by adding the possibility to adopt every type of available solar technologies on each roof (PV, solar thermal and PVT), together with stratified thermal storages and electrical batteries in each building. Based on the implemented roof space constraint, it is possible for the optimizer to select solutions featuring multiple solar technologies or mixed orientation of the solar surfaces. As an example, for building 5, figure 35 shows two of the multiple solutions which are considered by the solar optimization pre-processor to select the best ones in terms of specific productivity and coverage of the building consumption. After the pre-processing, for each building with a flat roof, the scenario file is filled with 4 possible field layout for each technology (2 for panels installed on portrait arrangement and 2 for panel installed on East-West structures, for PV, ST and PVT), while in the case of a slanted roof there is only 1 case for each side of the roof and for each technology.

Table 11 shows the summary results for the optimization of the district energy system based on cost and environmental impact, while table 12 and table 13 present the optimized capacities, for each building and each technology, for cost and environmental impact optimization, respectively. From these tables, it can be noted that the cost-optimized district features a larger PV surface and no electrical storage capacity (i.e., *eES*) which increases the shares of renewable electricity sold to the grid and its connected revenue. When the

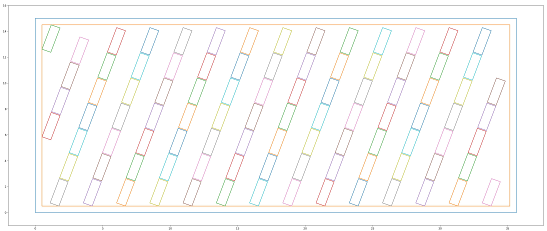

(a)

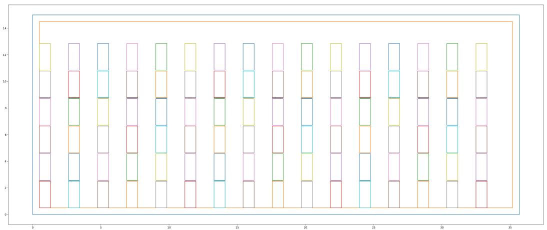

(b)

Figure 35: 2 of the more than 20 solar field arrangements considered in the solar pre-processing for building 5: a) portrait layout, oriented full south with 46° tilt, b) portait layout, aligned on the short side, with 36° tilt.

Table 11: Summary results of cost and environmental impact optimization of the energy system of the typical swiss district with internal electrical and thermal grids.

Parameter	**Cost Optimization**	**EnvImpact Optimization**	**Unit**
Electricity Resource Cost	512947	526506	CHF/y
Investment Cost	623898	858848	CHF/y
FeedIn Revenue	14186	0	CHF/y
HP Capacity	1143	1291	kW
TES Capacity	269	265	m^3
eES Capacity	0	2395	kWhe
PV Capacity	947	896	kWp
PVT Capacity	0	0	m^2
ST Capacity	284	357	m^2
EnvImpact Electrical Consumption	340873	293345	kg CO_2 eq/y
EnvImpact HP	22199	25073	kg CO_2 eq/y
EnvImpact TES	6592	6495	kg CO_2 eq/y
EnvImpact PV	35712	33777	kg CO_2 eq/y
EnvImpact ST	1202	1513	kg CO_2 eq/y
Total System Annual Cost	1122659	1385354	CHF/y
Total System Annual Environmental Impact	406577	360204	kg CO_2 eq/y

target is the minimization of the total environmental impact of the system, the solar thermal collector surface is increased to the maximum area possible on the roof of building 1, where the TES and the GWHP generator are located. Probably due to the impact of distribution losses on the financial viability of solutions based on solar thermal technology, this latter is not chosen for the other buildings, even in the case of environmental impact minimization. The PVT solution is never chosen by the optimizer, probably due to its costs and reduced performance for DHW production. The district optimized for its environmental impact features a large electrical storage capacity, so as to maximize the self-consumption and reduce the renewable electricity fed to the grid. Interestingly, the cost-optimized thermal storage has a larger capacity than the environmental optimum, even if their capacities are quite similar. The optimal capacity of the GWHP, on the other hand, increases in the environmental optimization case, due to the effect of the environmental impact of heat losses: with a larger heat pump capacity at its disposal, the energy production system is able to answer energy demand peaks with reduced reliance on the thermal energy storage content and reduced thermal losses. To gain deeper insight on the sensitivity of the optimized energy system architecture to changes to the objective function of the optimization process, a multi.objective optimization was also performed. Figure 36(a) shows the Pareto front for the combined cost-environmental impact optimization performed on the idealized Swiss district under investigation, while 36(b), instead, shows the total capacities installed by technology and by optimization run, ordered by increasing environmental impact and decreasing cost. These results have been compiled by performing a first cost optimization with no constraint on the environmental impact, a successive environmental optimization with no cost constraint and then iterating with successively smaller values of total environmental impact. In the stacked capacity plot, the capacity for ST and PVT, originally in m^2, is evaluated under the assumption of exposing the solar panel to an irradiance of $1000\,W\,m^{-2}$ while operating at 65 °C for ST and 35 °C for PVT, with an ambient temperature of 15 °C. Analogously, the capacity for the TES, output in m^3, is translated to kW h by assuming a uniform temperature increase of the water-based storage from 35 °C to 65 °C.

Table 12: Cost-optimized capacities of the energy generation technologies for each of the district building.

Building	**GSHP Capacity [kW]**	**PV Capacity [kWp]**	**ST Capacity [m^2]**	**Storage Capacity [m^3]**
Building 1	1098	0	284	260
Building 2	0	182	0	0
Building 3	0	83	0	0
Building 4	0	127	0	0
Building 5	0	71	0	0
Building 6	0	63	0	0
Building 7	0	163	0	0
Building 8	0	162	0	0
Building 9	0	96	0	0
Building 10	0	0	0	0

Table 13: Capacities of the energy generation technologies for each of the district building under environmental impact minimization.

Building	**GSHP Capacity [kW]**	**PV Capacity [kWp]**	**ST Capacity [m^2]**	**Storage Capacity [m^3]**
Building 1	1246	0	357	256
Building 2	0	190	0	0
Building 3	0	83	0	0
Building 4	0	87	0	0
Building 5	0	71	0	0
Building 6	0	63	0	0
Building 7	0	163	0	0
Building 8	0	162	0	0
Building 9	0	76	0	0
Building 10	0	0	0	0

Optimization of a decentralized district energy system

Another type of typical district is characterized by the adoption of decentralized solutions for heat generation that do not foresee the adoption of an internal thermal distribution grid. Contemporary decentralized solutions consists mainly in the adoption of ASHP installed locally at every building of the district. Also in this case, to derive a base case scenario for the comparison against the optimized neighborhood, it is possible to run the optimization without allowing the installation of solar technologies or that of electrical storage units. Table 14 shows the ASHP and TES capacities for each district building following a cost and an environmental impact

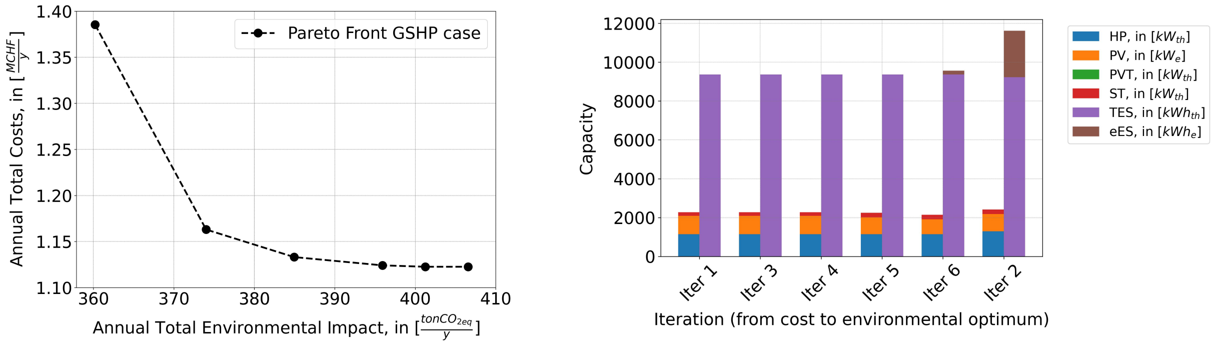

(a) (b)

Figure 36: Results of the multi-objective optimization performed on the typical Swiss district with thermal and electrical distribution grids: (a) Pareto front; (b) staked capacities of heat generators and energy storage

optimization of the base case (i.e., no solar or eES storage). Cost-optimized ASHP capacities are sensibly smaller than those from the environmental impact optimization, set-aside for Building 4 (B1004) and building 8 (B1013). Once the optimization is run for the environmental impact minimization, also TES capacities increase with respect to the cost-optimized case. This behavior points to an increase in the capacity of the energy system to buffer energy production and delay its distribution to time-slots featuring (e.g.) an electricity mix with a lower total environmental impact.

Table 14: Capacity data for each district building in the base case of a decentralized energy system according to cost and environmental impact optimization

Opt_type	Entity	Building_1	Building_2	Building_3	Building_4	Building_5	Building_6	Building_7	Building_8	Building_9	Building_10	Units
Cost	ASHP_cap	255	68	519	40	137	60	60	153	206	116	kWh
Cost	TES_cap	38	10	93	10	23	10	10	31	35	19645	m^3
Env	ASHP_cap	297	92	591	30	167	75	75	119	244	141	kWh
Env	TES_cap	60	19	132	16	35	15	15	51	52	29660	m^3

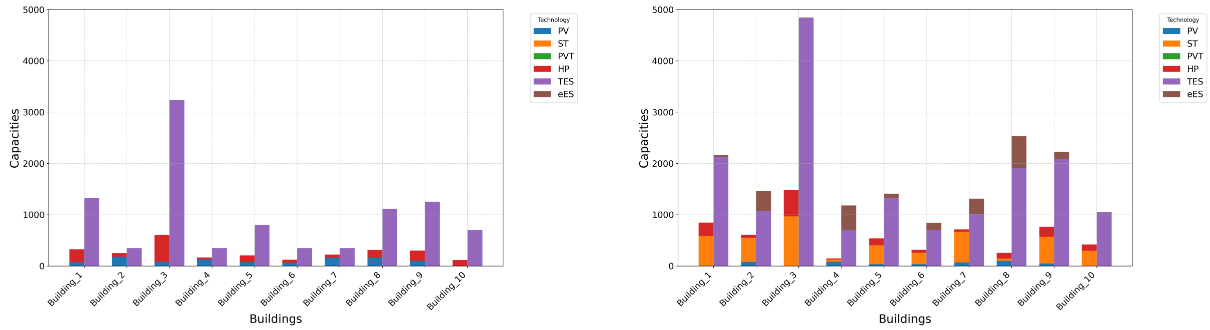

(a) (b)

Figure 37: Capacities of energy generators or storage resulting from separate cost and environmental impact optimizations performed on the typical Swiss district without district heating network but with internal electric grid.

Once the decentralized district is optimized by adopting renewable energy subsystems (PV, ST or PVT) and electrical storage, the energy system architecture changes, as shown by figure 37. For the case without internal district heating network, the cost optimized architecture of the energy system doesn't include solar thermal and PVT technologies, due to their costs. Yet, when the optimization is run to find the minimum environmental impact of the energy system, solar thermal technology is widely adopted, together with a certain level of electrical storage. Between cost and environmental optima, TES capacity, increases uniformly trough the building portfolio, pointing to the positive impact that self-consumption has on the environmental impact of the overall system. From the comparison of the two architectures shown in figure 37, it can be noticed that ASHP capacities decreases as soon as ST technology is adopted in the energy system. The increase of electrical storage at the environmental optimum is an indication, moreover, that the optimizer prioritize self-consumption of renewable electricity rather than its sale to the grid. From a deeper look to the technology mix of the environmental optimum system of figure 37 (b), one can notice that the optimizer has selected multiple solar technologies for the same building roof. The "Roof area" constraint assures that the total footprint of each type of solar field is compatible with the available surface, taking into account safety distances from roof edge and minimal pathways between solar strings.

Table 15: Solar field capacities resulting from the environmental optimum in the decentralized district case.

Field Version	Building_1	Building_2	Building_3	Building_4	Building_5	Building_6	Building_7	Building_8	Building_9	Building_10
pv_1	8	0	0	0	34	0	69	0	0	0
pv_2	0	0	0	0	0	0	0	0	0	0
pv_3	0	0	0	0	0	0	0	0	48	0
pv_4	0	80	0	84	0	33	0	101	0	0
ST_1	209	0	0	0	0	0	218	0	0	109
ST_2	0	0	0	0	0	0	0	0	0	0
ST_3	0	0	133	0	73	0	0	0	0	0
ST_4	0	170	219	15	61	83	0	16	189	0
pvt_1	0	0	0	0	0	0	0	0	0	0
pvt_2	0	0	0	0	0	0	0	0	0	0
pvt_3	0	0	0	0	0	0	0	0	0	0
pvt_4	0	0	0	0	0	0	0	0	0	0

Table 15 shows the inventory of solar solutions selected by OptimEase for the environmental optimum: for each solar technology (PV, ST, PVT), the optimizer has evaluated 4 types of solar fields at each building roof. Once the optimization finished, by combining the results and the problem configuration scenario file, the type of solar fields to be adopted for each building roof can be derived. As an example, for the decentralized system under study, based on the the solar cases written on the scenario file by the optimizer and shown in table 16, and based on the results of table 15, Building 5 should be equipped as follows:

- 34 kWp of PV panels mounted on an East-West structure with 20° tilt aligned on the long side of the roof and featuring a footprint factor (i.e., the ratio between the effective solar surface and the roof area) of more than 65%;
- 73 m^2 of solar collectors in portrait arrangement exposed full south, with a 7° tilt and featuring a footprint factor of about 56%;
- 61 m^2 of solar collectors in portrait arrangement exposed full south, with a 34° tilt and featuring a footprint factor of only 42%

The combination of these 3 solar solutions allow optimizing the decentralized energy system of Building 5. Analogously for the rest of the buildings, different solar fields are combined to maximize the energy demand coverage. It is noteworthy that the combination of the two solar collector fields featuring 7° and 34° tilts has the effect of "fattening" the solar productivity in mid season increasing the thermal demand coverage.

Optimization of a biomass based centralized district energy system

Another example of Swiss typical neighborhood features an internal district heating based on biomass boilers, together with an inner electrical grid for self-consumption and direct access to the electricity market. It is of interest to investigate wat is the impact of SolHood optimization on such energy system architecture. As done before-hand, a cost-optimization run is performed for the system with biomass boiler as sole generator

Table 16: Solar cases considered by the optimizer and (in yellow) those which have been selected for the environmental optimum solution.

Label	Tilt [°]	Absolute Azimuth [°]	Layout	Footprint Ratio [%]	Alignment	Demand coverage [%]	Specific Productivity [kWh/m^2/y]
pv_1	20	200	east-west	65.9%	long	34%	230
pv_2	20	180	east-west	61.0%	south	33%	230
pv_3	7	110	portrait	59.3%	long	33%	238
pv_4	36	180	portrait	42.4%	south	29%	258
pvt_1	20	200	east-west	65.9%	long	35%	$230_e + 1035_{th,SH}$
pvt_2	20	180	east-west	61.0%	south	34%	$230_e + 1036_{th,SH}$
pvt_3	7	110	portrait	59.3%	long	33%	$238_e + 1069_{th,SH}$
pvt_4	36	180	portrait	42.4%	south	30%	$258_e + 1163_{th,SH}$
ST_1	20	200	east-west	65.9%	long	40%	760
ST_2	20	180	east-west	61.0%	south	40%	761
ST_3	7	180	portrait	56.5%	south	39%	817
ST_4	36	180	portrait	42.4%	south	37%	864

Table 17: Summary of system architectures selected for the case of district with biomass boiler-based heating network an for three optimization targets: minimum cost, minimum environmental impact and 50 % of the minimum environmental impact

	PV			ST			Wood			TES			eES		
	cost	env	50% max	cost	env	50% max	cost	env	50% max	cost	env	50% max	cost	env	50% max
B_1	182	190	152	357	357	357	1850	1850	1850	145	145	145	0	0	0
B_2	64	64	64	0	0	0	0	0	0	0	0	0	0	491	132
B_3	108	87	87	0	0	0	0	0	0	0	0	0	0	362	0
B_4	71	71	45	0	0	0	0	0	0	0	0	0	0	485	99
B_5	49	49	49	0	0	0	0	0	0	0	0	0	0	159	0
B_6	82	82	82	0	0	0	0	0	0	0	0	0	0	277	0
B_7	162	104	104	0	0	0	0	0	0	0	0	0	0	452	97
B_8	96	76	76	0	0	0	0	0	0	0	0	0	0	586	119
B_9	0	0	0	0	0	0	0	0	0	0	0	0	0	429	0
B_10	0	0	0	0	0	0	0	0	0	0	0	0	0	0	0
Tot	814	723	659	357	357	357	1850	1850	1850	145	145	145	0	3241	447
Units	kW_e	kW_e	kW_e	m^2	m^2	m^2	kW_th	kW_th	kW_th	m^3	m^3	m^3	kWh_e	kWh_e	kWh_e

to establish a base case. For the same building energy demand reported in 10, the optimization framework selects a minimal architecture featuring a biomass boiler with a capacity of 1850 kW_{th} and a thermal storage of about 145 m^3. Once the optimization process done, a series of solar technologies are adopted based on the adopted optimization target, as shown in Table 17, to reach the various optimization targets imposed, as shown in Table 18. While solar thermal technology is systematically adopted at the location of the TES, it is also systematically excluded from the other buildings more distant from the TES due, probably, to the impact of heat losses on the viability of solar thermal solutions. Photovoltaic installations are, instead, selected for the majority of buildings in order to cover the electricity demand of the district. PVT collectors are, again, not selected on the account, probably, of their non-optimal cost and environmental impact. eES technology is adopted to decrease the environmental impact of the electricity production sub-system as it allows increasing electricity self-sufficiency at the expense of the feed-in tariff income.

Table 18: Summary of environmental impact, cost, sufficiency ratios, and capacities for various optimization targets and the base case of biomass-based centralized energy system.

	Base case	Cost	Env	50% env	Unit
Total environmental impact	428.61	385.8	347.9	368.5	tonnCO_2eq/y
Total cost	1.16	1.05	1.29	1.08	million CHF/y
Sufficiency ratio (elec.)	-	28%	43%	41%	-
Sufficiency ratio (thermal)	-	4%	4%	4%	-
Wood boiler capacity	1.854	1.850	1.850	1.850	MW_{th}
TES capacity	145	154	154	154	m^3
eTES capacity	0	0	3243	447	kWh_e
PV capacity	0	814	724	661	kWp
PVT capacity	0	0	0	0	m^2
ST capacity	0	357	357	357	m^2

5.2 Operation optimization

This section presents the results obtained from the implementation of the Model Predictive Control (MPC) strategy described in Section 4.1.3. Moreover, the system being analyzed was presented previously in Section 4.1. In order to evaluate the performance of the optimizer (optihood), a comparative analysis is carried out against the baseline Rule-Based Control (RBC) strategy defined in Section 4.1.2. The assessment focuses on the Key Performance Indicators (KPIs) established in Section 2.7: specifically the overall operational cost, the CO_2 impact, and the grid flexibility factor.

The primary objective of the optimization function within optihood was the minimization of operational costs. Consequently, the optimizer modulates the system's energy flows to shift consumption to periods of lower electricity tariffs. Table 19 summarizes the annual results for the base case (RBC) versus the optimized case (MPC).

Table 19: Annual performance comparison between Rule-Based Control and optihood optimization (MPC). Percentage improvements achieved using MPC compared to RBC are also listed.

Scenario	Total OPEX Cost [CHF]	CO_2 Impact [-]	Flexibility Factor [-]
Base Case (RBC)	13 902	9.26	-0.2503
With optihood (MPC)	13 319	9.37	0.0878
Improvements	**+4.19 %**	**-1.18 %**	**+33.81 %**

As anticipated, the implementation of optihood resulted in a reduction of the total system cost from 13902 CHF to 13319 CHF, representing a saving of 4.2%. Furthermore, the Grid Flexibility Factor showed a substantial improvement. While the base case resulted in a negative flexibility factor (-0.2503), indicating a grid-stressing behavior, the optimized control shifted this value to a positive range (0.0878). This represents an absolute increase of 33.81%, demonstrating that the system became significantly more grid-supportive by shifting loads away from peak periods. Under the RBC strategy, the system activated heat pumps strictly based on immediate thermal demand, often coinciding with peak consumption hours. Conversely, the MPC effectively utilized the thermal mass of the storage tanks as a buffer by pre-charging them during periods of low electricity prices.

It is noted that the CO_2 impact increased slightly from 9.26 to 9.37. This behavior is attributed to the formulation of the objective function, which targeted cost minimization exclusive of emissions. In this specific simulation scenario, periods of low electricity prices did not always correlate perfectly with low grid carbon intensity. This finding suggests that for future applications where decarbonization is the priority, a multi-objective optimization function should be employed to balance the trade-off between economic savings and environmental impact.

To understand the source of the cost reductions, it is necessary to analyze the dynamic behavior of the control signals. Figure 38 illustrates the correlation between the dynamic electricity price and the activation of the heat pump over a representative period where the control works as intended.

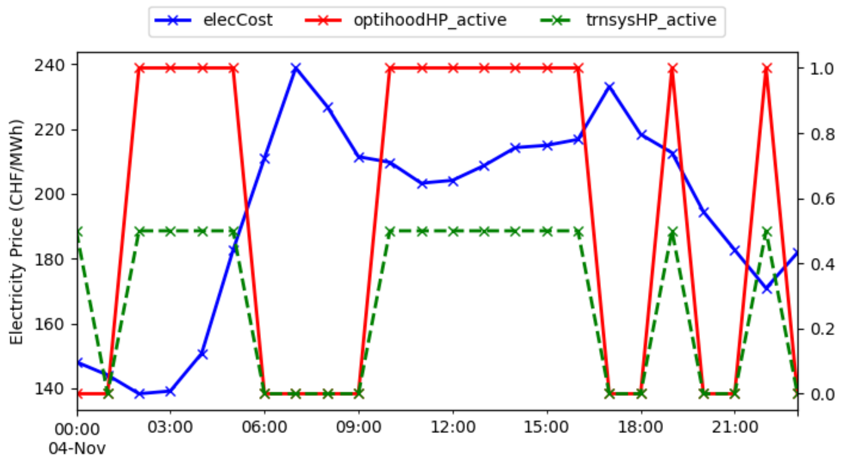

Figure 38: Comparison of electricity price signal (blue) against optihood activation control signal (red) and TRNSYS actual operation (green).

The blue line represents the electricity price [CHF/MWh], while the red line represents the binary activation signal sent by optihood (1 for active, 0 for inactive). As observed in the interval between 10:00 and 16:00, the optimizer identifies a period of low electricity prices. Consequently, optihood commands the heat pump to activate (switch to state 1) to pre-charge the thermal storage, taking advantage of the favorable tariff. Conversely, during price peaks (e.g., around 08:00 and 19:00), the optimizer keeps the heat pump deactivated to avoid high costs. The green line represents the actual status of the heat pump in the TRNSYS simulation, which attempts to follow the optimized control actions.

While the cost reduction of 4.2% is positive, it falls short of the theoretical potential of approximately 8% observed in initial optimization runs. This deviation is caused by a discrepancy in the fidelity of the component models used in the optimizer versus the detailed physics-based models in TRNSYS.

Specifically, there was a mismatch in the Heat Pump (HP) modelling. The optimizer modeled the HP as a modulating unit, capable of adjusting its thermal output to meet specific energy targets precisely. Whereas, the TRNSYS digital twin (Type 977) operated as a non-modulating, fixed-speed unit. This discrepancy led to operational conflicts. When optihood calculated an optimal trajectory requiring partial energy delivery, it sent an "ON" command. The TRNSYS model, being non-modulating, responded by activating the heat pump at nominal (full) power. This often resulted in an over-delivery of thermal energy, causing the temperatures in the Domestic Hot Water (DHW) tanks to rise significantly above the target set-points.

To prevent dangerous overheating and ensure the physical validity of the simulation, a safety override was implemented in the co-simulation interface. The TRNSYS controller was modified to ignore the "ON" command from optihood if the DHW tank temperature exceeded a safety threshold. This behavior is clearly observed in Figure 39, which shows a longer simulation duration.

As seen in Figure 39, there are moments where the red line (optihood request) is high, but the green line (TRNSYS status) drops to zero (and vice versa). Instances where the optihood request is active but the TRNSYS status drops to zero represent the safety controller overriding the optimizer to prevent overheating.Conversely, the TRNSYS status activates without an optimizer request when the water temperature in

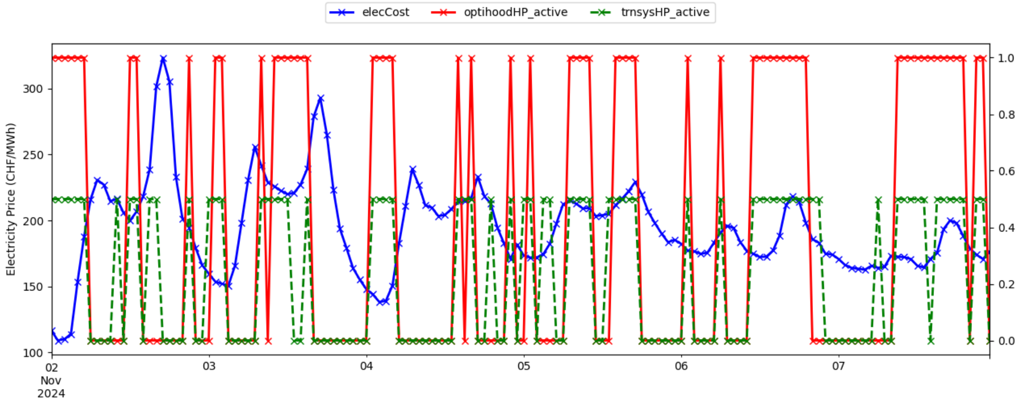

Figure 39: Impact of safety overrides on operation. Despite continuous activation signals from optihood (red blocks), TRNSYS operation (green) cycles on and off due to DHW tank temperature limits.

storage tank falls below a lower-bound threshold. This rule-based intervention ensures minimum temperature maintenance; however, relaxing this threshold could allow the optimizer to dictate the heat pump activation more effectively. These limitations reduced the effective utilization of low-price periods, thereby limiting the achieved cost savings to 4.2%. It is concluded that aligning the component definitions, specifically utilizing modulating heat pump models in the TRNSYS system simulation, would allow the system to fully exploit the optimization strategy and achieve savings closer to the theoretical 8%.

5.3 Case Studies

The objective of the case studies is to evaluate the potential, applicability, and usability of the proposed method by implementing the developed optihood framework (Section 2.1) in real-world scenarios. This analysis primarily aims to identify optimization opportunities for both current and future implementations while assessing the effectiveness of the framework. The results from the case studies are expected to yield recommendations that could inform the development of similar future neighborhoods.

In this chapter, we will present and discuss the applicability of the optimization framework on two case studies. During the proposal phase, the neighborhood "Kreuzstrasse Zollikofen" (project of Meili Management AG) was identified as the first case study. However, during the course of the project, it was found that the required data to setup the neighborhood within the optihood framework could not be made available. Therefore, another real case with office buildings in Zurich was selected. The second case study is the Ecothierrens neighborhood in the canton of Vaud.

5.3.1 Office District Zurich

Description of the district

The first case study conducted by SPF-OST consists of a small neighborhood of 6 office buildings (constructed between 1995-2004) in Zurich with a total energy reference area of 26 728 m^2 including a small living space of 193 m^2. The heating demands of these buildings are currently met using fossil-based technologies (gas/oil-fired boilers). Figure 40 shows a representation of the considered office district with 6 buildings. An overview of the energy reference area and annual energy demands of each building is given in Table 20. Due to lack of available monitoring data, the demand profiles were evaluated for each office building (and also for residential space heating in Building 6) using the demand profile generator of the nPro design tool[14]. This tool provides

[14]https://www.npro.energy/

demand profile generation methods for different types of buildings (residential, office, shops, etc.) based on the energy reference area and the building subcategory. The nPro tool defines several building subcategories relevant for Switzerland (e.g. Minergie building standards). The 'multi family house constructed between 1995-2004' building category was used for the residential space, while for offices the subcategory 'existing' denoting the existing office building stock in Switzerland was considered. The specific annual energy demand assumptions used within this case study from the nPro tool are summarized in Table 21. In order to account for the randomness associated with the use of DHW and electricity, the standard demand profiles from nPro tool were shifted using random time shifts sampled from a Gaussian normal distribution. These fixed-profiles with random time shifts were then used for the electricity and domestic hot water demands of each building.

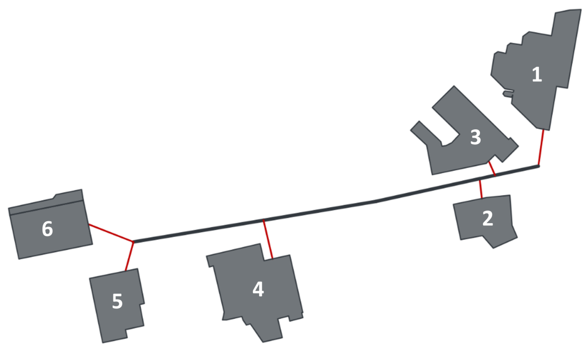

Figure 40: Schematic representation of the considered office district in Zurich.

Table 20: Overview of energy reference area and annual energy consumption demands.

Building	Residential space [m^2]	Office space [m^2]	Electricity demand [MWh/y]	DHW demand [MWh/y]	SH demand [MWh/y]
1	0	10080	454	81	1240
2	0	1548	70	12	190
3	0	4834	218	39	595
4	0	3380	152	27	416
5	0	3994	180	32	491
6	193	2892	134	27	397

Table 21: Specific annual energy demands for office and residential spaces assumed within the case study.

Building usage	Electricity demand [kWh/m^{2}y]	DHW demand [kWh/m^{2}y]	SH demand [kWh/m^{2}y]
Office	45	8	123
Residential	22	21	88

Instead of using fixed profiles for space heating, we used the 3R3C building model (described in section 2.2.3) to model the annual space heating demand of each building. The thermal comfort temperature range of 22 °C to 24 °C was assumed during day and 20 °C to 24 °C at night. Thermal capacity and window area (including a factor for shading) were estimated based on the energy reference area, the year of construction and the following additional sources/assumptions:

- Total envelope area from eValo and 3D swisstopo.

- Infiltration through the building envelope was estimated with 0.2 W/(m^{2}K).
- Shading factor of 0.2 (reduction of g-value due to active blinds).
- Window g-value and u-value were based on "Merkblatt Fenster – Das Fenster in der Energieberechnung".
- Opaque components u-value was obtained from eValo.
- Thermal mass between 0.1–0.15 kWh/(m^{2}K) was assumed based on SIA 380/1:2016.

Internal heat gains within the buildings were calculated based on SIA 2024, by multiplying the specific values with the energy reference area. SIA 2024 provides the standard hourly profiles for heat gains resulting from occupancy and equipment for different types of buildings (including offices and residential spaces). Figure 41 shows the normalized internal gain profiles from SIA (per unit reference area) for offices and residential buildings. Internal heat gains arise from the occupants, lighting and equipment. The y-axes represents the normalized internal gains, where 100% denotes the maximum magnitudes. These maximum magnitudes of internal gains (per unit reference area) would be different depending on the building type (office or residential) and the type of internal gain (occupant, light or equipment). Table 22 lists the magnitudes of maximum internal gains per unit energy reference area for offices and residential buildings. Furthermore, for offices we assume reduced internal heat gains during weekends. The internal gains due to occupant and light were reduced to 20% (from hour 8 to 18) and 0% otherwise. The internal gains from equipment in offices were reduced to 10% (all day on a weekend). While, for residential buildings we assume the same internal gains profile for weekend and weekday. The internal heat gains for the mixed-use building (building 6) were calculated separately for the office and residential spaces. The fitting method described in section 2.2.3 was then used to obtain the effective thermal resistances for each building. After evaluating the parameters associated with the 3R3C building model, these parameters were setup in the required input format for the optihood framework. The building model parameters obtained for each building in the district are given in Table 23.

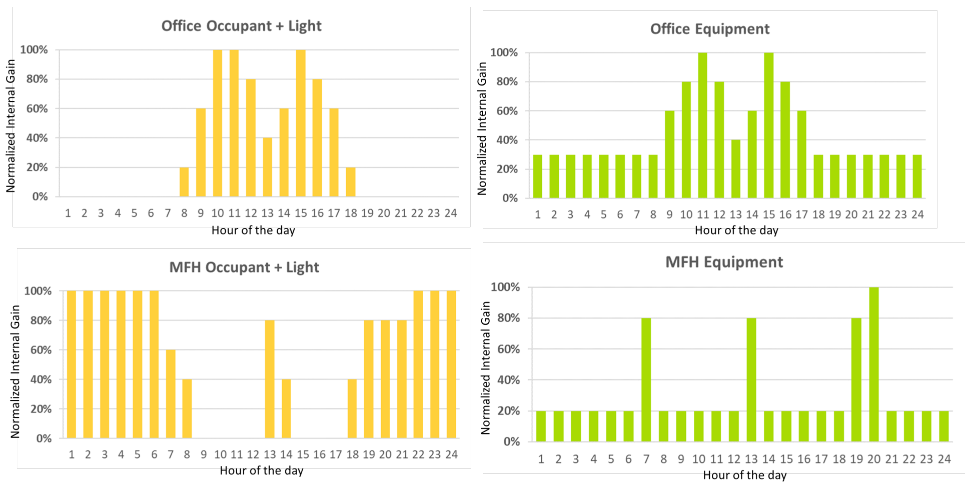

Figure 41: Normalized internal gain profiles (per unit energy reference area) for offices and residential buildings, obtained from SIA 2024.

Moreover, the weather data for Zurich including the ambient temperature, global and diffuse solar radiation on a horizontal plane was obtained from MeteoSwiss. We used the weather data of a typical year in Zurich during the simulations. A fixed grid-electricity tariff of 20 Rp./kWh was assumed along with dynamic hourly carbon emissions for grid electricity (Jobard et al. (2022)). The hourly emissions are based on life-cycle impact assessment, i.e. global warming potential over a span of 100 years (Section 2.6.1).

Table 22: Maximum magnitudes (100% in Figure 41) of internal gains per unit energy reference area, based on SIA 2024.

Building type	Internal gain type	Maximum magnitude [W/m^2]
Office	Occupant	8.4
	Light	9.8
	Equipment	15
Residential	Occupant	2.4
	Light	7.7
	Equipment	10

Table 23: Evaluated parameters for 3R3C building model (Section 2.2.3) showing the effective thermal resistances (R) and capacities (C) of three different thermal elements (heat distribution system, indoor air mass, and building wall/envelope).

Building	Window area [m^2]	$R_{distribution}$ [K/kW]	$C_{distribution}$ [kWh/K]	R_{indoor} [K/kW]	C_{indoor} [kWh/K]	R_{wall} [K/kW]	C_{wall} [kWh/K]
1	261	0.0442	2.17	0.0053	8.11	0.1002	1512
2	84	0.0661	0.33	0.0079	1.25	0.1499	232.2
3	121	0.0655	1.04	0.0079	3.89	0.1485	725.1
4	36	0.0944	0.73	0.0113	2.72	0.2139	507
5	127	0.0718	0.86	0.0086	3.21	0.1627	599.1
6	123	0.0770	0.67	0.0092	2.48	0.1746	462.75

Formulation of optimization scenario

In this case study, we investigated the optimal energy system designs within the office district by considering four scenarios:

- LT-DH: This case refers to a Low-Temperature District Heating (where distribution temperatures range around 10 °C to 20 °C) with a central borehole field, decentral heat pumps (GSHP) and decentral thermal energy storages. The decentral units (GSHPs and storages) are employed within each building for local heat production and use. The optimizer would select the installed capacities of the decentral GSHPs and storages. The central borehole field is implemented exclusively as a heat source for the GSHPs (without regeneration). Electricity could be provided using grid electricity, PV and/or electrical batteries. The optimizer decides whether to install PV and batteries, and if installed, which capacities to employ.
- HT-DH-HP-PV: In this case, we consider a High-Temperature District Heating (70 °C to 80 °C) with a central air-source heat pump (ASHP) and a central water-based thermal energy storage. The central ASHP produces heat which is stored in a central water-based thermal energy storage and then distributed at 70 °C to the heat consumers (or buildings). The installed capacities of ASHP and storage are obtained from optimizations. The choice between the electricity production technologies is the same as in LT-DH.
- HT-DH-HP-PV-FPC: This case is again a high-temperature district but with a combination of a central ASHP and central solar thermal field, which is composed of flat plate collectors (FPCs). In addition, a central thermal energy storage is employed. Similar to the previous cases, the capacities of each component are obtained from optimizations. Also, the choice between the electricity production technologies is the same as in LT-DH and HT-DH-HP-PV cases.

- HT-DH-HP-PVT: This is the third configuration considered with a high-temperature district. The central heat production technology in this case is a covered PVT collector field, which is complemented by a central thermal energy storage system for the storage of the produced heat. The capacities of the PVT collectors and thermal energy storage will be calculated on the basis of optimizations. As in all previous cases, the electricity production technologies remain the same.

We prepared the optimization scenarios for each of the above-mentioned cases. PV installation was always considered to be rooftop, while considering the maximum available area and roof orientation for PV installation. The total available roof area for each building, together with the orientation of the roof were obtained from the application sonnendach.ch[15] and are given in Table 24.

Table 24: Available roof area and roof orientation for PV installation.

Building	Roof surface area [m^2]	Roof Alignment	Roof pitch
1	691	0° North	0°
2	464	0° North	0°
3	667	0° North	0°
4	22	76° East	32°
4	22	256° West	32°
5	506	0° North	0°
6	773	0° North	0°

Results of optimization

Table 25 presents the installed capacities of different system components for the cases LT-DH, HT-DH-HP-PV, HT-DH-HP-PV-FPC and HT-DH-HP-PVT. The capacities selected during both cost and environmental optimizations are shown. The maximum available capacity limited by the available roof area is chosen for PV installation in both cost and environmental optimizations. This is observed for every case where PV technology can be selected. Furthermore, while there are no electrical batteries in the cost optimum solutions, batteries able to store of 3 to 4 hours the PV peak power capacity are installed in the environmental optimizations. Moreover, the capacity of borehole field in cost optimization of LT-DH case was observed as 672 kWh, which remained nearly the same during environmental optimization (675 kWh).

Figure 42 shows the total annualized cost (calculated using Eq. 26) per unit energy demand and the annual GHG emissions (from Eq. 27) per unit energy demand for the cost optimum solution in each of the four considered cases. While, Figure 43 illustrates the same results for the environmentally optimum solutions in each case.

It can be seen that HT-DH-HP-PV-FPC configuration is both the cost and environmentally optimum configuration out of the four cases evaluated. In the cost optimum, HT-DH-HP-PV-FPC case has 18 % lower cost with marginally higher (~1.5 %) emissions compared to the LT-DH case. Notably, The HT-DH-HP-PV configuration performs quite close to the HT-DH-HP-PV-FPC case, showing a cost difference of less than 1 % and 6 % higher emissions. The environmental optimum HT-DH-HP-PV-FPC exhibits the same PV capacity as the cost optimum, although with higher installed capacities for FPC and ASHP. The increase in ASHP size is a direct consequence of the massive reduction in Thermal Energy Storage (TES) capacity. With a diminished thermal buffer, the heat pump requires a higher peak capacity to cover demand spikes that the storage would otherwise smoothen out. The environmental optimum solution also includes an electrical battery. The cost of environmental optimum is 1.4 times higher than that of the cost optimum solution, however the impact is 17 % lower.

[15] `https://www.uvek-gis.admin.ch/BFE/sonnendach/`

Table 25: Installed capacities of system components during cost and environmental optimizations for different considered cases.

Case		PV [kW_p]	GSHP [kW]	ASHP [kW]	FPC [m^2]	PVT [m^2]	Thermal storage [m^3]	Battery [kWh]
LT-DH	cost	314.5	692.8	-	-	-	57.5	-
	env	314.5	670.3	-	-	-	87.8	929
HT-DH-HP-PV	cost	314.5	-	564.2	-	-	1245.9	-
	env	314.5	-	756	-	-	92.3	939.7
HT-DH-HP-PV-FPC	cost	314.5	-	547.4	849	-	1012.1	-
	env	314.5	-	569.9	7258.8	-	174.3	1164.5
HT-DH-HP-PVT	cost	-	-	554.4	-	338.8	1121	-
	env	-	-	646.1	-	1880.9	133.3	1235.5

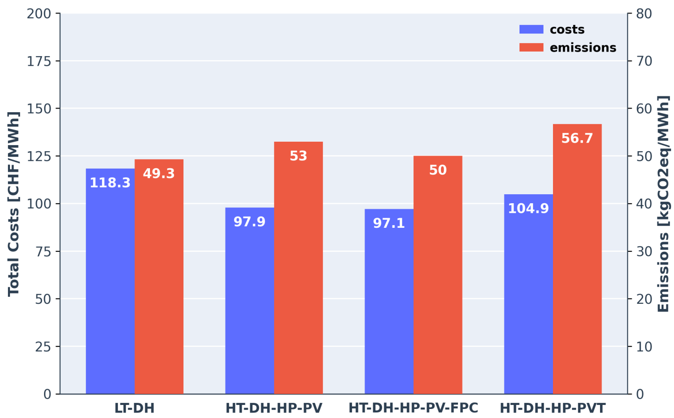

Figure 42: Total annualized cost per unit energy demand and emissions per unit energy demand for the **cost optimum** solutions in each of the considered cases.

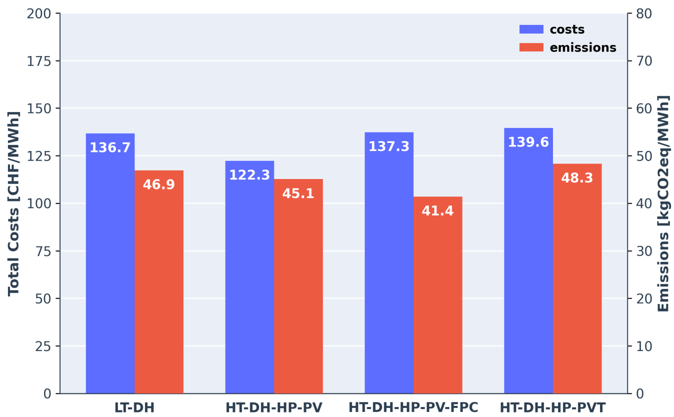

Figure 43: Total annualized cost per unit energy demand and emissions per unit energy demand for the **environmental optimum** solutions in each of the considered cases.

A distinct contrast is observed between the optimal storage sizing strategies for the centralized (HT-DH) and decentralized (LT-DH) networks. The centralized configurations use large thermal buffers to decouple heat generation from demand. The specific storage volume for the centralized cases (HT-DH variants) lies in the range of 0.3 m^3/MWh to 0.4 m^3/MWh of the total annual thermal demand (SH + DHW). This relatively large sizing allows the central generation units to operate continuously during favorable economic windows.

Conversely, the decentralized storage capacities in the LT-DH case are significantly smaller, with an overall specific size of 0.02 m^3/MWh. In the LT-DH configuration, the storage acts primarily as a short-term buffer for the decentralized heat pumps rather than a load-shifting asset for the grid, as the thermal inertia of the building mass (activated via the 3R3C model) provides the necessary flexibility.

The installed capacities of the heat pumps in all scenarios are significantly lower than what would be prescribed by conventional sizing standards. Traditional sizing typically aims to cover peak loads with a safety margin, resulting in 1800 h to 2200 h of operation on a very cold year. In contrast, the optimizer minimizes the investment cost by downsizing the heat pump and forcing it to run in baseload operation. This results in extremely high full load hours (flh): approximately 5000 flh for LT-DH case, and greater than 6000 flh for HT-DH cases. This operational strategy relies heavily on the thermal storage to manage peak demand periods, effectively flattening the heat pump's output profile. Additionally, the optimizer uses a standard weather data profile for system dimensioning, instead of an extremely cold year.

In the HT-DH-HP-PV-FPC cost-optimum scenario, the solar collector field size is effectively 849 m^2. Relative to the total thermal demand of the district, this corresponds to a specific collector area of approximately 0.24 m^2/MWh. This is considerably smaller than typical solar thermal system designs, which aim for higher fractional coverage. The optimization suggests that for this specific tariff structure and demand profile, a small field acting as a summer-load provider is more economically efficient. The specific yield of the field is approximately 500 kWh/m^2a, which is consistent with typical performance values for flat plate collectors.

The contribution of the solar thermal field to the total district heating demand is quantified by the solar fraction.

$$\text{Solar Fraction} = \frac{Q_{solar}}{Q_{total\_demand}} = \frac{423\ \text{MWh}}{3547\ \text{MWh}} = 11.9\% \tag{39}$$

This fraction highlights the role of the solar thermal integration as a baseload provider. With an effective area of 849 m^2, the field is able to cover a significant portion of the domestic hot water demand and distribution losses during the summer. However, the system continues to rely on the heat pumps to cover the bulk of the space heating demand during the winter months (as shown in Figure 44). Additionally, the ~12 % solar fraction represents an economic optimum where the cost of increasing the collector area (and the requisite storage to manage the excess summer heat) outweighs the marginal benefits of electricity savings.

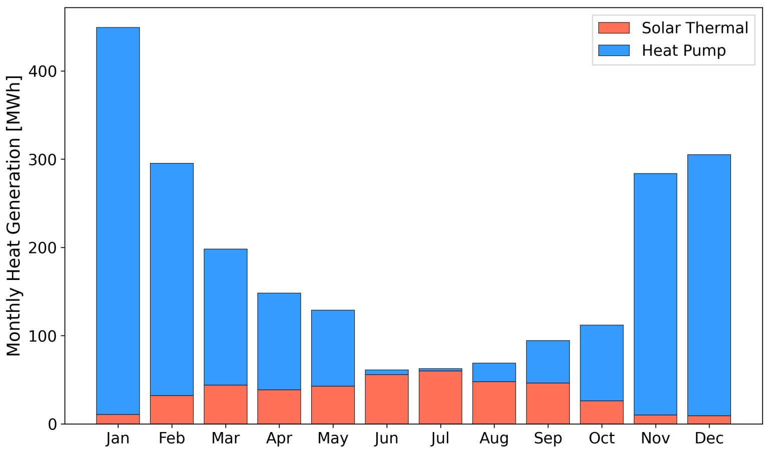

Figure 44: Monthly thermal energy generation for the cost-optimal HT-DH-HP-PV-FPC scenario. The solar thermal field (red) is sized to cover the baseload demand in summer, while the heat pump (blue) covers the peak heating loads in winter.

It is important to note that these sizing and operational findings are intrinsically linked to the specific cost assumptions and demand profiles modeled in this study. However, while the exact numerical values are specific to the demand category of this office district, the observed trends (particularly regarding high heat pump utilization and the economic trade-offs of storage sizing) are expected to be applicable to similar district typologies and boundary conditions.

To further evaluate the economic and operational performance of the selected optimal configuration, key performance indicators (KPIs) for the HT-DH-HP-PV-FPC case were analyzed. Table 26 compares the average system electricity cost, system self-sufficiency, and the Levelized Cost of Heat (LCOH) for both the cost and environmental optimization strategies. Note that these KPIs were defined previously in Section 2.7. A considerable disparity is observed in the LCOH between the two strategies, as anticipated. While the cost-optimal solution achieves a competitive LCOH of 7 Rp/kWh$_{th}$, the environmental optimum sees this figure rise to 11 Rp/kWh$_{th}$. This substantial increase ($\approx$ 57 %) aligns with the previously discussed rise in annualized costs and is driven by the extensive investment in capacity (larger FPC field and battery storage) required to marginally reduce emissions. It is important to note that the LCOH values presented here represent the cost of heat generation and storage only. The capital costs associated with the construction of the district heating network (piping, trenching, and civil works) are excluded from this calculation, as the network topology remains the same across all the considered scenarios. Consequently, the full-system LCOH would be higher than the generation-only figures reported here.

The system electricity costs, representing the cost of electricity consumed from the grid and self-generated PV, increases from 18 Rp/kWh in the cost optimum to 24 Rp/kWh in the environmental optimum. This increase is attributed to the inclusion of the electrical battery storage in the environmental scenario; while the battery reduces grid dependency, the amortization of its capital cost raises the effective cost of the stored electricity utilized by the system. However, these higher specific costs in the environmental optimum yield an improvement in energy independence. The system self-sufficiency rises from 18.7 % to 22.6 %. This improvement indicates that the combination of increased thermal storage, electrical batteries, and a larger solar thermal contribution allows the district to decouple itself further from the external electrical grid, although at a significant financial cost.

Table 26: Comparison of KPIs (defined in Section 2.7) for the HT-DH-HP-PV-FPC configuration under cost and environmental optimization strategies.

KPI	Cost Optimum	Environmental Optimum
System Electricity Cost [CHF/kWh]	0.18	0.24
Self-Sufficiency [%]	18.7	22.6
LCOH [CHF/kWh$_{th}$]	0.07	0.11

5.3.2 Ecothierrens

The second case study is presented here and consists of a small eco-district, called Eco-Thierrens, made of 3 buildings built between 2015 and 2017, located in Thierrens, near Yverdon-Les-Bains, in Switzerland (Figure 45). The eco-district has a total energy reference area of 1856 m^2 and it is made mainly of residential spaces, as shown in Table 27. To derive the hourly profiles of the EcoThierrans district energy demand, CEA was used to model the district based on new building archetypes defined based on the LESOSAI reports submitted during the administrative procedures of the district construction. The eco-district current energy supply system is shown in Figure 45. Its heating supply system is based on an air-source heat pump supplying heat to a 85 m^3 thermal energy storage (TES) located outdoors and fed (originally) by PVT collectors, too. A small internal thermal network connects the buildings to the TES and allows heat distribution for space heating and domestic hot water preparation. Photovoltaic (PV) panels installed on building roofs generate electricity, which can be utilized on-site, stored in batteries within the buildings, or fed into the local grid under the Swiss national feed-in tariff program.

Figure 45: View of EcoThierrens, an eco-district located in Thierrens, in Switzerland.

Table 27: Values of reference energy surface, net volumes and target/limit values for space heating according to SIA380/1

Thermal zone	Building category	A_e [m^2]	A_w/A_e	Vol. net [m^3]	Q_{lim} [MJ/m^2]	Type*
Heated area A	multi-residential	648.4	1.668	1667.8	151.1	A1
Heated area B	multi-residential	514.7	1.812	1311.5	159.8	A1
Heated area C	multi-residential	693.0	1.782	1735.2	158	A1
Total		**1856.1**	**1.751**	**4714.6**	**156.1**	
Correction of $C_{h/m}$ as a function of the yearly average temperature θ_{es} : -7.5%						
A1: New construction		A2: Refurbishing		A3: Extension		A4: Change of destination

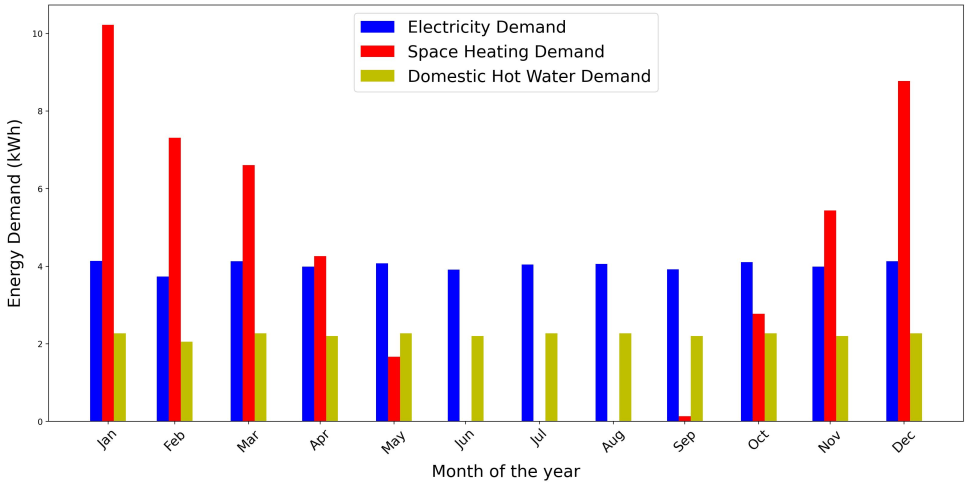

Figure 46: Montly profile of aggregated energy demand of the district Eco-Thierrens for space heating, DHW production and electricity.

The eco-district features several solar surfaces already installed on the slanted roof of the building. ST or PVT collectors are installed on the south-ward roof surfaces, oriented 45° South-East, while PV panels are installed on the slopes oriented 45° North-West. Table 28 shows the values used as input on the scenario configuration file (i.e, *Hood* tab). For this particular case study, the optimization has been limited to select the size of PV and ST solar fields, each installed on a different slope of the building roofs, and determine the optimal capacity for the main heat generator, a propane based air-source heat pump. As shown in Table 29, between cost optimization (i.e., iteration 1) and environmental optimum (i.e., Iteration 2), an electrical storage capacity of more than 40 kWh is added to the architecture, together with 200 m^2 of solar collectors on the southernmost slopes, while PV capacity decreases. Notably, while the cost of the system increases by only 20 %, the environmental impact of the optimized solution is reduced threefold.

Table 28: Input provided at the "Hood" tab in the scenario configuration file.

Parameter	**Building C**	**Building B**	**Building A**
ID	1	2	3
latitude (°)	46.70269	46.703	46.70271
longitude (°)	6.75851	6.7583	6.75815
bld_orientation (°)	135	225	135
short_side (m)	14	12.5	14.61
long_side (m)	20	14.6	16
busy_area (m^2)	2	2	2
pv	1	1	1
solarCollector	1	1	1
pvt	0	0	0
Roof_tilt (°)	35	35	35
Roof_Ridge	L	S	L

Table 29: Results of multicriteria optimization for the EcoThierrens case study

Parameter	**Iteration 1**	**Iteration 2**	**Unit**
Electricity Resource Cost	14617	10990	CHF/y
Investment Cost	63298	79426	CHF/y
FeedIn Revenue	3107	363	CHF/y
HP Capacity	31	32	kW
TES Capacity	85	85	m^3
eTES Capacity	0	43	kWhe
PV Capacity	31	26	kWp
ST Capacity	0	202	m^2
Total system annual cost	74809	90053	CHF/y
Total system annual environmental impact	12275	4242	kg CO_2 eq

6 Conclusions and outlook

The project SolHOOD facilitated the development and extension of the python-based optimization framework "optihood" for smart planning and control of energy systems in neighborhoods. This framework was significantly extended by implementing validated models for solar technologies (including flat plate collectors, PV and PVT collectors), a building model (3R3C) to replace the static heating demand profiles, thermal energy storage model, and functionality to serve as an MPC algorithm, among other developments. Optihood is open-source, with the code available (and actively maintained) on GitHub[16] and a comprehensive online documentation[17]. Furthermore, the project developed an innovative methodology for constructing Typical Electricity Years (TEY) specifically adapted to Switzerland, aligning with Typical Meteorological Year (TMY) data. This method effectively captures the temporal variability of greenhouse gas (GHG) emissions, reflecting dynamic changes in the electricity system. By integrating TEY profiles into building energy simulations, the project improves the precision of energy system performance evaluations by integrating dynamic electricity modeling into the planning of sustainable energy systems at the neighborhood level. The project, moreover, defined a comprehensive set of Key Performance Indicators (KPIs) to assess energy systems from several viewpoints, taking into account economic, environmental, and operational aspects. Indicators such as Net Present Value (NPV), Levelized Cost of Energy (LCOE), Global Warming Potential (GWP), self-sufficiency, and the grid flexibility factor provide a robust basis for comparing different configurations and operational strategies. These KPIs allow considering dynamic electricity pricing and operational constraints to achieve optimal energy system performance, balancing cost and sustainability objectives.

The project also tackled the optimization of energy system design by analyzing representative neighborhood typologies and boundary conditions for solar technologies. A statistical study of Swiss districts identified key features for categorizing various neighborhood types, with a subset of a "2000 Watt" district serving as a reference model for optimization. Such data-driven approach has been adopted with the aim of ensuring that the results of the optimization are practical and adaptable to different urban contexts. The integration of solar energy solutions and the challenges posed by it related to regulations, safety standards, and limitations on available roof space have been also addressed. Furthermore, the project introduced a pre-processing methodology for solar radiation modeling to optimize the configuration of solar panels, including their tilt, orientation, and layout.

The application of the optihood framework to two distinct case studies, an office district in Zurich and the residential Eco-Thierrens district, yielded critical insights regarding optimal system topologies. In the Zurich office district case study, a centralized High-Temperature District Heating (HT-DH) network powered by a central air-source heat pump (ASHP) and flat plate collectors (FPC) proved to be both the economic and environmental optimum. It is important to note that the optimization scope was strictly limited to DH solutions (low and high-temperature), excluding decentralized alternatives such as gas boilers or ASHPs without a DH connection. Compared to a decentralized Low-Temperature (LT-DH) alternative with ground-source heat pumps, the centralized solution offered an approximate 18 % reduction in total annualized costs. A key finding regarding component sizing was the economic viability of downsizing heat pumps to run in baseload operation (achieving >6000 full load hours), while relying on significant thermal storage capacities ($0.3\,m^3/MWh$ to $0.4\,m^3/MWh$) to manage peak demands. The integration of solar thermal energy played a crucial role, covering approximately 12 % of the demand (primarily summer baseload), with a specific yield of $500\,kWh/m^2a$. Moreover, maximizing the rooftop installation of PV panels in districts was suggested during both the economic and environmentally perspectives. The Eco-Thierrens case study highlighted the trade-offs between economic and environmental objectives. While cost optimization focused on standard capacities, the environmental optimization required the integration of significant electrical battery storage (>40 kWh) and the addition of $200\,m^2$ of solar thermal collectors. Notably, while the environmental optimum increased the total annual system cost by approximately 20 %, it resulted in a threefold reduction in the annual environmental impact (from 12.3 $tonnCO_2eq$ to 4.2 $tonnCO_2eq$). It is worthwhile to note that these results are based on the specific assumptions made for the costs and GHG emissions. The results, therefore, are expected to provide

[16] https://github.com/SPF-OST/optihood

[17] https://optihood.readthedocs.io/

recommendations for future neighborhoods with similar energy demands and building types.

Lastly, the project successfully demonstrated the potential of optihood as an MPC strategy for district heating operation. Comparing the MPC strategy against a standard Rule-Based Control (RBC), the optimization achieved a validated cost reduction of 4.2 %. More significantly, the MPC transformed the system's interaction with the electrical grid. The Grid Flexibility Factor improved by 33.8 %, shifting from a negative value (grid-stressing) to a positive value (grid-supporting). This was achieved by effectively utilizing thermal storage to shift heat pump activation to periods of low electricity prices, decoupling thermal demand from electricity consumption. However, the analysis revealed a slight increase in CO_2 emissions (+1.18%) under the MPC strategy. This occurred because periods of low electricity prices did not perfectly correlate with low grid carbon intensity, highlighting that single-objective cost optimization does not automatically yield environmental benefits.

Outlook and recommendations

While the results affirm the validity of the developed framework, the following areas are identified for future work and development:

- **High-Fidelity Model Alignment:** The MPC analysis revealed a performance gap between the theoretical potential (approx. 8 % savings) and the achieved results (4.2 %). This was primarily due to a discrepancy between the modulating heat pump model used in the optimizer and the non-modulating (on/off) physics-based model in the TRNSYS simulation. Future implementations must ensure stricter alignment between the optimization models and the physical hardware (or digital twins) to avoid safety overrides that limit performance.
- **Multi-Objective MPC:** Given that cost-optimized control slightly increased emissions, future control strategies should implement multi-objective optimization functions. These should weigh real-time pricing against dynamic carbon signals to balance economic savings with decarbonization goals.
- **Scalability of Hybrid Solar Configurations:** While this project demonstrated the cost-effectiveness of solar thermal as a baseload provider in the specific context of the Zurich case study, future work should investigate the scalability of this finding. Further research is required to categorize which specific neighborhood typologies and demand profiles favor hybrid PV-Solar Thermal configurations over PV-only solutions. Additionally, the sensitivity of these hybrid designs to future fluctuations in electricity prices and collector costs should be analyzed to provide generalized design guidelines.
- **Data-Driven Generalizability:** The identification of representative district typologies establishes a framework for extending these findings beyond the specific case studies. Future work should focus on automating the mapping of these optimized archetypes to broader urban planning datasets to facilitate large-scale energy planning.

In conclusion, SolHOOD has successfully developed a robust and open-source framework for optimizing district energy systems. The results demonstrate that through careful design optimization and predictive control, district energy systems can achieve significant cost reductions and grid flexibility improvements, paving the way for the sustainable energy transition of the building stock.

7 National and international cooperation/Publications

The SolHOOD project placed a strong emphasis on knowledge transfer and collaboration across both academic and industrial sectors. To ensure a broader application of the project results, the team engaged in active dissemination through open-source software releases, scientific publications, and direct technology transfer mandates with industry partners.

- The extensions to the open-source *optihood* framework were published on GitHub, with a set of examples illustrating its functionalities. An online documentation was prepared describing the different component models and providing guidelines for use. The documentation is accessible at `https://optihood.readthedocs.io/`.
- We participated in the *oemof* user developer meeting held in Flensburg, Germany during 18-20 May 2022, and presented the *optihood* framework. The meeting served as a platform for knowledge exchange as well as provided networking opportunities with the developers of the *oemof* package (which *optihood* is based on).
- The *optihood* framework was presented at the SPF Industrietag (Industry day) on 08 March 2023. This annual event organized by SPF brings together several industry professionals and provided us with a platform for knowledge exchange/networking with industries.
- One peer-reviewed article was presented at the scientific conference CISBAT, held during 13-15 September 2023 in Lausanne:
  - Neha Dimri, Daniel Zenhäusern, Daniel Carbonell, Xavier Jobard, Vincent Jacquot, Agnès François, Massimiliano Capezzali, Marten Fesefeld, *Optihood – a multi-objective analysis and optimization framework for building energy systems at neighborhood scale*, Journal of Physics Conference Series 2600, 082027, DOI: 10.1088/1742-6596/2600/8/082027
- We secured the following cooperation with the industries based on the developments made and experience gathered during the SolHOOD project:
  - A mandate from Energie 360° (March 2023 – September 2023) for the use of *optihood* to study the flexibility potential in a district heating network.
  - A successful first attempt of an experimental MPC-run of *optihood* with Yuon Control AG (February 2024 - September 2024).
- Cooperation is also taking place with SPF's own follow-up projects which use *optihood* as an optimization tool. These include GISOptiTES and DecenTGrids within the BFE programme on Solar Heat and Heat Storage, and SolIceTES in the BFE programme Heat Pump and Refrigeration Technologies.

References

Afjei, T. and Wetter, M. (1995). Yearly Utilization Model YUM WP, HolzBenutzerhandbuch mit Beispielen. Technical Report INFEL/KRE, Zürich.

Carbonell, D., Battaglia, M., Philippen, D., and Haller, M. Y. (2018). Numerical and experimental evaluation of ice storages with ice on capillary mat heat exchangers for solar-ice systems. *International Journal of Refrigeration*, 88:383–401.

Carbonell, D., Birchler, D., Hobé, A., and Ruesch, F. (2024). *IceGrids - Implementation of ice storage tanks into 5GDHC networks as seasonal storage or load shifting element*. Institut für Solartechnik SPF for Swiss Federal Office of Energy (SFOE), Research Programme Solar Heat and Heat Storage, CH-3003 Bern.

Carbonell, D., Philippen, D., Granzotto, M., and Haller, M. Y. (2016a). Simulation of a solar-ice system for heating applications. System validation with one-year of monitoring data. *Energy and Buildings*, 127(0):846 – 858.

Carbonell, D., Philippen, D., and Haller, M. Y. (2016b). Modeling of an ice storage buried in the ground for solar heating applications. Validations with one year of monitored data from a pilot plant. *Solar Energy*, 125:398–414.

Carbonell, D., Philippen, D., Haller, M. Y., and Frank, E. (2015). Modeling of an ice storage based on a de-icing concept for solar heating applications. *Solar Energy*, 121:2–16.

Diane, v. G., Jakob, R., and Loïc, P. (2021). Solcad – rapport final. potentiel du solaire thermique dans les chauffages à distance en suisse.

EnDK (2008). Modèle de prescriptions énergétiques des cantons (mopec) - edition 2008. *Konferenz Kantonaler Energiedirektoren*.

Faria, P., Lezama, F., Vale, Z., and Khorram, M. (2121). A methodology for energy key performance indicators analysis. *Energy Informatics*, 4.

Frischknecht, R., Jungbluth, N., Althaus, H.-j., Doka, G., Heck, T., Hellweg, S., Hischier, R., Nemecek, T., Rebitzer, G., Spielmann, M., and Wernet, G. (2007). ecoinvent report n°1: Overview and Methodology. Technical Report 1, Swiss Centre for Life Cycle Inventories, Dübendorf, CH.

Hilpert, S., Kaldemeyer, C., Krien, U., Günther, S., Wingenbach, C., and Plessmann, G. (2018). The open energy modelling framework (oemof) - a new approach to facilitate open science in energy system modelling. *Energy Strategy Reviews*, 22:16–25.

Hoffmann, M., Puranik, S., Juanpera, M., Martín-Rapún, J. M., Tuiskula, H., and Blechinger, P. (2020). Investment planning in multi-vector energy systems: definition of key performance indicators. In *CIRED 2020 Berlin Workshop (CIRED 2020)*, volume 2020, pages 158–161.

Holmgren, W., Hansen, C., and Mikofski, M. (2018). pvlib python: a python package for modeling solar energy systems. *Journal of Open Source Software*, 3(29):884.

Iturralde, J., Alonso, L., Carrera, A., Salom, J., Battaglia, M., and Carbonell, D. (2019). *Energy demands for multi-family buildings in different climatic zones*.

Jobard, X., Demonchy, G., Lasvaux, S., Frossard, M., Dimri, N., and Zenhäusern, D. (2022). Optim-ease - deliverable wp1: Buildings demand, technolgies, lca and lcc data methodology. Technical report.

Jones, E., Oliphant, T., Peterson, P., et al. (2001). SciPy: Open source scientific tools for Python.

Katrin, M., Sarah, A., Heike, Z., and Fabian, K. (2021). Standards et labels de la construction durable en suisse.

KBOB, ecobau, and IPB (2022). Kbob-empfehlung 2009/1:2022: Ökobilanzdaten im baubereich, stand februar 2022. koordinationskonferenz der bau- und liegenschaftsorgane der öffentlichen bauherren c/o bbl bundesamt für bauten und logistik.

Lund, P. D., Lindgren, J., Mikkola, J., and Salpakari, J. (2015). Review of energy system flexibility measures to enable high levels of variable renewable electricity. *Renewable and Sustainable Energy Reviews*, 45:785–807.

Mavrotas, G. (2009). Effective implementation of the ε-constraint method in multi-objective mathematical programming problems. *Applied Mathematics and Computation*, 213(2):455–465.

Minergie (2011). The minergie-standard for buildings.

Péan, T., Costa-Castelló, R., and Salom, J. (2019). Price and carbon-based energy flexibility of residential heating and cooling loads using model predictive control. *Sustainable Cities and Society*, 50:101579.

Péan, T. Q., Salom, J., and Ortiz, J. (2017). Potential and optimization of a price-based control strategy for improving energy flexibility in mediterranean buildings. *Energy Procedia*, 122:463–468. CISBAT 2017 International ConferenceFuture Buildings & Districts – Energy Efficiency from Nano to Urban Scale.

Quiquerez, L. (2017). *Décarboner le système énergétique à l'aide des réseaux de chaleur: état des lieux et scénarios prospectifs pour le canton de Genève*. PhD thesis, UNIGE.

Rüdisüli, M., Teske, S. L., and Elber, U. (2019). Impacts of an increased substitution of fossil energy carriers with electricity-based technologies on the swiss electricity system. *Energies*, 12(12).

Siemens Industry, I. (2014). Managing energy using key performance indicators. Technical report, Siemens Retail & Commercial Systems.

SPADOM. Ville de lausanne, service des parcs et des domaines, végétation et panneaux solaires.

Stocker, T. F., Qin, D., Plattner, G.-K., Tignor, M., Allen, S. K., Boschung, J., Nauels, A., Xia, Y., Bex, V., and (eds.), P. M. M. (2013). Climate Change 2013: The Physical Science Basis. Contribution of Working Group I to the Fifth Assessment Report of the Intergovernmental Panel on Climate Change.

SUVA (2022). Travaux sur les toits. pour ne pas tomber de haut. Technical report, SUVA.

SUVA, Swissolar, des édifices Suisse, E., suissetec, and swiss safety (2022). Énergie solaire: intervenir en toute sécurité sur les toits. montage et entretien d'installations solaires. Technical report, SUVA.

The CEA team (2024). The city energy analyst (version 3.38.0).

Yang, Y., Jurasz, J., Li, H., Lydia, A., Syrri, A., and Yan, J. (2020). Key performance indicators on flexibility of a multi-energy system. In *Applied Energy Symposium 2019: Low carbon cities and urban energy systems*.

Zenhäusern, D., Bamberger, E., and Baggenstos, A. (2017). Pvt wrap-up energiesysteme mit photovoltaisch-thermischen solarkollektoren. Technical report, EnergieSchweiz, Bundesamt für Energie BFE.

A Appendix A

A.1 Parametric calculation for ground-source and air-source heat pump

The default geothermal heat pump implemented within the framework is ProDomo brine/water heat pump from Cadena Systems AG. The fitted data using the approach described in section 2.2.1 is shown in Figure A1. Table A1 defines the fitted coefficients for the geothermal heat pump.

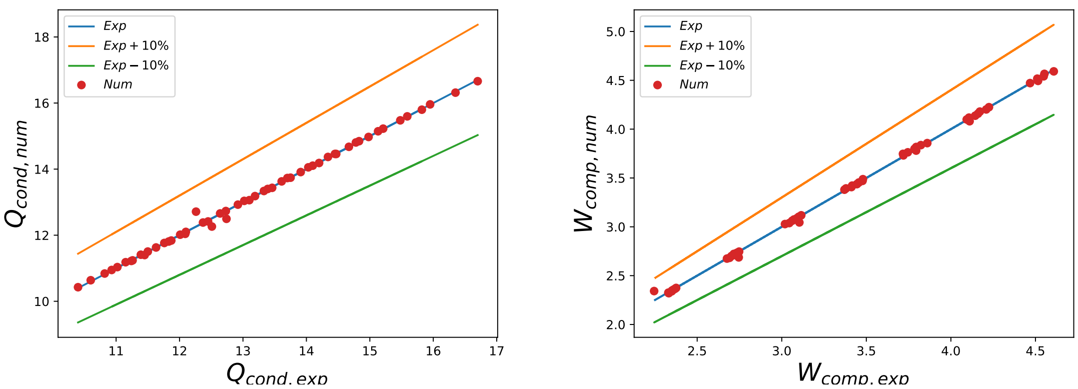

Figure A1: Differences between experiments and fitted data of Q_{cond} and W_{comp} for ground-source heat pump

The HP08L-M-BC air/water heat pump from Heliotherm was implemented as the default air-source heat pump within the framework. The fitted data and the corresponding coefficients for air-source heat pump are given in Figure A2 and Table A2, respectively.

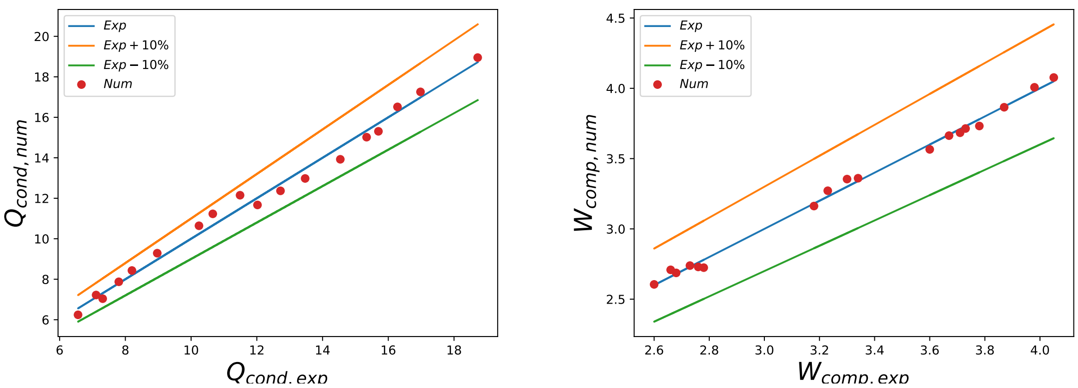

Figure A2: Differences between experiments and fitted data of Q_{cond} and W_{comp} for air-source heat pump

Table A1: Fitted coefficients for the ground-source heat pump.

Coefficient	Description	$[kW]$
bq_1	1^{st} *condenser polynomial coefficient*	1.3898e+01
bq_2	2^{nd} *condenser polynomial coefficient*	1.1484e+02
bq_3	3^{rd} *condenser polynomial coefficient*	-9.3634e+00
bq_4	4^{th} *condenser polynomial coefficient*	-1.7942e+02
bq_5	5^{th} *condenser polynomial coefficient*	3.4234e+02
bq_6	6^{th} *condenser polynomial coefficient*	-1.2497e+01
bp_1	1^{st} *compressor polynomial coefficient*	1.5999e-01
bp_2	2^{nd} *compressor polynomial coefficient*	-1.2369e+00
bp_3	3^{rd} *compressor polynomial coefficient*	1.9939e+01
bp_4	4^{th} *compressor polynomial coefficient*	1.9345e+01
bp_5	5^{th} *compressor polynomial coefficient*	7.1057e+00
bp_6	6^{th} *compressor polynomial coefficient*	-1.4048e+00
$\dot{m}_{cond}$	3055.36 $[kg/h]$	
$\dot{m}_{evap}$	2865.59 $[kg/h]$	
COP_{nom} (A0W35)	4.64	
$Q_{cond,nom}$ (A0W35)	12.49 $[kW]$	
$Q_{evap,nom}$ (A0W35)	9.80 $[kW]$	
$W_{comp,nom}$ (A0W35)	2.69 $[kW]$	
RMS_{COP}	$9.78e-03$	
$RMS_{Q_{cond}}$	$8.06e-02$	
$RMS_{W_{comp}}$	$2.02e-02$	
Fit model	Inlet/Outlet Temperature	

Table A2: Fitted coefficients for the air-source heat pump.

Coefficient	Description	
		$[kW]$
bq_1	1^{st} *condenser polynomial coefficient*	1.1833e+01
bq_2	2^{nd} *condenser polynomial coefficient*	9.6504e+01
bq_3	3^{rd} *condenser polynomial coefficient*	1.4496e+01
bq_4	4^{th} *condenser polynomial coefficient*	-5.0064e+01
bq_5	5^{th} *condenser polynomial coefficient*	-1.3360e+02
bq_6	6^{th} *condenser polynomial coefficient*	-1.2497e+01
bp_1	1^{st} *compressor polynomial coefficient*	6.6610e-01
bp_2	2^{nd} *compressor polynomial coefficient*	-2.2365e+00
bp_3	3^{rd} *compressor polynomial coefficient*	1.5541e+01
bp_4	4^{th} *compressor polynomial coefficient*	2.5705e+01
bp_5	5^{th} *compressor polynomial coefficient*	-1.7407e+01
bp_6	6^{th} *compressor polynomial coefficient*	3.8145e+00
$\dot{m}_{cond}$	2900.00 $[kg/h]$	
$\dot{m}_{evap}$	7250.00 $[kg/h]$	
COP_{nom} (A0W35)	4.23	
$Q_{cond,nom}$ (A0W35)	11.50 $[kW]$	
$Q_{evap,nom}$ (A0W35)	8.78 $[kW]$	
$W_{comp,nom}$ (A0W35)	2.72 $[kW]$	
RMS_{COP}	$1.07e-01$	
$RMS_{Q_{cond}}$	$3.78e-01$	
$RMS_{W_{comp}}$	$3.16e-02$	
Fit model	Inlet/Outlet Temperature	

A.2 Building RC model

The nomenclature for the configuration parameters, exogenous inputs, boundary parameters, state variables and decision variables of the RC building model is given in Table A3. The temperature of each thermal space is influenced by the exogenous input parameters, temperature and heat flows from the adjoining thermal spaces. The state space equations of the building are given in Table A4.

Table A3: Variables and parameters of the building RC model.

Nomenclature:	
$R \in R^+$	Thermal resistance between states [K/kW]
$C \in R^+$	Thermal capacity of the state [kWh/K]
$gA \in R^+$	Total aperture area of the windows [m^2]
$Q \in R$	Heating power [kW]
$T \in R$	Temperature [K]
$\epsilon_t^{ind} \geq 0$	Violation of indoor comfort temperature range at time t [K]
$T_t^{amb} \in R^+$	Ambient outside air temperature at time t [K]
$I_t^H \in R^+$	Total horizontal irradiation at time t [kW/m^2]
$Q_t^{occ} \in R$	Internal heat gains from occupants at time t [kW]
Superscripts and Subscripts:	
ind	Indoor air state
$wall$	Wall and building mass state
dis	Distribution system state
$stor-dis$	From the storage tank to the distribution system
min	minimum
max	maximum
t	at t^{th} time step

Table A4: State space differential equations of the building RC model.

State-space equations:
$C_{ind} \cdot \dot{T}^{ind} = \frac{1}{R_{ind}}(T^{wall} - T^{ind}) + gA \cdot I^H + Q^{occ}$
$C_{wall} \cdot \dot{T}^{wall} = \frac{1}{R_{ind}}(T^{ind} - T^{wall}) + \frac{1}{R_{wall}}(T^{amb} - T^{wall})$
$C_{dis} \cdot \dot{T}^{dis} = \frac{1}{R_{dis}}(T^{ind} - T^{dis}) + Q_t^{stor-dis}$

The relations between the temperatures of different thermal spaces (represented by the state space differential equations) in the form of discrete linear difference equations are given by:

$$\begin{bmatrix} T_{t+1}^{ind} \\ T_{t+1}^{wall} \\ T_{t+1}^{dis} \end{bmatrix} = A^{build} \cdot \begin{bmatrix} T_t^{ind} \\ T_t^{wall} \\ T_t^{dis} \end{bmatrix} + B^{build} \cdot Q_t^{stor-dis} + C^{build} \cdot \begin{bmatrix} I_t^H \\ Q_t^{occ} \\ T_t^{amb} \end{bmatrix} \tag{A1}$$

where, A^{build}, B^{build} and C^{build} are the matrix coefficients of discretization.

The constraints on the initial temperatures of the thermal spaces are given by:

$$\begin{bmatrix} T_0^{ind} \\ T_0^{wall} \\ T_0^{dis} \end{bmatrix} = \begin{bmatrix} T_{init}^{ind} \\ T_{init}^{wall} \\ T_{init}^{dis} \end{bmatrix} \tag{A2}$$

where, T_{init} denotes the initial temperature of a given thermal space.

The acceptable upper and lower limits on indoor temperatures are defined by the constraint:

$$T_{min}^{ind} - \epsilon_t^{ind} \leq T_t^{ind} \leq T_{max}^{ind} + \epsilon_t^{ind} \tag{A3}$$

The permissible range of heating power delivered by the distribution system is modelled by the following constraint:

$$Q_{min}^{stor-dis} \leq Q_t^{stor-dis} \leq Q_{max}^{stor-dis} \tag{A4}$$

A.3 "weather" class

The class "weather" implemented under Python downloads solar radiation data from the PVGIS database and outputs an excel file containing query results.

By default, downloaded data contain the annual hourly profile of the Typical Meteorological Year (TMY[18]) for a location assigned in a source file, which defaults to "Scenario.xls". Optionally, the class allows to download historical hourly values of solar radiation measurements instead of TMY data sets.

Together with solar radiation and air temperature data, the "weather" class provides the annual hourly profile of the soil temperature, used in geothermal probe computations. A seasonality model is applied to the mean surface soil temperature measured at the nearest Meteosuisse station to derive the temperature that the heat transfer fluid of a geothermal probe would have at the location of interest.

The use to create an instance "meteo" of class "weather" is as follows:

$$meteo = weather(source = "scenario.xls", target = "weather.csv")$$

where:

- "scenario.xls" is the source file providing input values (latitude, longitude, azimuth and tilt of solar surface);
- "weather.csv" is the output file to which the output data are written. In particular, the following data are written in the output file:
  - air temperature, given in [°C];
  - global irradiance on the horizontal plane, in $[\frac{W}{m^2}]$;
  - diffuse irradiance on the horizontal plane, in $[\frac{W}{m^2}]$;

[18] A Typical Meteorological Year (TMY) is a set of meteorological data with data values for every hour in a year for a given geographical location. For each month in the year, the data have been selected from the year that was considered most "typical" for that month.

- soil temperature, in [°C].

Several class attributes and methods are available:

- $weather.get\_scenario()$: method to get input data from the source file and populate the class attributes;
- $weather.get\_TMY()$: method to download PVGIS TMY hourly data for the location specified in the source file;
- $weather.get\_hourly()$:method to download PVGIS historical hourly data for the location specified in the source file;
- $weather.get\_TMY\_formatted()$: same as get_TMY() but including the output format based on the default field labels;
- $weather.get\_stn()$: Geopanda based method to locate the Meteosuisse soil temperature station nearest to the project site specified in the source file;
- $weather.get\_soil()$: method to get the 2021 measurement hourly values for the surface soil temperature as measured in the nearest Meteosuisse station;
- $weather.compute\_soil()$: method to compute the temperature annual hourly profile of a geothermal probe installed at the location of interest;
- $weather.save\_DB()$: method to save data to the target file;
- $weather.lator.longor.azor.tilt$: attributes to store coordinates, tilt and azimuth (populated from the source file at instance creation)

A.4 Ground source temperature hourly profile

As mentioned beforehand, the "weather" class provides the annual hourly temperature profile of the heat transfer fluid of the borehole heat exchanger, used for the computation of the geothermal HP. To do this, first the nearest Meteosuisse station with 2021 soil temperature measurements is identified among the 63 stations available in the file "Soil_stn.csv". Then, a simple seasonality model is applied to compute the mean "soil temperature", i.e. the temperature at which the heat transfer fluid in a geothermal probe would exit the soil, by assuming it to be variable between 0°C at the end of February and the annual mean surface temperature at the end of summer (see Figure A3):

$$T_{soil} = 0\ ^{\circ}\mathrm{C} + \frac{< T_s > - 0\ ^{\circ}\mathrm{C}}{2} \left(sin \left(2\pi \cdot \frac{dayN - 155}{365} \right) + 1 \right) \tag{A5}$$

where:

- $< T_s >$ is the annual mean surface temperature;
- dayN is the day-number, with 155 corresponding to the 28 of February.

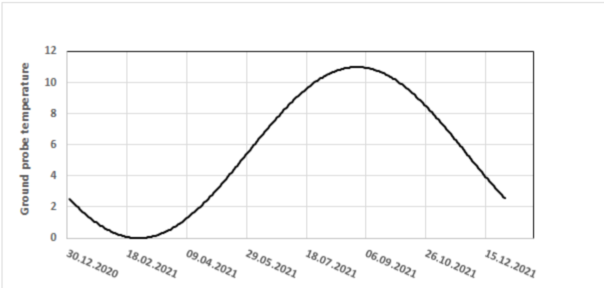

Figure A3: The seasonal soil temperature profile is computed as a sinusoidal profile between a minimum soil temperature of 0°C at the end of winter and a maximum temperature at the end of the summer given by the annual mean surface soil temperature.

A.5 The "calepinage" class

The "Calepinage" class, implemented in Python and utilizing the "Shapely" package, offers a robust method for calculating the optimal number of panels that can be accommodated on a rectangular-shaped roof with arbitrary orientation. Specifically tailored to the geometric characteristics of a reference solar panel of width w and length l, the class employs a sophisticated algorithm. This algorithm first computes the optimal distance between rows, strategically minimizing shading during the winter solstice at the latitude of installation. Subsequently, it maximizes the utilization of available space by efficiently filling the roof with the greatest possible number of panels.

The class takes as input the following series of data, with default values provided in parentheses:

- $orientation$ (180): the orientation of the building in degrees, following the convention where 180° represents South, 90° corresponds to East, 270° indicates West, and 360°/0° denotes North;
- lat (42.6): the latitude at the center of the building roof; used to determine the optimal row distance to avoid reciprocal shadowing of the panel rows at noon on Winter solstice;
- W (10): width of the rectangular shaped roof, in $[m]$;
- L (10): length of the rectangular shaped roof, in $[m]$;
- w (1): panel width, in $[m]$;
- l (2.05): panel length, in $[m]$;
- $tilt$ (20): panel tilt, used to compute the horizontal projection of the panel in a portrait installation arrangement, in [°];
- $tilt\_EW$ (20): tilt of individual panels in an East-West installation arrangement, in [°];
- d_W (0.5): distance from the roof edge on the short side of the building, in $[m]$;
- d_L (0.5): distance from the roof edge on the long side of the building, in $[m]$;
- d (0.6): minimum distance between rows, to ensure a pathway for operational and maintenance activities, in $[m]$;
- off_pnl (0.07): collector spacing along each collector row, in $[m]$;
- f_orient (False): boolean to consider collectors oriented towards South (True) or orient them parallel to the main building axis (false);
- f_EW (False): boolean to enable (True) or disable (False) E-W installation arrangement calculations;

- f_plot (False): boolean to enable plotting the collector arrangement on the rectangular shaped roof.

The use to create an instance "Roof" of class "calpinage" for a 20 m by 10 m roof oriented 45° East to retrieve the maximum number of 2 by 0.75 m collectors that can be installed with a tilt of 33°, facing south in portrait arrangement, is as follows (see Figure A4):

$$\begin{aligned} Roof = Calpinage(orientation = 90 + 45, w = 0.75, l = 2, W = 10, L = 20, tilt = 33, \\ f\_EW = False, f\_plot = True, f\_orient = True) \end{aligned} \tag{A6}$$

While the use to create the same instance for a roof oriented 15° West in East-West arrangement would be the following (see Figure A5)):

$$\begin{aligned} Roof = Calpinage(orientation = 180 + 15, w = 0.75, l = 2, W = 10, L = 20, tilt = 33, \\ f\_EW = True, f\_plot = True, f\_orient = True) \end{aligned} \tag{A7}$$

The "calpinage" class, besides providing the option to plot the surface studied, e.g. roof, and the collector arrangement, outputs the total number of panels and the ratio of roof surface covered by the collectors. It has to be noted, that each E-W collector arrangement corresponds to 2 collectors installed side-by-side at a customized tilt. As an example, in the case of Figure A4, 36 panels can fit the roof with orientation 45° E in portrait arrangement, while in the case of Figure A5, 50 panels can be installed on the 15° W oriented roof in E-W layout, featuring a coverage ratio of 31.6 % and 43.8 %, respectively.

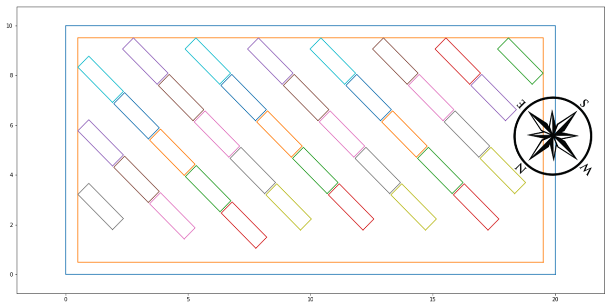

Figure A4: Graphical output of the *"Roof"* instance of class *"calpinage"* for a 20 m by 10 m roof oriented 45° East filled with 2 m by 0.75 m collectors installed with a tilt of 33°, facing south and in portrait arrangement.

Class use-case example

Figure A6 shows the district Im Lenz in Lenzburg, one of the "2000 Watt" sites, which can be considered an example of Swiss typical district. The highlighted building features an 11 m by 50 m rectangular shaped roof and it is located at Niederlenzer Kirchweg 8 in Lunzburg. The building has its short axis oriented towards 10° West and according to the adopted convention, it has an azimuth of 190°. It is assumed that solar panels of rectangular shape with dimensions 2 m by 1 m are installed, either in portrait layout or East west arrangement. Collectors can be installed aligned with the building or facing south, if in portrait arrangement, or along the North-South direction, if in East-West arrangement.

The python instruction to create a class named roof_1 of type "Calpinage" in the case of the building in Lenzburg (i.e., latitude of 47.39°N) with solar panels in portrait layout, facing south and featuring a tilt of 30°, and with a minimum row distance of 0.6 m, is the following:

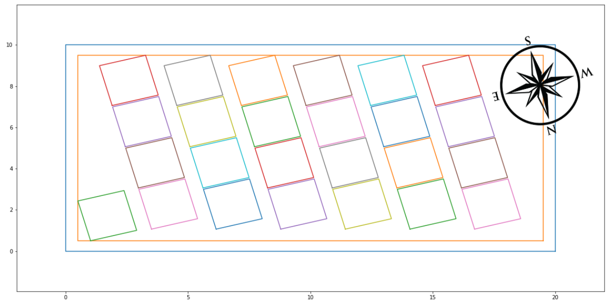

Figure A5: Graphical output of the *"Roof"* instance of class *"calpinage"* for a 20 m by 10 m roof oriented 15° West filled with 2 m by 0.75 m collectors installed in an East-West structures with default tilt.

Figure A6: "2000 Watts" site Im Leinz in the city of Lenzburg: google map aerial view (left pane) and site representation under City Energy Analyst (right pane).

Figure A7: Panel arrangement according to portrait layout (left pane) and east-west structures (right pane).

$$\begin{aligned} roof\_1 = Calpinage(orientation = 190, lat = 47.39, w = 1, l = 2, W = 11, L = 50, tilt = 30, \\ f\_EW = False, f\_plot = True, f\_orient = True, d\_rows = 0.6) \end{aligned} \tag{A8}$$

while the one to perform the same calculation in the case of east-west arrangement would be the following:

$$\begin{aligned} roof\_1 = Calpinage(orientation = 190, lat = 47.39, w = 1, l = 2, W = 11, L = 50, tilt_EW = 20, \\ f\_EW = True, f\_plot = True, f\_orient = True, d\_rows = 0.6) \end{aligned} \tag{A9}$$

The graphical output for the previous instructions is shown in Figure A8 and Figure A9 for portrait and east-west layout, respectively. Table A5 shows the number of panels that can be installed on the same roof in portrait layout and in East-west arrangement for several tilt values, together with the fill-in ratio calculated assuming the default distance between collector and roof edge (i.e. d_L = d_W = 0.5 m), and default minimal spacing between neighboring rows (i.e., 0.6 m).

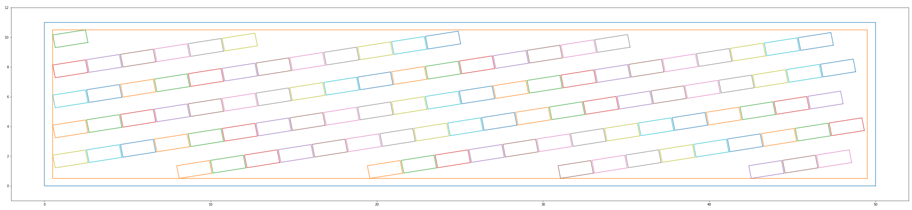

Figure A8: Panel placement on the roof according to South alignment and in portrait layout.

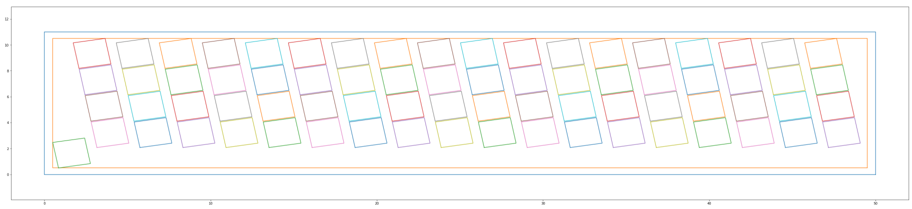

Figure A9: Panel placement on the roof according to North-South alignment in East-West layout.

Table A5: Number of panels and fill-factor for the building roof under study for several values of panel tilt installation.

Panel tilt	Number of panels		Fill-factor	
	Portrait	EW	Portrait	EW
20	120	146	48.9%	59.6%
30	105	154	42.8%	62.8%
40	95	170	38.8%	69.4%